UNIVERSITY OF BIRMINGHAM

DEGRADATION OF PURE MAGNESIUM ALLOYS

IN

SIMULATED BODY FLUID

By

Hamidreza Hodaeian

A thesis submitted to

The University of Birmingham

for the degree of

MASTER OF RESEARCH

School of Metallurgy and Materials
College of Engineering and Physical Sciences
University of Birmingham
March 2013

ABSTRACT

Biodegradable bone implants have the ability to be resorbed or dissolved and finally removed from the human body after the healing process. Therefore, there is no need to have a second operation for the patients, resulting in lower costs imposed on the health care system. Polymers and ceramics are common biodegradable implants used in the human body but their mechanical properties are poor for load bearing applications. Therefore, application of a metal instead of a polymer or ceramic would be more appropriate. Magnesium has the potential to become a promising biodegradable bone implant. Magnesium gradually degrades in the human body and also has no adverse side effects on the human body. Furthermore, its mechanical properties are closer to the mechanical properties of bone, compared to other metallic implants such as stainless steels, Co-Cr alloys and titanium alloys. Therefore, metallic bone implants made by magnesium would be more biocompatible with bone tissue and the occurrence of stress shielding would be less compared to other metallic implants. However, magnesium degrades very quickly in the physiological environment where the pH ranges from 7.4 to 7.6 and the implant may be degraded completely before the healing process is finished. It is important to study the corrosion process of magnesium alloys in order to control the corrosion rate in the body during the approximately 12-18 week period in which it maintains its mechanical integrity until the bone tissue is completely healed.

The corrosion behaviour of 5 types of samples; cast commercial pure magnesium ingot (A), cast commercial pure magnesium solidified at 2 rates (B and C), extruded commercial pure magnesium (D) and extruded super pure magnesium (E), were studied in tests involving 480 hour immersion in Simulated Body Fluid (SBF). Weight loss, pH changes and the rate of release of magnesium ions were measured. Furthermore, SEM (Scanning Electron Microscopy), EDX (Energy Dispersive X-ray spectroscopy) and XRD (X-ray Diffraction) were conducted on the surface of the specimens.

The weight loss of extruded samples (E and D) was about 7 to 20 times lower, compared to the cast samples (A, B and C), which indicated a higher corrosion resistance for the extruded samples. In addition, the extruded samples (D and E) showed a higher reproducibility and greater uniformity of corrosion compared to the cast samples (A, B and C) after 480 hour immersion in SBF.

The main reason for such a difference in the corrosion behaviour, reproducibility and uniformity of corrosion of the samples was related to the presence of porosity within the specimens associated with the casting of the alloy. Plastic deformation reduced and eliminated most of the casting defects, including porosity, in the extruded samples (D and E). Also, magnesium hydroxide formation was prevented in the extruded samples (D and E). Therefore, the extruded samples showed higher corrosion resistance, reproducibility and uniformity of corrosion compared to the cast samples (A, B and C).

ACKNOWLEDGEMENTS

Firstly, I would like to thank my supervisors, Dr. Artemis Stamboulis and Dr. W. D. Griffiths. It was my great fortune to have them as my advisors. I cannot adequately express my gratitude for their everlasting support, criticisms, motivations…

I am tremendously grateful for all the support and time they have given me over the course of my project and writing up period. Without their support, I feel that I would not have been able to complete this work. As a result of their guidance I have further developed my skills and experience, which I am sure, will be invaluable in the future. Working with them was full of learning and the most enjoyable experience I have ever had…

I would also like to thank the Department of Metallurgy and Materials, University of Birmingham for use of their facilities and equipment. I am thankful to the staff of the department of Metallurgy and Materials. Especially, I would like to thank Paul Stanley and Theresa Morris for their help in SEM.

I would also like to express my gratitude to Dr. Stephanie Handley-Sidhu at School of Geography, Earth and Environmental Sciences for her helping on Ion Chromatography measurements.

I am also particularly grateful to Dr. Jackie Deans at School of Chemistry for her support and guidance during XRD measurements.

In addition, I would like to thank all those in the biomaterials group who have helped me throughout my project.

Finally, I would give my special appreciation to my parents Mr. Mohammadreza Hodaeian and Mrs. Masoumeh Hodai for their consistent support, patience and understanding during my postgraduate study in the University of Birmingham. Without their support, I could not complete my degree.

TABLE OF CONTENTS

LIST OF FIGURES

LIST OF TABLES

CHAPTER 1: Literature Review

1.1 Introduction

Biodegradable bone implants have the ability to be spontaneously resorbed or dissolved and finally removed from the human body after the healing process [1, 2]. Hence, it is more convenient for patients to have biodegradable implants instead of non-biodegradable ones due to problems related to non-biodegradable implants such as mismatch between the implant and the body or inflammation [1]. Also, if the implant is biodegradable, there is no need to have a revision surgery in order to remove the implant [1, 3]. This is desirable because revision surgery leads to side effects and might cause pain to the patient, and it imposes higher health costs on society and the health care system [4, 5].

Polymers and ceramics are the most common materials used for biodegradable bone implants but their mechanical properties are not appropriate for load bearing applications [2]. The high fracture toughness and mechanical strength of metallic materials make them a more appropriate choice for load bearing applications where high fracture toughness is important. However, the problem of most metallic materials currently used in the biomedical industry, including titanium alloys, stainless steels and cobalt-chromium based alloys, which are not biodegradable, is the release of metallic ions induced by corrosion or wear which can be toxic, and can result in inflammation of the tissue and inevitable implant failure. In addition, metal implants exhibit high elastic modulus, much higher compared to the stiffness of bone (Table 1.1). This can result in stress shielding which can prevent stimulation of bone growth and remodelling, leading to a reduction in implant stability [4].

Magnesium is a lightweight metal which has low density (1.74 g/cm3) and good mechanical properties and has good potential for applications in aerospace, automotive industry, telecommunication, computer hardware, hand held tools, microelectronics and as biodegradable bone implant in the medical field [1, 4, 6]. Some of the properties of magnesium such as its elastic modulus, density and

yield strength are very close to bone when compared to other implants, resulting in reduction of stress shielding and better bone formation (Table 1.1).

Table 1.1 Mechanical and physical properties of various implant materials compared to natural bone tissue [4, 77].

Implant materials	Fracture toughness (MPam $^{1/2}$)	Elastic modulus (Gpa)	yield strength (Mpa)	Density (g/cm^3)
Natural bone	3-6	3-20	130-180	1.8-2.1
Magnesium	15-40	41-45	65-100	1.74-2.0
Ti alloy	55-115	110-117	758-1117	4.4-4.5
Co-Cr alloy	N/A	230	450-1000	8.3-9.2
Stainless steel	50-200	189-205	170-310	7.9-8.1
Synthetic hydroxyapatite	0.7	73-117	600	3.1
PLLA	0.93	2.5	60	1.23-1.25

Osteoconductive and osteoinductive properties have been observed in magnesium alloys such as Mg-Mn-Zn leading to bone bonding and bone formation, respectively [1]. Also, revision surgery will not be required because magnesium and its alloys when in contact with an aqueous environment e.g. the physiological environment, corrodes and eventually degrades. Magnesium ions are non-toxic and can be excreted from the body via the kidneys. No remarkable side effects related to magnesium ions in the human body have been observed [2-4, 7]. But the limitation of magnesium usage in the body relates to its corrosion rate, which for pure magnesium is very high in the physiological environment where the pH ranges from 7.4 to 7.6. Therefore, they can lose their mechanical integrity very fast before the healing process is completed [1-4, 8].

It is important to study the corrosion process of magnesium alloys in order to control the corrosion performance in the body during the approximately 12-18 week period, during which it can maintain its mechanical integrity till the bone tissue is completely healed [1, 4].

There are different methods that can be used in order to control the corrosion rate of magnesium including surface treatment, purification of magnesium, alloying of magnesium with other elements such as Al, Zn and RE elements and controlling the microstructure by optimising the grain size and the

presence of intermediate phases. The latter, and particularly the amount and distribution of grain size and intermetallic phases, play the most important role in the corrosion process of magnesium [1, 3, 8].

1.2 Corrosion types and mechanism in magnesium alloys

The poor corrosion resistance of magnesium alloys firstly stems from internal galvanic corrosion, due to the presence of inhomogeneities such as second phases and impurities in the alloy. Secondly, the formation of magnesium hydroxide on the surface, which is not as stable as the passive films formed on stainless steel and aluminium, is another important reason for poor corrosion resistance [9-12]. However, formation of a partially protective layer on the surface inhibits general corrosion in magnesium alloys, therefore, localized corrosion is the common type of corrosion [13].

1.2.1 Galvanic corrosion

Magnesium is highly reactive owing to its very low electrochemical potential. Therefore, the metallic phases ,which can be found, whether in pure magnesium or magnesium alloys, increase the occurance of internal galvanic attack [12]. This galvanic attack mostly leads to severe localized corrosion next to a cathodic second phase [10]. Formation of some large pits was observed by Song et al. [14] next to a cathodic second phase in a Mg-Zn-Y-Zr wrought alloy which could be due to micro galvanic corrosion induced by the second phase. Cathodes are classified into external and internal cathodes. The metals in contact with magnesium are known as external cathodes and the second phases and impurities in the alloy are called internal cathodes (See figure 1.1) [10].The most common impurity and internal cathode in magnesium alloys is Iron [12].

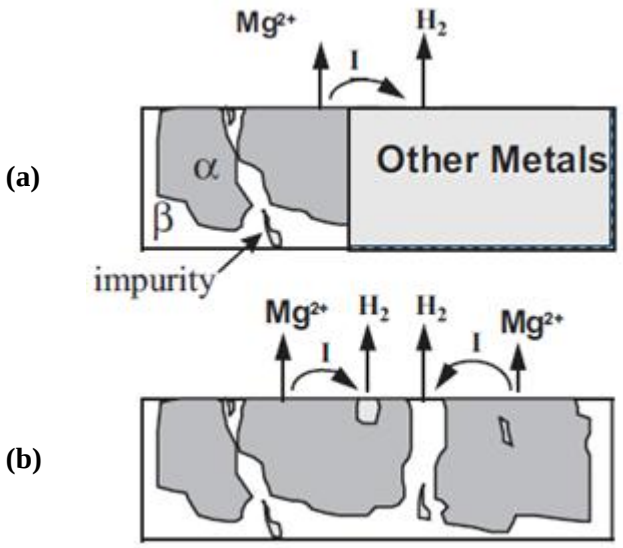

Figure 1.1 (a) External and **(b)** Internal galvanic corrosion in magnesium alloy [10].

1.2.2 Pitting corrosion

The presence of inhomogeneities due to coring and second phases within the alloy [15], and the breakdown of a passive layer on the alloy surface, leads to pitting corrosion in metals [16]. Corrosion pits in magnesium alloys occur adjacent to second phases such as $Al_{12}Mg_{17}$ and AlMn, because of the local breakdown of passivity and formation of an electrolytic cell between the cathodic second phases and the anodic magnesium matrix [17]. The mechanism of pitting corrosion in AM60 magnesium alloy is shown in Figure 1.2.

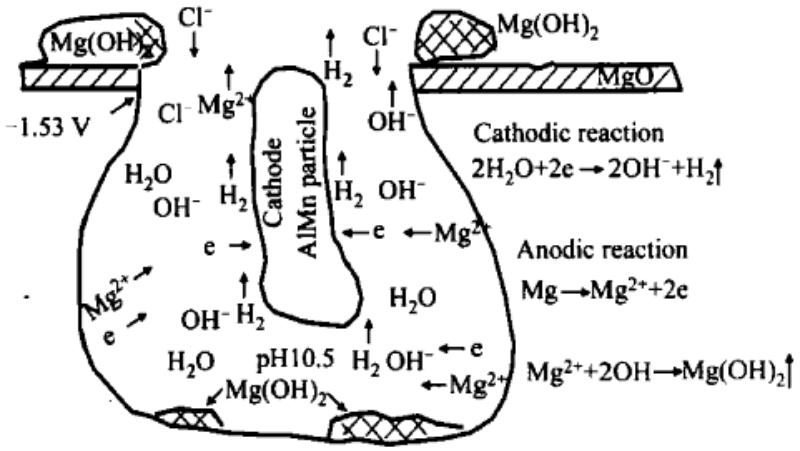

Figure 1.2 Mechanism of pitting corrosion in AM60 magnesium alloy [17].

The corrosion mechanism reactions in magnesium alloys lead to hydrogen evolution and the formation of magnesium hydroxide [10, 12, 13, 17-19];

Anodic reaction: $Mg \longrightarrow Mg^{2+} + 2e$ (A)

Cathodic reaction: $2H_2O + 2e \longrightarrow 2H_2 \uparrow + 2OH^-$ (B)

Complete reaction: $Mg^{2+} + 2H_2O \longrightarrow Mg(OH)_2 + 2H_2 \uparrow$ (C)

Evolution of hydrogen during dissolution of magnesium stems from two different reactions. One of them is due to the electrochemical reaction, which leading to formation of hydrogen in the cathodic reaction. The other one is the reaction between Mg^+ and water, which directly results in production of hydrogen. Hydrogen evolution is one of the procedures which could be used for measuring the corrosion performance of magnesium alloys by means of the amount of hydrogen evolved due to the exposure of magnesium alloy to an aqueous solution. In fact, the amount of measured hydrogen evolved during dissolution of the magnesium alloy is equivalent to the measured weight loss of the metal because the evolution of one mole hydrogen gas is equivalent to the dissolution of one mole of dissolved magnesium alloy in the corrosive solution [10, 12, 13, 17-19].

Huber [10, 12] and Fruhwirth et al. [20] stated that the magnesium hydroxide film is primarily magnesium oxide, which is quickly replaced by magnesium hydroxide with higher stability. In general, $Mg(OH)_2$ film is considered as a crystalline film, but Hanawalt stated that this film can be partly or fully amorphous [10, 12]. Non-crystalline films can provide higher protection against environments containing corrosive ions compared to the crystalline films, because they indicate higher ductility and higher resistance to breaking down [12].

1.2.3 Intergranular corrosion

In general, intergranular corrosion does not happen in magnesium alloys because most of the second phases precipitated along the grain boundaries are cathodic to the matrix. Hence, the grains will be anodic to the grain boundaries and areas adjacent to the grain boundaries corrode mostly and grain boundaries will be maintained intact [10, 12].

1.2.4 Crevice corrosion

Elimination of oxygen within a crevice, and the presence of a cathodic area outside the crevice with a high concentration of oxygen, can lead to the development of an anodic area within the crevice and consequently crevice corrosion. In fact, the difference in oxygen concentration between anodic and cathodic areas leads to crevice corrosion. Because there is no sensitivity to difference in oxygen concentration in the corrosion of magnesium, crevice corrosion does not appear in magnesium alloys [10, 12].

1.2.5 Filiform corrosion

This type of corrosion occurs under protective coatings. Hence, it is not common for uncoated magnesium alloys [10]. But filiform corrosion was observed for uncoated AZ91 (Mg - 9 wt% Al, 1 wt% Zn) alloy [10]. Also, Ghali et al. [19] observed this type of corrosion with an uncoated AZ31 alloy.

1.2.6 Stress corrosion cracking (SCC)

Stress corrosion cracking (SCC) occurs when both tensile loading and corrosive environments combine together and lead to cracking in materials [21]. Magnesium alloys have the susceptibility of SCC in chloride containing environments [22-25]. SCC can be found mostly in the form of transgranular corrosion in magnesium alloys, but precipitation of $Mg_{17}Al_{12}$ along the grain boundaries in Mg-Al-Zn alloys can lead to intergranular SCC [10, 12]. The possibility of SCC will increase in

magnesium alloys with higher mechanical strength [26]. Therefore, SCC is less common in cast alloys and mostly happens in wrought alloys in the location of twins [10, 12]. Orthopaedic implants such as pins and screws will be affected by tension and compression stresses in the body [26]. Also, brittle cracks associated with SCC stem from sharp contours, corrosion pits and micro-cracks [27]. Therefore, the possibility of SCC in orthopaedic implants made by magnesium alloys could be high, firstly, because of the sharp contours in temporary implants such as pins and screws and, secondly, because of the pitting corrosion which occurs easily in chloride solutions for magnesium alloys [5, 28, 29]. Stress corrosion cracking (SCC) is not only limited to magnesium alloys. Stress assisted failures for implant devices made by stainless steel and titanium alloys have also occurred [30-32]. The susceptibility of the magnesium alloys to stress corrosion cracking can be increased by the addition of alloying elements such as Al and Zn [10].

1.2.7 Corrosion fatigue

The mechanism of cracking in corrosion fatigue is the same with Stress Corrosion Cracking (SCC), but the loading stress in corrosion fatigue is cyclic whereas in SCC it is sustained [21]. Gu et al. [33] investigated the fatigue and corrosion fatigue behaviours of extruded WE43, (Mg - 4 wt% yttrium, 3 wt% RE) and die-cast AZ91D alloys in air and SBF (Simulated Body Fluid), respectively. They recorded a fatigue limit of 50 MPa at 10^7 cycles and 20 MPa at 10^6 cycles for die-cast AZ91D in air and SBF, respectively. In addition, a fatigue limit of 110 MPa at 10^7 cycles and 40 MPa at 10^7 cycles was recorded for extruded WE43 in air and SBF, respectively. Also, they observed that both alloys under cyclic loads had increased corrosion rate in SBF compared to an immersion test with no cyclic loading. They concluded that the corrosion fatigue cracks started from pits in SBF and micro-pores in air [33]. Furthermore, Bhuiyan et al. [34] reported a loss of fatigue strength in extruded AZ80-T5 magnesium alloy which was related to the formation of pits in corrosive environments.

1.3 Magnesium alloys in biomedical applications

The selection of alloying elements is important due to their effects on the corrosion and mechanical properties of the metal. For biomedical applications, other issues including toxicity and biocompatibility are very important [5]. Mostly magnesium is alloyed with Al, Rare Earth(RE) elements, Zr, Zn, Li and Mn for various engineering applications [19]. The most common magnesium alloying elements used for biomedical purposes are Al, Zn, Ca, Mn and RE elements (Table 1.2) [5].

Table 1.2 Common magnesium alloying elements used for biomedical applications [5].

Family	Representative alloys	Alloying elements (wt.%)			Main phases
Pure Mg	Mg [11]				Mg
Mg–Al–Zn	AZ31 [11,12]	3Al	1Zn		Mg; $Mg_{17}Al_{12}$
	AZ91 [11,13]	9Al	1Zn		
Mg–Ca	Mg–*x*Ca [11,14,15] (*x* = 1, 2, 3, 4, 5, …)	*x*Ca			Mg; Mg_2Ca
Mg–Zn–Ca	Mg–1Zn–1Ca [16]	1Zn	1Ca		Mg; Mg_2Ca; $Ca_2Mg_6Zn_3$
Mg–Zn–Mn–Ca	Mg–2.0Zn–1.2Mn–1Ca [17]	2Zn	1.2Mn	1 Ca	Mg; Mg_2Ca; $Ca_2Mg_6Zn_3$; $Ca_2Mg_5Zn_{13}$
Mg–Si–Ca		1Si	1Ca		Mg; Mg_2Si; SiMgCa
Mg–Zn	Mg–*x*Zn [11,13,18,19] (*x* = 1, 3 10)	*x*Zn			Mg; MgZn Mg_2Zn_3 Mg_7Zn_3
Mg–Zn–Mn	Mg–1Mn–1Zn [20]	1Mn	1Zn		Mg; MgZn Mg_2Zn_3 Mg_7Zn_3
Mg–Mn	Mg–1Mn [11]	1Mn			Mg; Mn
RE containing magnesium alloy	LAE442 [8,12]	4Li	4Al	2 RE	Mg; $Al_{11}RE_3$;
	WE43 [8]	4Y	3RE		Mg; $Mg_{12}YNd$; $Mg_{14}YNd_2$
	ZE41 [11,13]	4Zn	1RE		Mg; MgZn(RE)
	AE44 [11]	4Al	4RE		Mg; $Mg_{17}Al_{12}$; $Al_{11}RE_3$; $Al_{12}RE$
	Mg–*x*Gd [21] (*x* = 5, 10, 15, …)	*x*Gd			Mg; Mg_5Cd
	WZ21 [22]	2Y	1Zn		Mg; $MgYZn_3$; Mg_7Zn_3; Mg_3YZn_6
	Mg–8Y [23]	8Y			Mg; $Mg_{24}Y_5$ Mg_2Y

1.3.1 Magnesium alloys with aluminium (Al)

Addition of aluminium to pure magnesium not only can result in improved mechanical properties but also can improve the corrosion properties of the alloy [35]. However, an increase in aluminium content in Mg-Al-Zn alloys led to a reduction of corrosion performance in SBF [3] because an increase in aluminium content increases the formation of $Mg_{12}Al_{17}$ phase, which can lead to more tendency of pitting corrosion in the alloy [5].

There is a controversy concerning the use of Al in the body or not. It was reported that aluminium in larger amounts can damage the neuron cells [36] and osteoblasts [37]. Also, it may lead to Alzheimer's disease [36, 38]. In addition, aluminium can combine with inorganic phosphates and

reduce the amount of phosphate ions in the body, leading to dementia [1, 39]. Therefore, it is important to control the amount of aluminium ions released from magnesium alloys in the body [5].

1.3.2 Magnesium alloys with calcium (Ca)

Calcium (Ca) is capable of improving the mechanical properties of the magnesium alloys and it does not cause any harmful effects in the human body [7, 40].

According to Wu et al. [41], an addition of calcium of up to 1 wt.% to AZ91 magnesium alloy will refine the microstructure and results in improvement of mechanical properties, but an addition of more than 1 wt.% Ca reduces the mechanical properties of AZ91 magnesium alloy, due to the reticular formation of the second phase of Al_2Ca [41, 42].

Wan et al. [40] reported that Mg-0.6Ca alloy improved the compressive strength and bending strength of pure magnesium. Also, it was stated that the elastic modulus and bending strength of this alloy were close to the properties of human cortical bone. However, the effect of calcium on the corrosion performance of magnesium alloys is not very clear. Kannan and Raman [28] indicated that addition of calcium to AZ91 resulted in improved corrosion resistance in modified simulated body fluid.

Wan et al. [40] indicated that addition of 0.6 wt.% calcium to pure magnesium increases the corrosion resistance signigicantly. Zhou et al. [43] concluded that addition of calcium had no detrimental effect on the corrosion of AZ91 magnesium alloy. But G. Neite et al. [44] named calcium as an element with a detrimental effect on magnesium corrosion.

1.3.3 Magnesium alloys with manganese (Mn), zinc (Zn) and rare earth elements (RE)

Addition of Mn to magnesium alloys does not affect the mechanical properties, but improves their corrosion performance [5]. But it was reported that Mn can lead to neurotoxicity [35].

Zn improves the mechanical properties of the magnesium alloys and does not show any side effects on the human body [1, 5, 45]. Also, Zn increases the corrosion performance of the magnesium alloys [1, 39]. Mg-6Zn indicated good biocompatiblity *in vivo* and zinc release had no side effects on the liver,

kidney and heart. *In vitro* cytotoxicity tests showed that Mg-6Zn was suitable for cellular application. Also, Mg-6Zn led to increased corrosion resistance compared to pure magnesium in SBF [38].

Corrosion performance, mechanical properties and creep resistance of magnesium alloys can be improved by rare earth elements (RE) [5]. Rare earth elements have shown anti-carcinogenic effects, however, they have also shown cytotoxicity [5] and hepatotoxicity [46]. High amounts of yttrium (Y) have caused changes in some genes and the DNA of rats [5, 38, 47]. Therefore, rare earth elements are not considered safe for applications in the body [2, 39].

Despite the usage of Al and RE containing magnesium alloys for biomedical applications (Table 1.2), they do not appear to be a suitable choice for application in the body which is why efforts have been made to use magnesium alloys that do not contain Al and RE elements or any other harmful metals [38].

A remarkable biocompatibility was observed both *in vitro* and *in vivo* for Mg-Ca [7] and Mg-Mn-Zn [48] alloys and Song [39] named calcium, zinc and manganese containing magnesium alloys as appropriate alloys for biomedical applications. Furthermore, Mg–6Zn, Mg–1Ca and Mg-0.6 Ca alloys have been considered as appropriate magnesium alloys to be applied as biodegradable implants [7, 40, 45].

1.4 Role of microstructure in corrosion performance of magnesium alloys

1.4.1 Microstructure definition

The microstructure of magnesium alloys plays a significant role in their corrosion behaviour. The microstructure of an alloy comprises the phases present, their distribution throughout the alloy and the grain size [1, 3, 49-51].

1.4.2 The dual role of the second phase

Addition of aluminium to magnesium alloys in certain amounts leads to the formation of a second phase, $Mg_{17}Al_{12}$ (β phase) [49]. Although, the β phase has acted as a corrosion barrier in Mg-Al alloys

such as AZ alloys [10, 49, 52] but the β phase can also act as an active cathode and increase the corrosion rate of the AZ alloys [10, 49, 53]. Song et al. claimed that the β phase plays a dual role in the corrosion of AZ alloys, depending on its amount and distribution [49, 50, 52]. The β phase would act as an anodic barrier against corrosion if it is distributed finely and continuous (high volume fraction of β phase). Otherwise, the β phase would act as a galvanic cathode and accelerates the corrosion of the alloy (low volume fraction of β phase) [10, 13, 49, 50]. Song also indicated that increasing the Al content can result in higher β phase volume fraction and continuous distribution of the β phase within the alloy. He stated that in permanent mould cast of Mg-5%Al alloy, the β phase acts as a galvanic cathode owing to the low volume fraction and its discontinuous distribution (Figure 1.3 - a), whereas in permanent mould cast of Mg-10%Al alloy (Figure 1.3 - b), the β phase acts as an anodic barrier due to the high volume fraction of β phase and its continuous distribution [49].

(a)

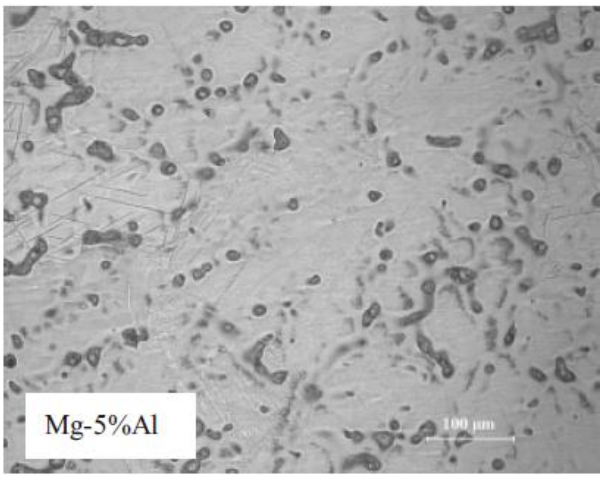

(b)

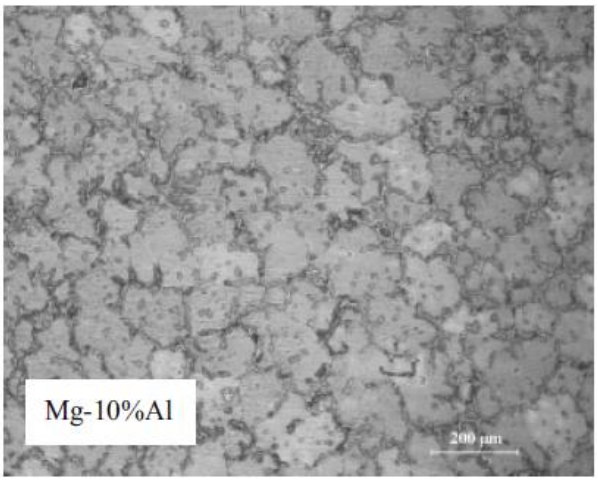

Figure 1.3 Distribution of β phase ($Mg_{17}Al_{12}$) in Mg-Al alloys**: (a)** Discontinuous distribution of β phase in Mg-5%Al **(b)** Continuous distribution of B phase in Mg-10%Al [49].

In addition, Song et al. showed that by increasing the distance from the skin to the interior of the specimen, the microstructure becomes coarser in the case of high pressure die-cast AZ91D (Figure 1.4) and the corrosion resistance decreases dramatically [50]. It was shown that the corrosion resistance of the skin with a high β phase ($Mg_{17} Al_{12}$) volume fraction and continuous distribution of β phase was 10 times more resistant than the interior of the specimen [49, 50].

(a)

(b)

(c)

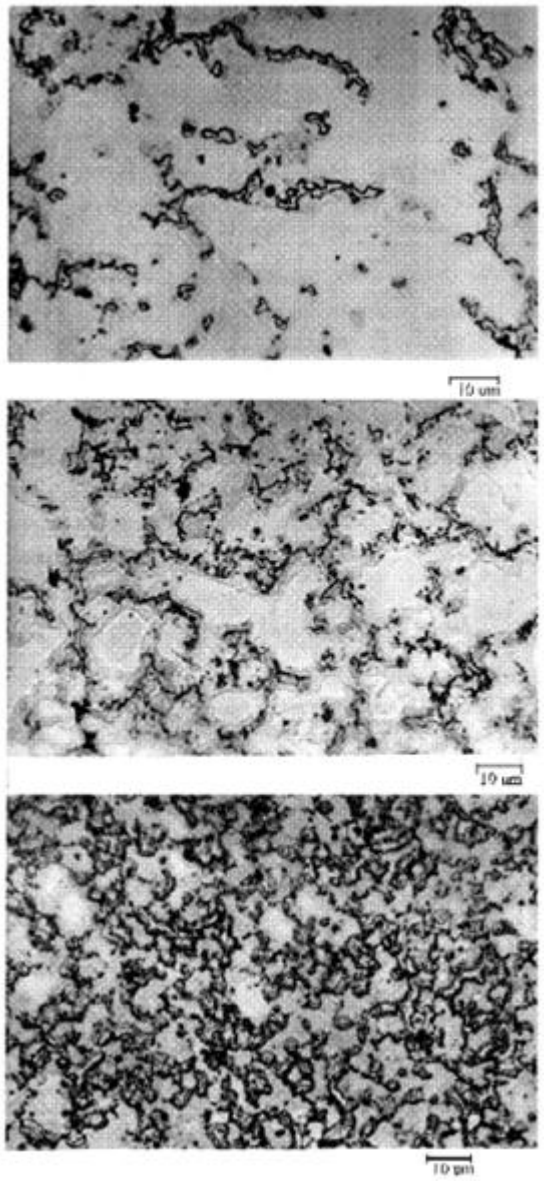

Figure 1.4 **(a)** centre area of AZ91D **(b)** edge area of AZ91D **(c)** skin of AZ91D [50].

1.4.3 Role of grain size

To some extent, the distribution of the second phase is associated with the grain size and grain refinement can lead to a more continuous distribution of the second phase and improve the corrosion performance of the alloy [49]. Song and StJohn [54] proved that refining the grains in MEZ alloy (Mg - Zn 0.5%, Mn 0.1%, Zr 0.1%, RE 2%) lead to a more fine and continuous distribution of the RE containing phase along the grain boundaries. This second continuous phase can inhibit the development of corrosion from the one grain to another.

Alvarez-Lopez et al. [1] studied the corrosion resistance of as-cast AZ31 magnesium alloys with different grain sizes in SBF. The results reported indicated a higher corrosion resistance for AZ31 magnesium alloys with the finest grain size. Ambat et al. [55] observed higher corrosion resistance for fine-grained die-cast AZ91D, compared to ingot cast AZ91D with a coarse grain size. Ballerini et al. [56] observed better corrosion performance in fine-grained die-cast AZ91 compared to sand-cast AZ91 with a coarse grain size. However, Ben-Haroush et al. [53] reported lower corrosion resistance for AZ80 magnesium alloys with finer grain size but the refined grains were obtained by hot extrusion not casting. Also, Kutniy et al. [57] refined the grain size of WE43 magnesium alloys by severe plastic deformation and the corrosion behaviour of the alloy was reduced. But Hong-fei et al. [58] observed higher corrosion resistance for refined grains obtained in extruded-drawn alloy, for a high purity of magnesium (99.95% purity).

1.5 Manufacturing process and its effect on the microstructure and corrosion performance of magnesium alloys

1.5.1 Casting

Casting is the most common manufacturing process to produce magnesium alloys, particularly when a high rate of production is required [50, 53]. Among the various casting methods, die-casting (HPDC) is the most common due to a high rate of production with a high quality produced economically [49, 50]. In spite of the application of die-cast magnesium alloys in some structural parts such as

automobile wheels, non-load bearing applications such as frames for electronics equipment have been the most widely used area for die-cast magnesium alloys [50]. AZ91D is one of the most widely used magnesium alloys and is capable of being applied in various temperature environments [49, 50]. For example, AZ91D has been considered as a promising alloy to be applied in powertrains, where the temperature is between 160 -200 °C [49]. But Kannan claimed that sand-cast AZ91 might be a better choice compared to die-cast AZ91 for biodegradable implants [8]. The solidification rate is high in die-casting and leads to higher fraction of β phase ($Mg_{17}Al_{12}$) [8, 50]. Hence, the dissolution of the grains in the die-cast alloy is faster compared to the coarse sand-cast alloy, which may lead to quick loss of mechanical properties in the die-cast alloy. On the other hand, the stability of β phase (Mg_{17} Al_{12}) is high in SBF. Therefore, the die-cast alloy may not be an appropriate choice for biodegradable implants owing to the presence of a high volume fraction of β phase (Mg_{17} Al_{12}) and its stability in SBF [8].

1.5.1.1 Porosity in casting

In general, casting results in the formation of pores in the specimen. The method of casting, the casting design and composition of the alloys determine the amount and form of porosity [30]. In most of the HPDC cast plates a non -uniformity can be observed in the appearance of the plates [49]. For example, figure 1.5–a shows the left side of the plate (HPDC AZ91D plate) is darker than the right side. After immersion of the plate in 5 wt % of NaCl solution for 4 hours (Figure 1.5-b), the results indicated that the corrosion was more severe in the dark areas. SEM examination showed many small pores in the dark areas, which were interconnected (Figure 1.6-a) and distributed under the surface of the plate (Figure 1.6-b). Fewer small pores were found in the bright areas, which were not interconnected (Figure 1.6-c) and distributed shallowly just beneath the surface (Figure 1.6-d). The pores in the dark areas, which formed mostly along the grain boundaries and next to the β phase ($Mg_{17}Al_{12}$), led to a reduction in the continuous distribution of the β phase and easier development of corrosion from grain to grain. But few pores in the bright areas, which also were found along the grain boundaries and next to the β phase, were not able to destroy the continuity of the β phase along the grain boundaries and

deteriorate the corrosion performance. Therefore, the effect of porosity on the intermetallics distribution can affect the corrosion performance of magnesium alloys [49].

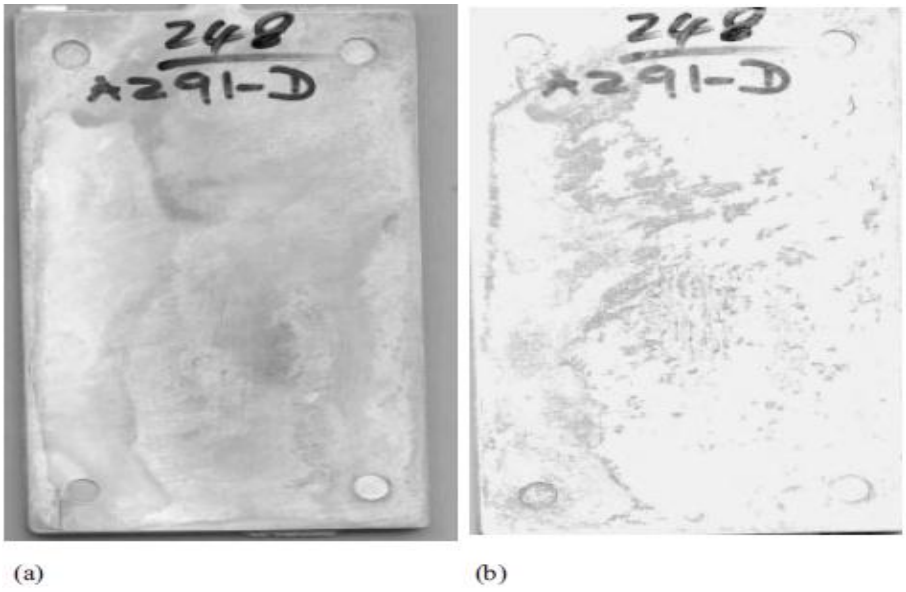

Figure 1.5 HPDC AZ91D plate **(a)** before immersion in 5 %wt NaCl **(b)** after immersion in 5 %wt NaCl for 4 hours [49].

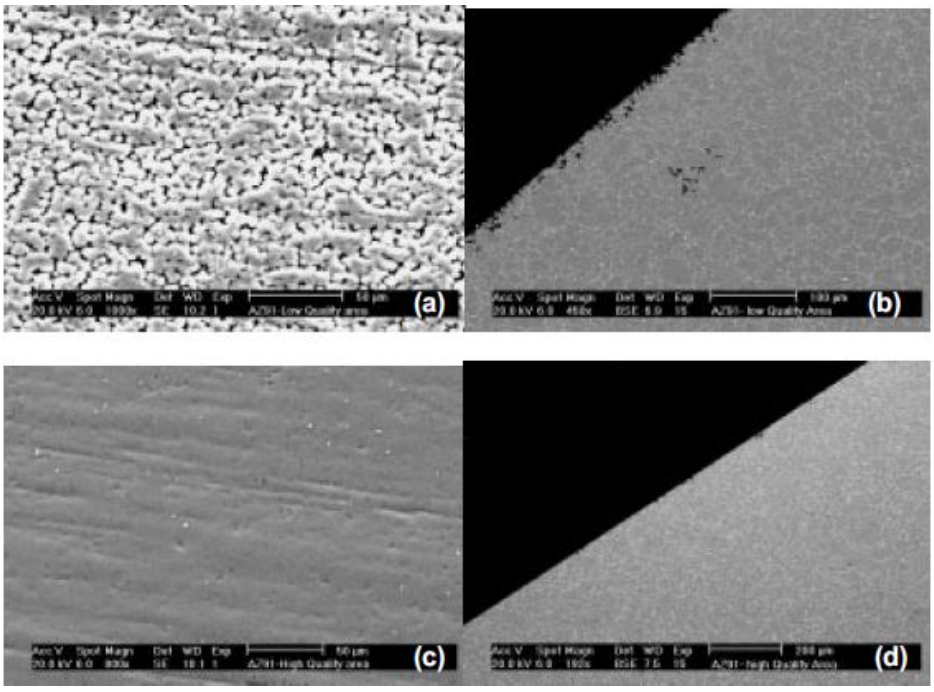

Figure 1.6 SEM micrograph of surface and cross section of dark and bright areas for HPDC AZ91D before corrosion**: (a)** surface of dark area **(b)** cross section of dark area **(c)** surface of bright area **(d)** cross section of bright area [49].

1.5.1.2 Solidification in casting

1.5.1.2.1 Solidification and second phase fraction

The solidification rate plays a role in determining the fraction of second phase formed because of segregation. In AZ91D, with an increase in distance from the surface, the microstructure becomes coarser and the β phase ($Mg_{17}Al_{12}$) fraction reduces. With increasing distance from the surface the solidification rate is reduced and consequently the β fraction is reduced and leads to less continuous distribution of the β phase along the grain boundaries. Hence, the galvanic accelerating role of β phase emerges. This suggests an improvement in the corrosion properties of magnesium alloys with increase in solidification rate can be obtained [50].

1.5.1.2.2 Solidification and grain size

The solidification rate has an important role in determining the grain size of the alloy. A rapid solidification rate leads to a finer grain size and a more continuous distribution of the β phase ($Mg_{17}Al_{12}$) and improves the corrosion performance of the magnesium alloy. In AZ91D, with increase in distance from the surface the grain size is increased and the β phase distribution becomes less continuous. Therefore, more severe corrosion occurs in the interior of the specimen [50].

1.5.1.2.3 Solidification and porosity

In AZ91D, a greater density of pores was observed in the interior of the specimen compared to the skin because of the slower solidification rate in the interior of the specimen. The presence of more porosity in the interior makes the area of exposure larger and damages the continuity of the β phase ($Mg_{17}Al_{12}$) and leading to a greater corrosion rate in the interior of the alloy. Rapid solidification, which causes finer and less porosity in the alloy, is more beneficial for the corrosion performance of magnesium alloys [49, 50].

1.5.2 Plastic Deformation

Application of cast magnesium alloys is superior to wrought magnesium alloys produced by extrusion, forging or rolling, but the wrought alloy products are still used in various applications. In recent years, the automotive industry has shown interest in the potential application of wrought magnesium alloys [11]. Most of the casting defects including porosity and inclusions are eliminated in wrought magnesium alloys and leads to improved mechanical properties compared to as-cast alloys. Remarkable grain refinement and strengthening can be obtained by plastic deformation, and plastically deformed alloys have superior mechanical properties. Therefore, wrought magnesium alloys have been paid much more attention in recent years [59-62].

However, there are limited numbers of slip systems in magnesium due to their hexagonal structure which cause difficulties to deform magnesium at room temperature. However, an increase in the number of slip systems at elevated temperatures increases the deform ability of magnesium alloys [53, 59, 62].

Kutniy et al. [57] studied the effect of severe plastic deformation on corrosion behaviour of WE43 magnesium alloy, and found it reduced corrosion performance. Ben-Haroush et al. [53] investigated the effect of hot extrusion on corrosion performance of AZ80 alloy. The as-cast AZ80 was extruded at 250°C, 300°C and 350°C in order to observe the differences in microstructure in these alloys, and how the microstructure was capable of affecting the corrosion performance of this alloy. The corrosion resistance of the alloys after extrusion decreased dramatically owing to the rearrangements of the second phases, caused by dynamic recrystallization during thermo-mechanical processing. Also, an increase in extrusion temperature during recrystallization resulted in increased grain size and more second phase rearrangements in the alloys. Hence, a less continuous distribution of the β phase ($Mg_{17}Al_{12}$) at higher extrusion temperatures occurred and caused a more severe corrosion rate in the alloy [53].

CHAPTER 2: Materials and Methods

2.1 Preparation of samples

The samples were classified into 5 different types; cast commercial pure magnesium ingot (A), more quickly solidified cast commercial pure magnesium (B), more slowly solidified cast commercial pure magnesium (C), extruded commercial pure magnesium (D) and extruded super pure magnesium (E).

Cast commercial pure magnesium ingot samples (A) were cut from ingots of commercial purity magnesium (> 99.5 wt% Mg) in a rectangular form, with dimensions 20x10x8 mm. In order to make the B and C types of samples, the same ingots of commercial purity magnesium were melted in a mild steel crucible in an induction furnace to a temperature of about 725^{o} C and cast into a rectangular plate die of dimensions 320x100x15 mm.

Two different solidification rates were used to prepare more quickly solidified cast (B) and more slowly solidified cast (C) types of samples by using two dies with two different temperatures. One of the dies was maintained at room temperature, and the other preheated to 700 ^{o} C in a resistance – heated furnace. The samples were cut from the plates with the dimensions 20x10x8 mm, as before.

In order to make the extruded commercial pure magnesium samples (D), an extruded rod of commercial purity magnesium (> 99.5 wt% Mg), with dimensions 25.4 mm diameter, was obtained from Magnesium Elektron (Manchester, UK). Samples were cut with the same dimensions 20x10x8 mm from this bar. In addition, extruded super pure magnesium samples (E) were cut from an extruded rod of super purity magnesium (99.95 wt% Mg; 0.02% Al, 0.02% Mn, 0.01 Si). The dimensions of the extruded rod of super purity magnesium were also 25.4 mm diameter, and it was obtained from GoodFellow (Cambridge, UK).

The samples were ground with SiC papers of grade 1200 and 2500 grit in order to remove any scratches remaining from the machining stage and to provide a reproducible surface. Each sample was then cleaned ultrasonically with ethanol for 10 minutes and dried in air.

2.2 Weight loss measurement and immersion test

Weight loss measurements were conducted in immersion tests, in order to investigate the degradation behaviour of magnesium *in vitro*. Simulated Body Fluid (SBF) was chosen as the *in vitro* environment, and was made following the method of Kokubo [63]. The list below is the chemicals used in 750 ml deionized water to prepare 1000 ml of SBF;

1) 7.996 g/l NaCl, ACS reagent, ≥ 99.5%.

2) 0.350 g/l $NaHCO_3$, ACS reagent, 99.7 – 100.3 %.

3) 0.224 g/l KCl, puriss. p.a., ≥ 99.5%.

4) 0.228 g/l $K_2HPO_4.3H_2O$, Reagent plus, ≥ 99.0%.

5) 0.305 g/l $MgCl_2.6H_2O$, purum p.a., ≥ 98%.

6) 40 cm^3 of 1 $Kmol/m^3$ HCl.

7) 0.278 g/l $CaCl_2$, ≥ 95%.

8) 0.071 g/l Na_2SO_4, Reagent plus, ≥ 99.0%.

9) 6.057 g/l $(CH_2OH)_3CNH_2$, Ultra pure Grade, ≥ 99.9%.

10) Appropriate amount of 1 $Kmol/m^3$ HCl in order to adjust the pH.

All chemicals were obtained from Sigma-Aldrich (Dorset, UK). The samples were suspended within the solution and the ratio of solution volume to sample surface area was about 1 mL/mm^2, following ASTM G31-72 [64]. Samples were placed in SBF with a pH of 7.4, maintained at a constant temperature of 37 ^{o}C in a water bath, and the sample weight was measured at different time intervals (after 6, 12, 24, 72, 120, 192, 264, 336, 408, 480 hour immersion). Prior to weighing, the samples

were washed with deionised water and dried in air. A summary of experimental method can be observed in figure 2.1. The number of repeated experiments for each type of sample was 5 and 25 experiments conducted in total.

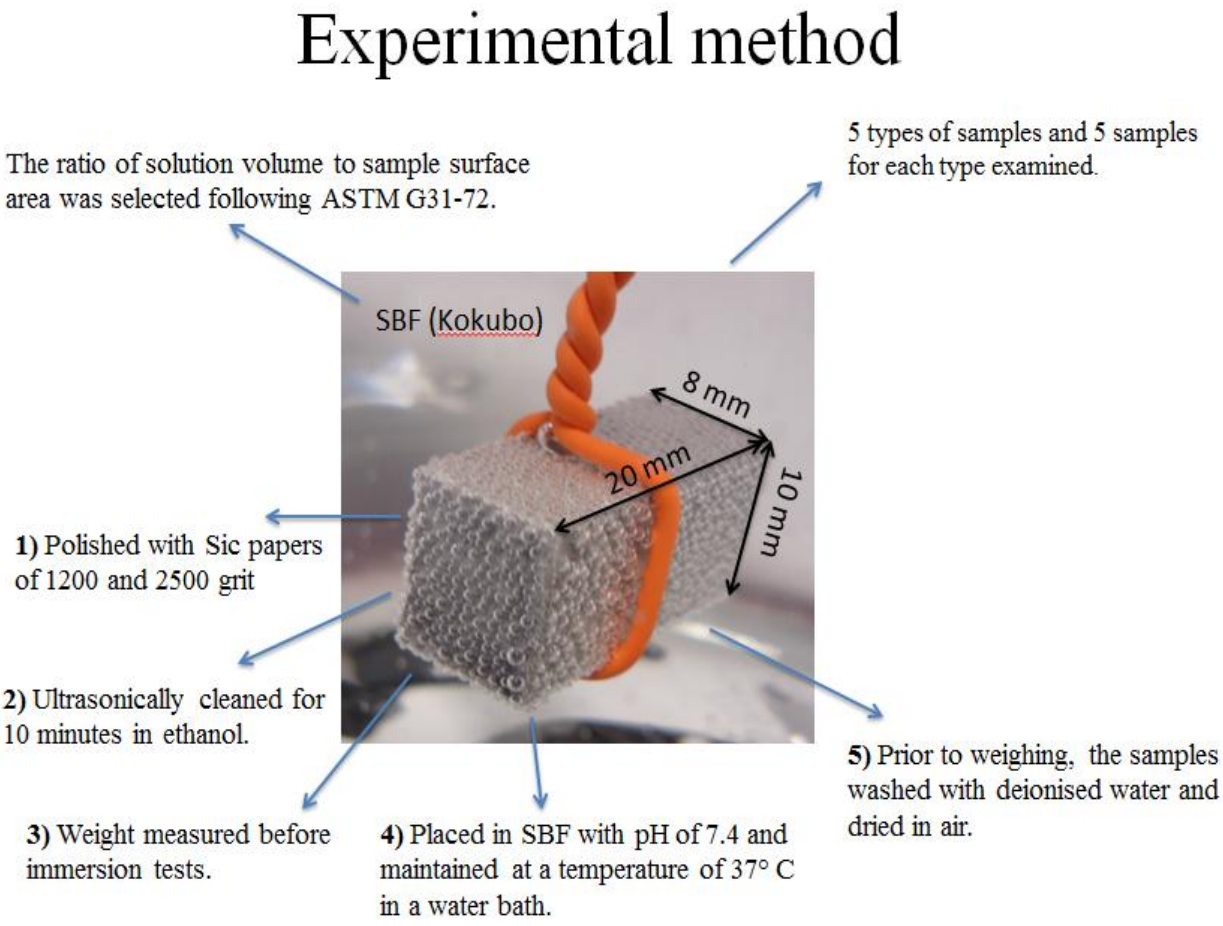

Figure 2.1 A summary of experimental method for doing immersion tests.

2.3 Measurement of pH value and magnesium ion release during corrosion in SBF

In addition to measuring the weight loss of the samples, changes in pH values were also recorded at various time intervals (after 6, 12, 24, 72, 120, 192, 264, 336, 408, 480 hour immersion). The pH meter was calibrated with buffer solutions before measuring the pH value of each solution at every time interval. Also, 5 ml of the solution of each immersed sample was taken at the various time intervals in order to measure the release of magnesium ions for each sample at every time interval. The release of magnesium ions (mg L^{-1}) was measured using a Dionex ICS-1100 ion chromatograph.

2.4 Characterization of materials using SEM, EDX and XRD

Scanning Electron Microscopy (SEM) analysis was conducted on the surface of samples after holding for different time intervals, using a JEOL 6060 SEM. A lower magnification was used in order to observe the difference in the surface morphology of each type of sample during corrosion, and to have a comparison between the surface morphology of each type of sample. A higher magnification was used in order to investigate the corrosion byproducts and their surface morphology.

In addition, SEM (Scanning Electron Microscopy) analysis was conducted on the etched surface of various pure magnesium alloy samples in order to observe the microstructure of the samples, including their grain structure, intermetallic content and distribution. Each type of sample was mounted and ground with SiC papers of 1200, 2500, 4000 grit and then polished to 0.25 μm. After polishing the samples, they were immersed in an etchant of 10 ml acetic acid and 80 ml deionized water for about 1minute at room temperature, as described in the ASM Metals Handbook [65], till the grain structure was revealed.

In addition to SEM analysis, Energy Dispersive X-ray spectroscopy (EDX) was used in order to determine the chemical composition of intermetallics and corrosion byproducts.

X-ray Diffraction (XRD) was used to detect the presence of different phases on the surface of each type of sample. XRD was conducted on the surface of each sample before and after immersion in SBF at the various time intervals, using an X-Ray Diffractometer D5005 (BRUKER Corporation). In order to scan the surface of each sample, the beam angle was adjusted to be between 10 to 85 º and the step size was 0.0147457 º. The total scan time for every test was 13 minutes.

In addition, Glancing Angling XRD was conducted on the surface of extruded super pure magnesium in order to find out more about the corrosion products formed on the surface of this sample type.

CHAPTER 3: Results

3.1 Weight loss measurements during corrosion in SBF

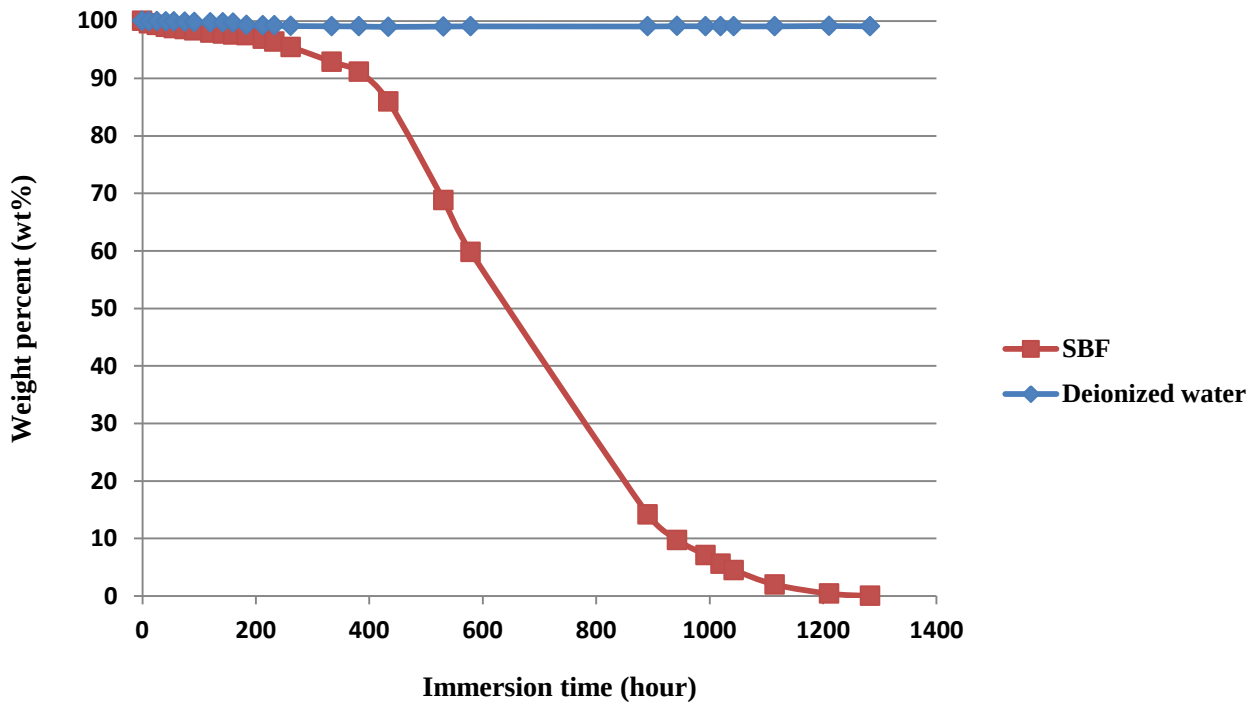

Figure 3.1 Weight percentage of cast commercial pure magnesium immersed in SBF and deionized water for 1283 hours.

In the first experiment, the cast commercial pure magnesium ingot samples were immersed in both SBF and deionized water to observe the difference in degradation in both solutions (Figure 3.1). No remarkable weight loss in deionized water was observed, whereas the sample immersed in SBF was completely degraded after 1283 hour immersion, which is about 8 weeks. According to these results, deionized water did not show the capability of being used as a representative medium for corrosion test. Furthermore, although, alloying is the most common method of modifying the corrosion performance of magnesium and can lead to improved mechanical and corrosion properties in the alloy [2-7] but it was chosen to work on magnesium in pure form to try to control the degradation behaviour of biodegradable magnesium component. Since, on the one hand, alloying means the release of ions of

the alloying element during corrosion which might lead to side effects in the body [1, 5, 35-39, 46, 47]. Also, the elements such as Calcium ,which did not show any side effects in the body and improved the mechanical properties of the magnesium alloys [7, 40], caused different corrosion behaviours in the magnesium alloys [28, 40, 43, 44].On the other hand, the total degradation time for the cast commercial pure magnesium sample immersed in SBF was about 8 weeks and close to the 12-18 weeks desirable for degradation of magnesium in the human body [1, 4]. Therefore, improved corrosion performance of magnesium by working on the pure magnesium alloys instead of alloying became the main purpose of this research.

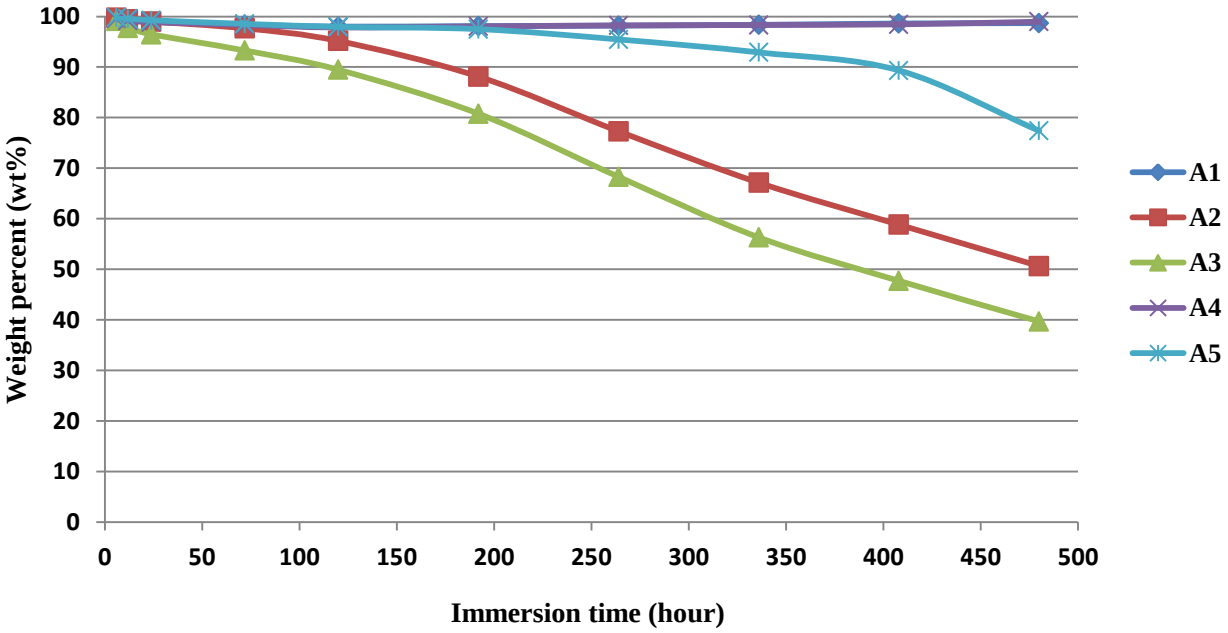

Figure 3.2 Weight percentage of cast commercial pure magnesium ingot samples (A_1 to A_5) during 480 hour immersion in SBF.

In figure 3.2, the difference in degradation behaviour of 5 samples of cast commercial pure magnesium ingot (A_1 to A_5) at various time intervals is shown. Weight loss was observed in all samples during 480 hour immersion in SBF. A_1 and A_4 indicated very similar degradation behaviour during the 480 hour immersion. A_5 showed similar degradation behaviour to A_1 and A_4 in the first 192

hours of immersion but its weight loss became more severe after 192 hours. The results in figure 3.2 showed a poor reproducibility for this type of sample.

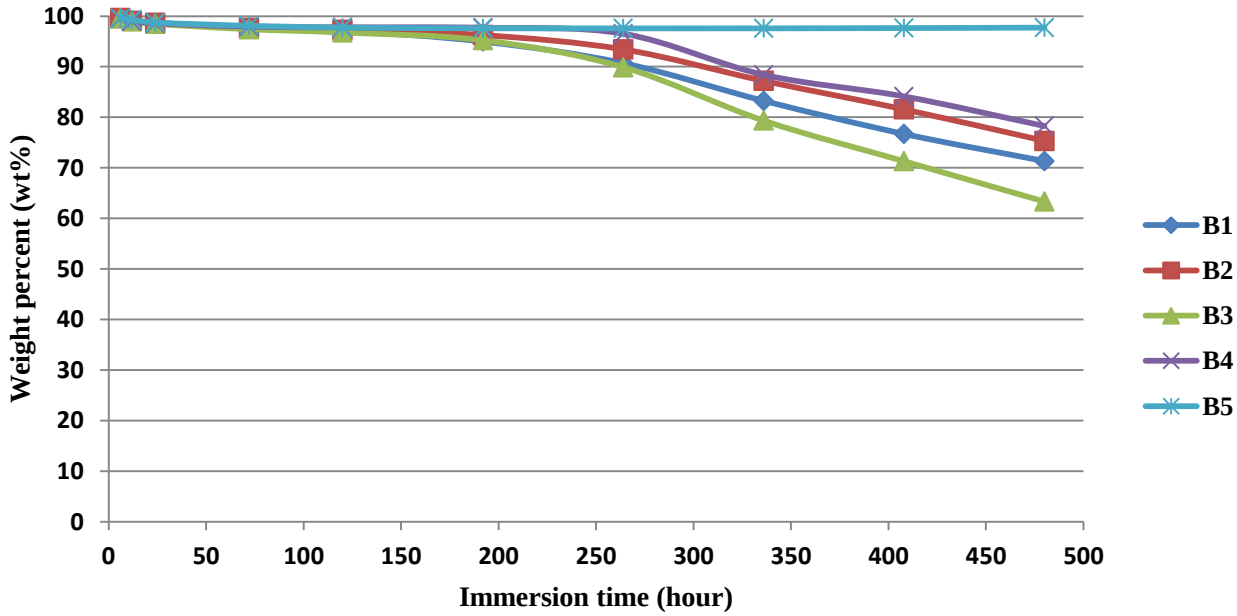

Figure 3.3 Weight percentage of more quickly solidified cast commercial pure magnesium samples (B_1 to B_5) during 480 hour immersion in SBF.

In figure 3.3, the difference in degradation behaviour of 5 identical samples of more quickly solidified cast commercial pure magnesium (B_1 to B_5) at various time intervals is shown. The degradation behaviour of B_1 to B_5 was very similar in the first 192 hour immersion in SBF, but their weight loss varied after this. B_5 had the lowest weight loss among all the samples during 480 hour immersion in SBF. The results also showed a poor reproducibility for this type of sample.

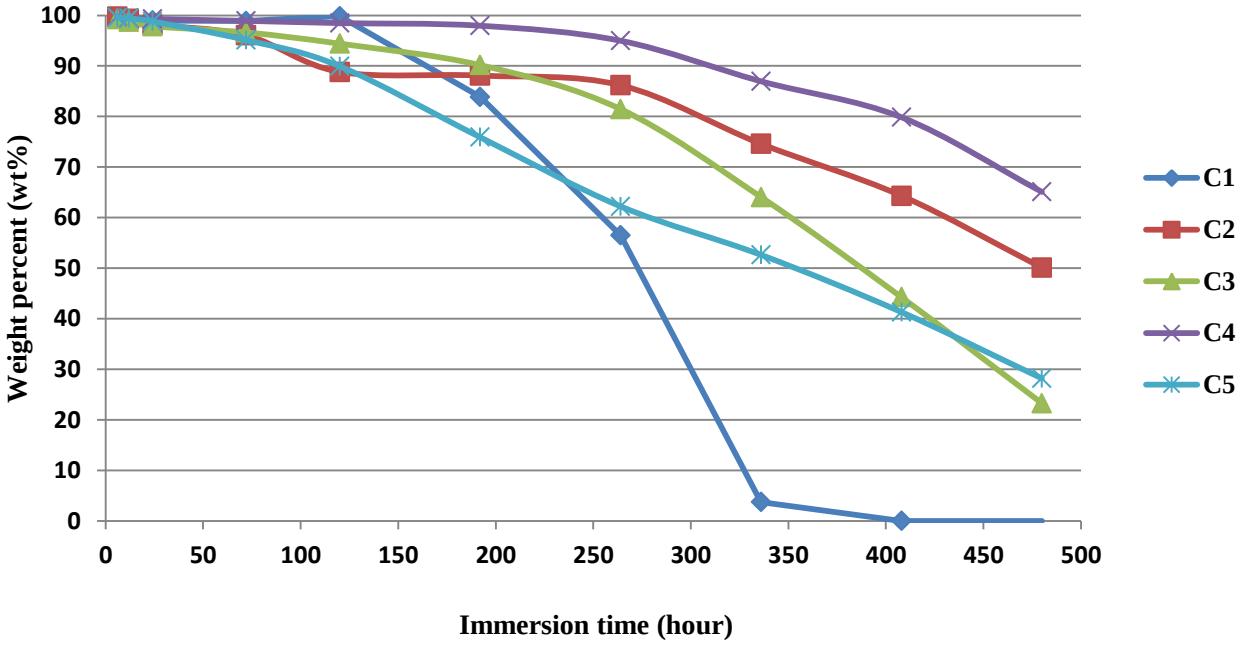

Figure 3.4 Weight percentage of more slowly solidified cast commercial pure magnesium samples (C_1 to C_5) during 480 hour immersion in SBF.

In figure 3.4, the difference in degradation behaviour of 5 samples of the more slowly solidified cast commercial pure magnesium (C_1 to C_5) at various time intervals can be observed. In the first 24 hour immersion all the 5 samples indicated almost similar degradation behaviour, whereas, after 24 hour immersion their degradation behaviour started to change completely. A rapid reduction of weight in sample C_1 occurred after 120 hour immersion, and it completely degraded after 408 hour immersion in SBF. The results therefore again showed a poor reproducibility for this type of sample.

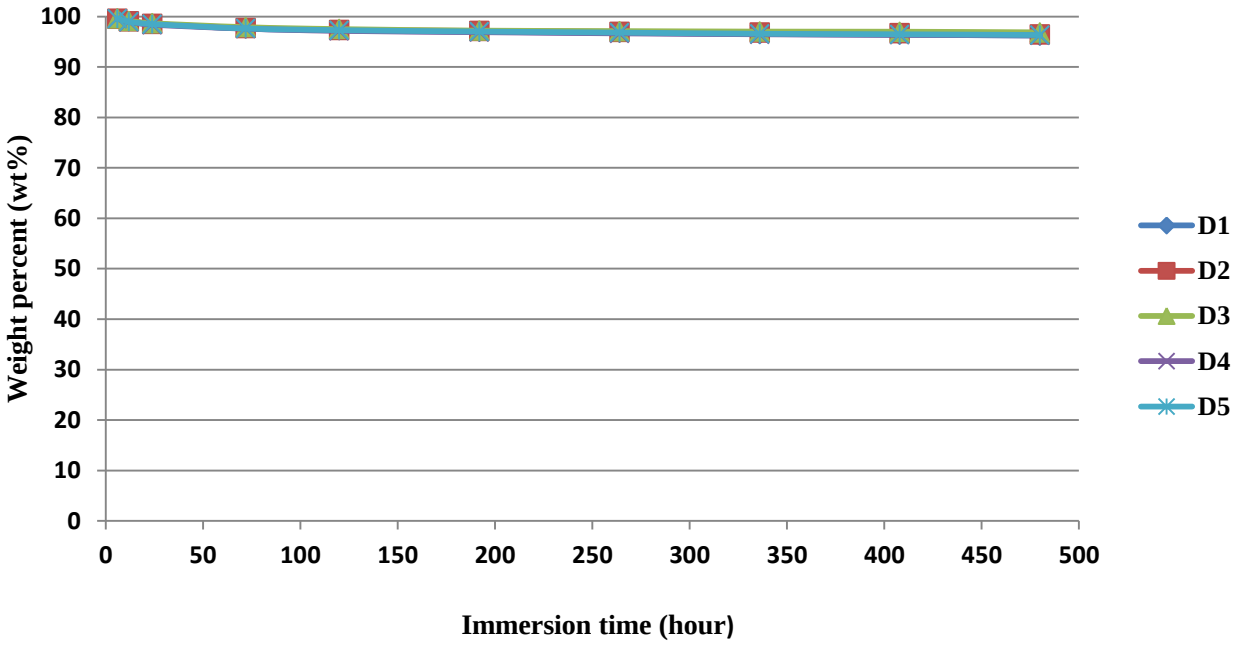

Figure 3.5 Weight percentage of extruded commercial pure magnesium samples (D_1 to D_5) during 480 hour immersion in SBF.

In figure 3.5, the difference in degradation behaviour of 5 samples of extruded commercial pure magnesium (D_1 to D_5) for various time intervals is shown. A similarity was observed in the degradation behaviour of all the samples at different time intervals during 480 hour immersion in SBF. The results showed a high reproducibility for this type of sample.

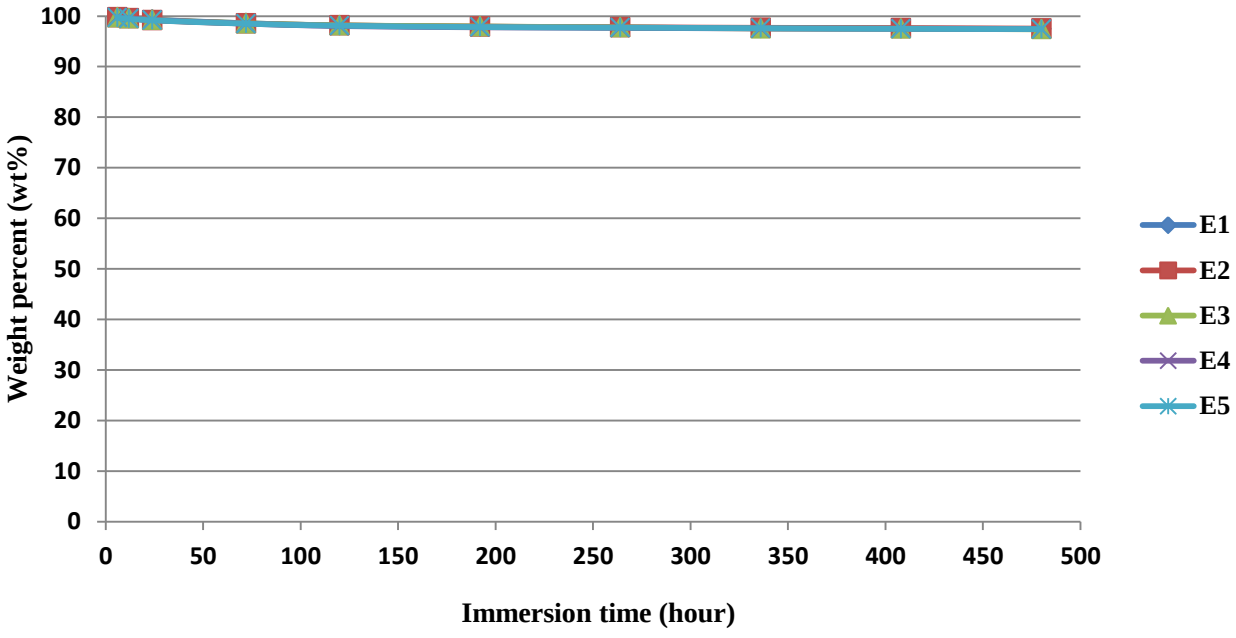

Figure 3.6 Weight percentage of extruded super pure magnesium samples (E_1 to E_5) during 480 hour immersion in SBF.

In figure 3.6, the difference in degradation behaviour of 5 samples of extruded super pure magnesium (E_1 to E_5) at various time intervals can be observed. There was again a similarity which was in the degradation behaviour of samples. This type of sample, also, indicated a high reproducibility, similar to the extruded commercial pure magnesium samples (D).

(a)

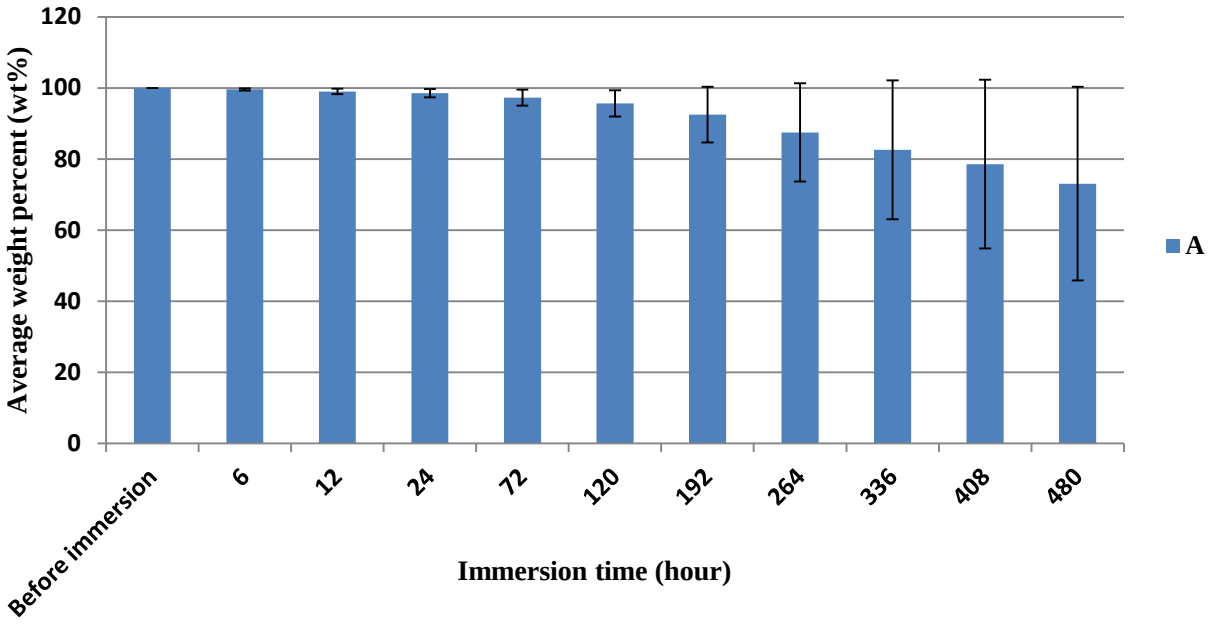

(b)

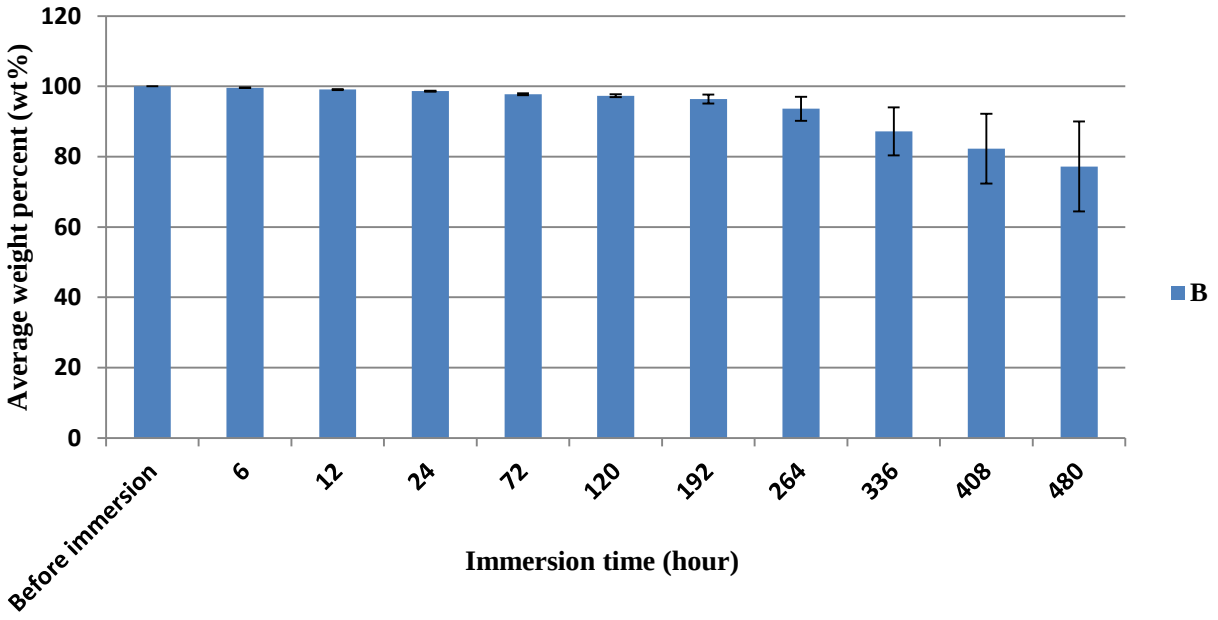

(c)

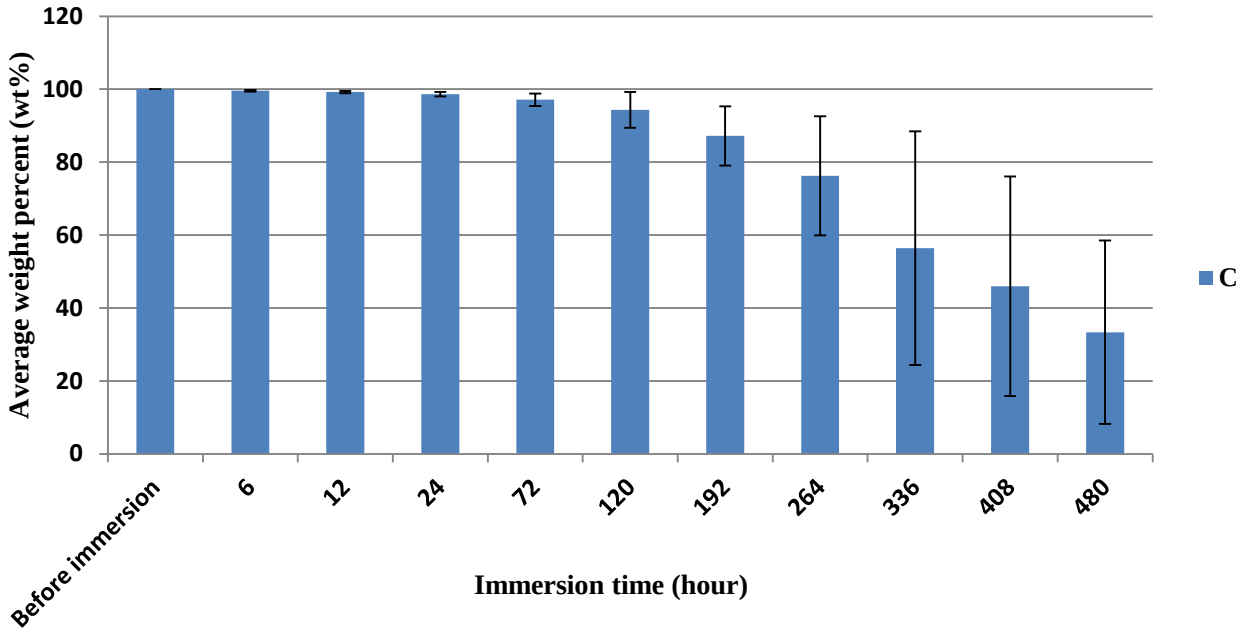
120
100
80
60
40
20
0
Average weight percent (wt%)
Before immersion
6
12
24
72
120
192
264
336
408
480
Immersion time (hour)
C

(d)

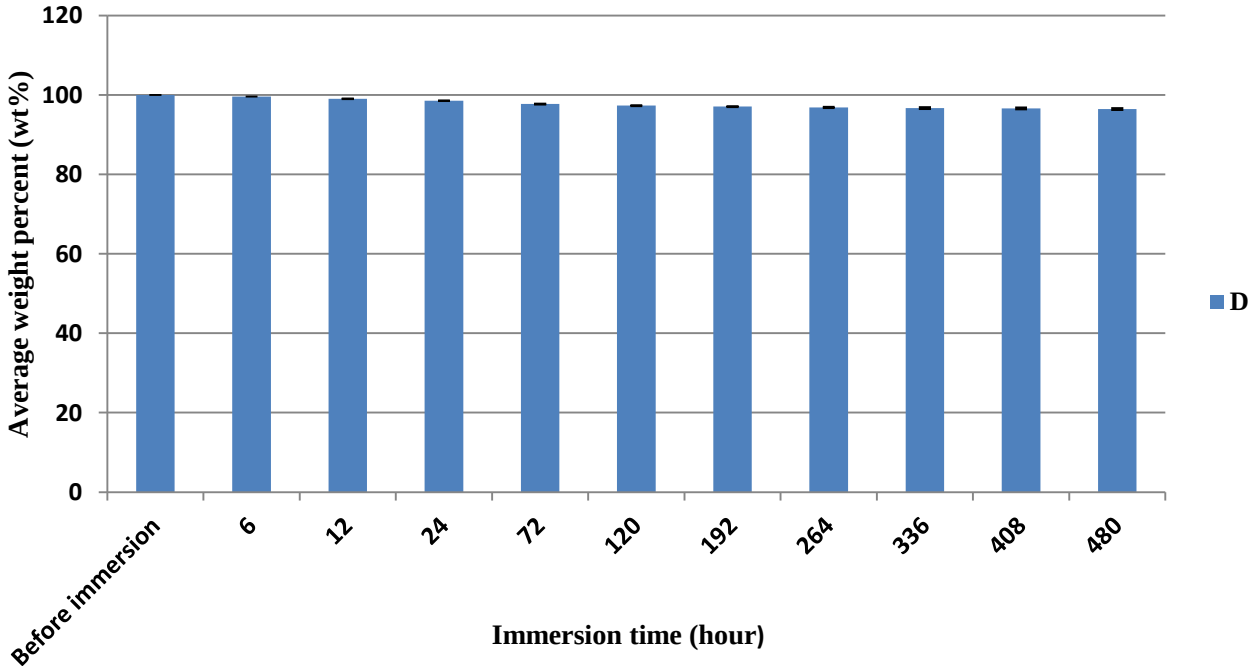
120
100
80
60
40
20
0
Average weight percent (wt%)
Before immersion
6
12
24
72
120
192
264
336
408
480
Immersion time (hour)
D

(e)

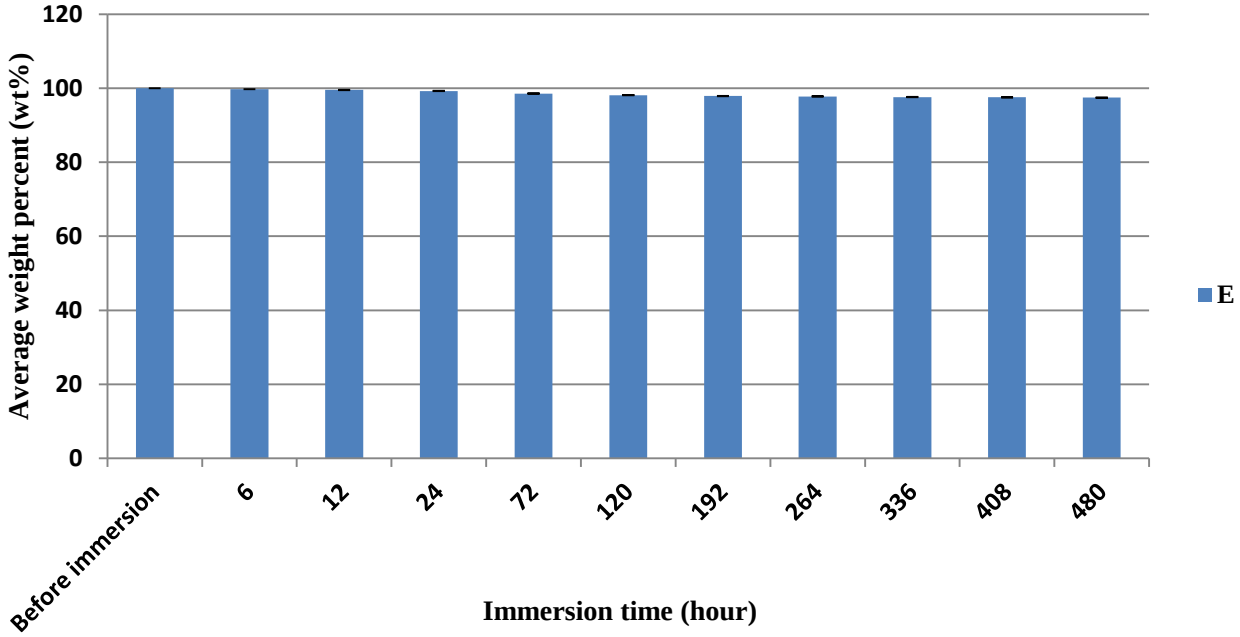

Figure 3.7 Average weight percentage of different types of samples **(a)** cast commercial pure magnesium ingot (A) **(b)** more quickly solidified cast commercial pure magnesium (B) **(c)** more slow solidified cast commercial pure magnesium (C) **(d)** extruded commercial pure magnesium (D) **(e)** extruded super pure magnesium (E).

The reproducibility of the different samples (A, B, C, D and E) is shown in figure 3.7 at different time intervals during 480 hour immersion in SBF. Each error bar indicates the standard deviation value of 5 samples tested for each type (A, B, C, D and E) at specific time intervals. The extruded samples (D and E) showed a higher reproducibility compared to the cast samples (A, B and C). In addition, the more quickly solidified cast sample (B) indicated the highest reproducibility among all the cast types of samples (A, B and C). The presence of high error bars for cast samples (A, B and C) originates from very diverse corrosion behaviours of 5 samples tested for each type (A, B and C) during immersion in SBF. This is mostly related to the manufacturing process of these samples and the presence of casting defects which will be explained in detail later on. Table 3.1 shows the standard deviation values of various types of samples during 480 hour immersion in SBF.

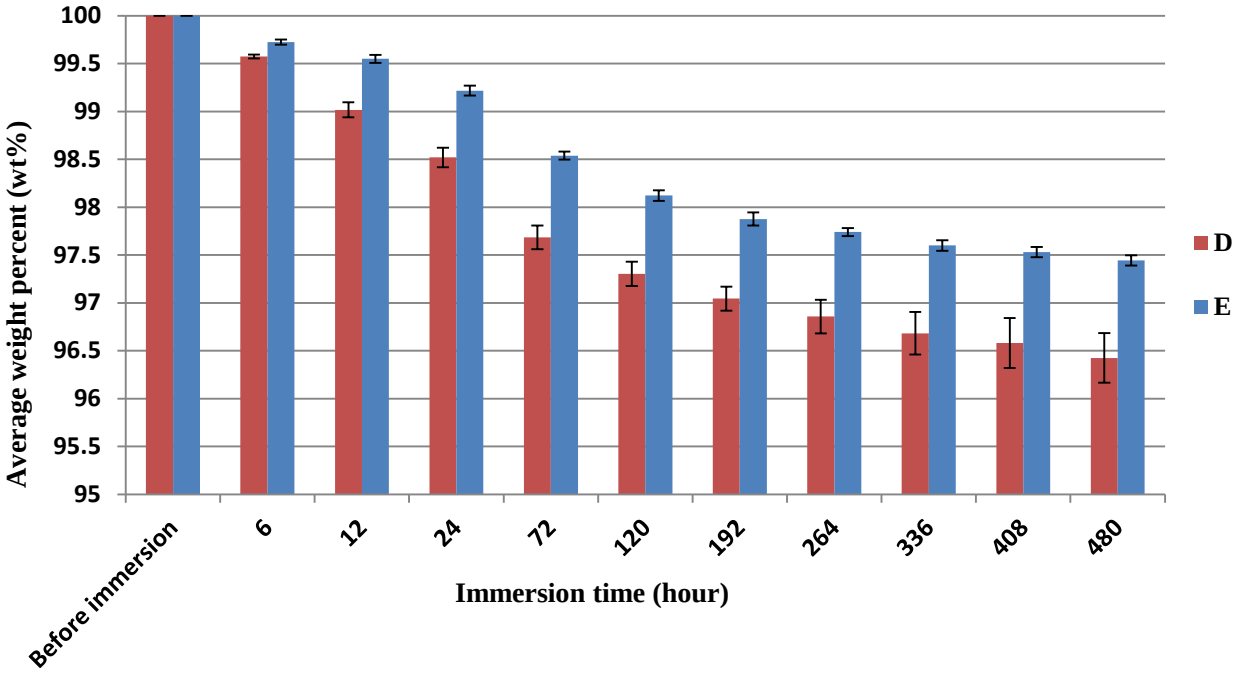

Figure 3.8 Average weight percentage of extruded commercial pure magnesium (D) and extruded super pure magnesium (E) from 95 to 100 (wt%) during 480 hour immersion in SBF .

Figure 3.8 shows more reproducibility for extruded super pure magnesium (E) than commercial purity (D).

Table 3.1 Standard deviation values (wt%) of various types of samples (A, B, C, D and E) during 480 hour immersion in SBF.

Time(h) / Sample	6	12	24	72	120	192	264	336	408	480
A	0.28	0.74	1.15	2.24	3.68	7.81	13.85	19.57	23.74	27.22
B	0.03	0.12	0.10	0.27	0.44	1.28	3.41	6.83	9.89	12.77
C	0.21	0.30	0.59	1.71	4.92	8.12	16.31	32.06	30.09	25.14
D	0.02	0.080	0.10	0.12	0.13	0.12	0.17	0.22	0.26	0.26
E	0.02	0.04	0.05	0.04	0.05	0.07	0.04	0.05	0.05	0.05

The reproducibility of samples: E > D > B > A > C

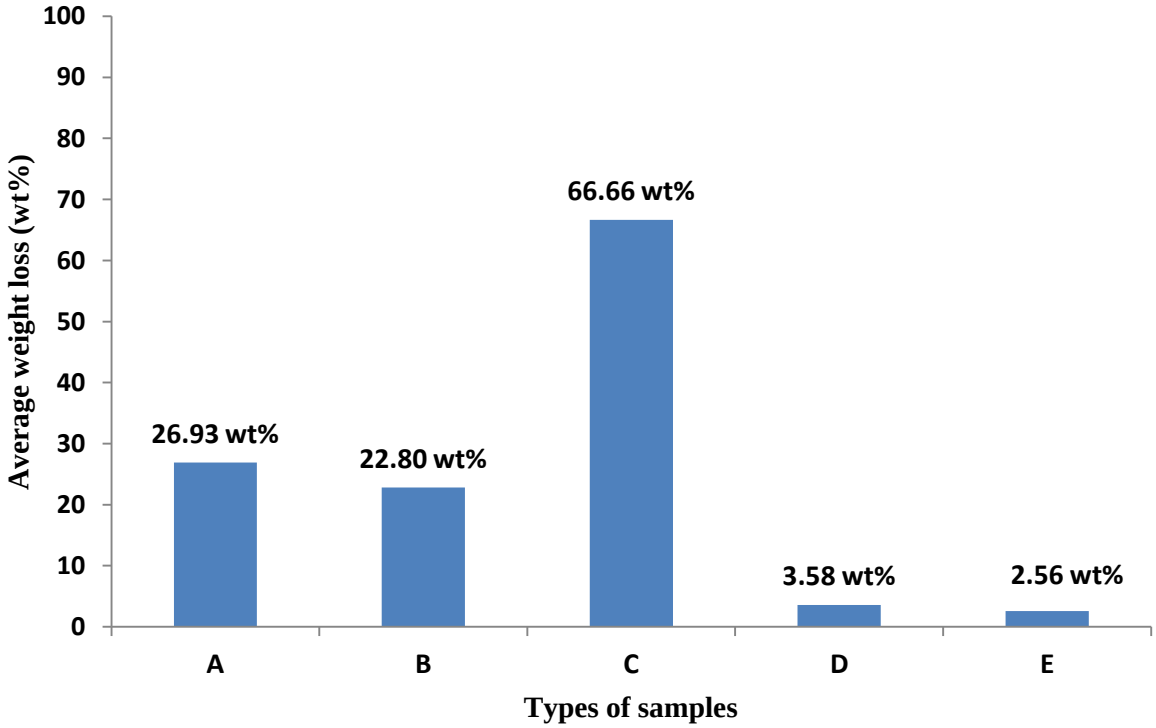

Figure 3.9 Average weight loss of cast commercial pure magnesium ingot (A), more quickly solidified cast commercial pure magnesium (B), more slowly solidified cast commercial pure magnesium (C), extruded commercial pure magnesium (D) and extruded super pure magnesium (E) after 480 hour immersion in SBF.

In figure 3.9, the average weight loss of the various types of samples (A, B, C, D and E) after 480 hour immersion in SBF shown. The weight loss of extruded samples (E and D) was about 7 to 20 times lower, compared to the cast samples (A, B and C), which indicated a higher corrosion resistance for the extruded samples. The extruded super pure magnesium (E) indicated the lowest weight loss of about 2.56 wt%, whereas, more slowly solidified cast commercial pure magnesium (C) showed the highest weight loss of about 66.66 wt%, after 480 hour immersion in SBF. More quickly solidified cast commercial pure magnesium (B) had the lowest weight loss among the cast samples (A, B and C).

Weight loss of samples: E < D < B < A < C

Corrosion resistance: E > D > B > A > C

3.1.1 An increase in weight with increased immersion time

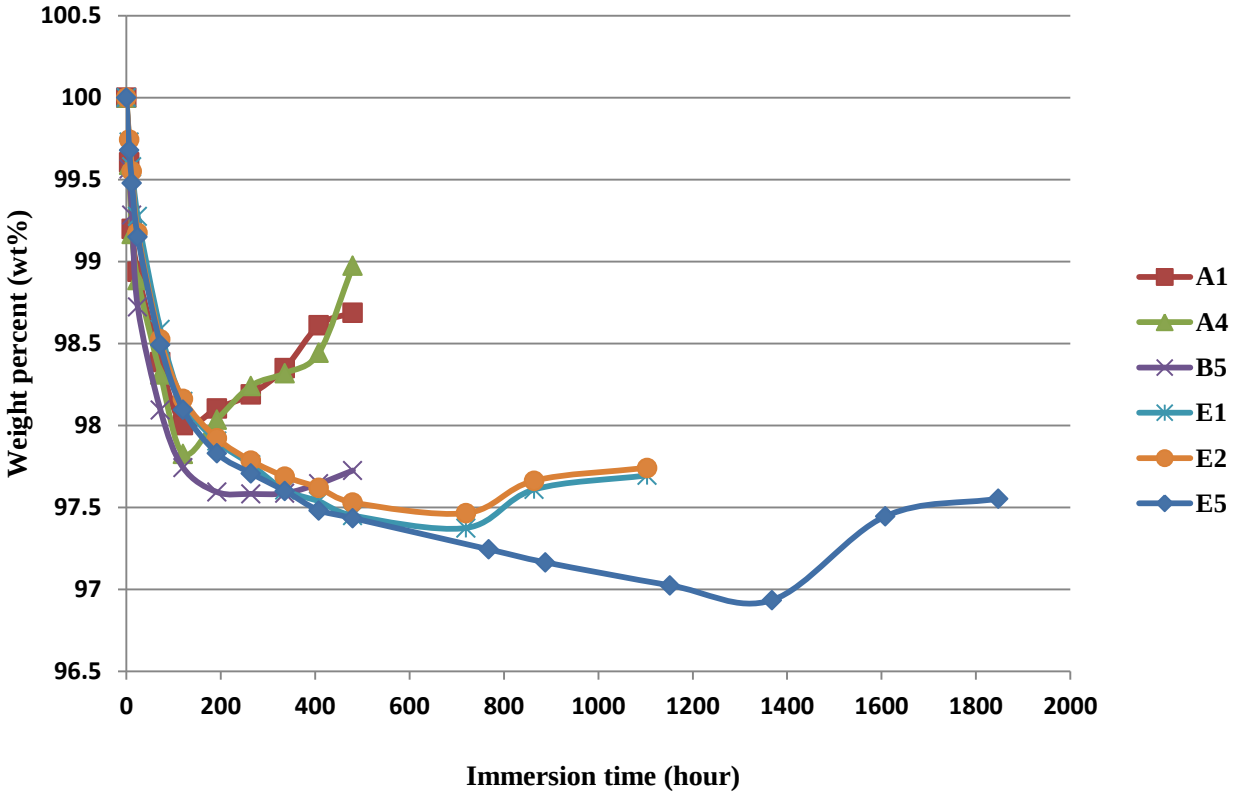

Figure 3.10 Weight percentage of cast commercial pure magnesium ingot (A_1 and A_4), more quickly solidified cast commercial pure magnesium (B5) and extruded super pure magnesium (E_1, E_2 and E_5) during immersion in SBF.

Increase in immersion time resulted in an increase in weight for some samples, such as A_1 and A_4, after 120 hour immersion in SBF, which was abnormal (Figure 3.10). Also, such behaviour was observed for one of the more quickly solidified cast commercial pure magnesium samples (B_5) after 336 hour immersion in SBF (Figure 3.10). But, such behaviour (an increase in weight with increased immersion time) did not happen for extruded super pure samples (E_1, E_2 and E_5) during 480 hour immersion in SBF. However, when the immersion time for 3 samples of extruded super pure magnesium (E_1, E_2 and E_5) increased to more than 480 hours, an incease in weight was observed (Figure 3.10). The weight of both E_1 and E_2 started to increase after 720 hour immersion in SBF and the weight of E_5 started to rise after 1368 hour immersion in SBF.

3.2 Results of pH measurements

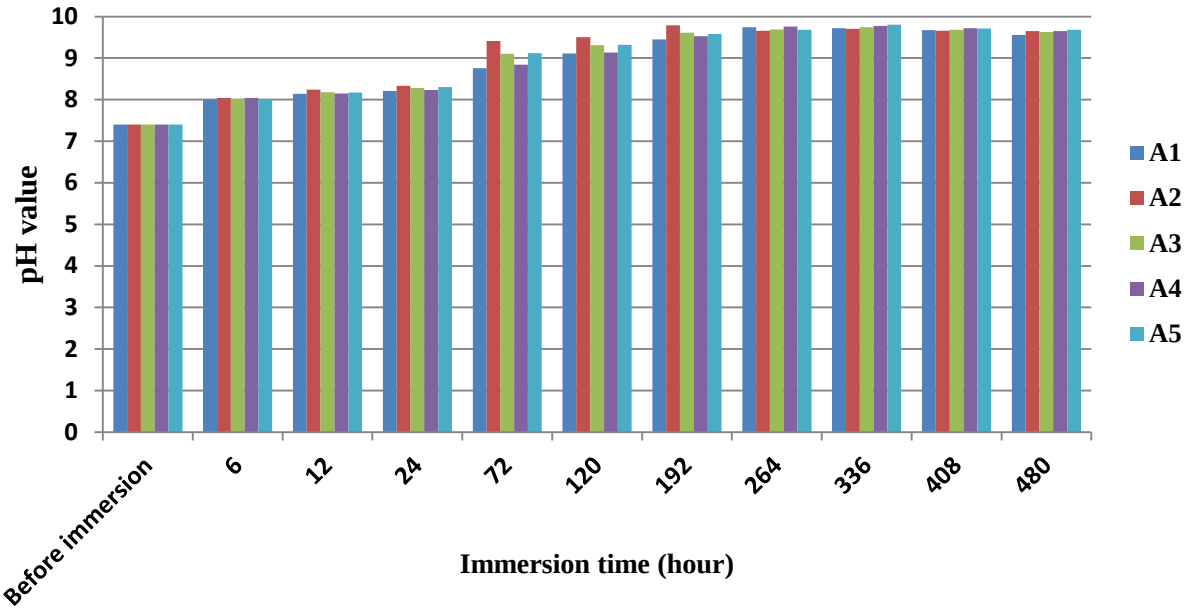

Figure 3.11 pH values of cast commercial pure magnesium ingot samples (A_1 to A_5) during 480 hour immersion in SBF.

In the cast commercial pure magnesium ingot samples (A_1 to A_5) increase in pH with increased immersion time occurred during the first 336 hour immersion in SBF followed by a reduction and then a stable pH occurred after 336 hour immersion (Figure 3.11). The pH value for A_2, A_3 and A_5 went above 9 at 72 hours immersion, whereas, for A_1 and A_4 this happened at 120 hour immersion. It was reported that the magnesium hydroxide film, which forms on the surface of corroded magnesium, becomes more protective above pH value of 9 [10, 12]. Therefore, it can reduce the corrosion rate of the specimen.

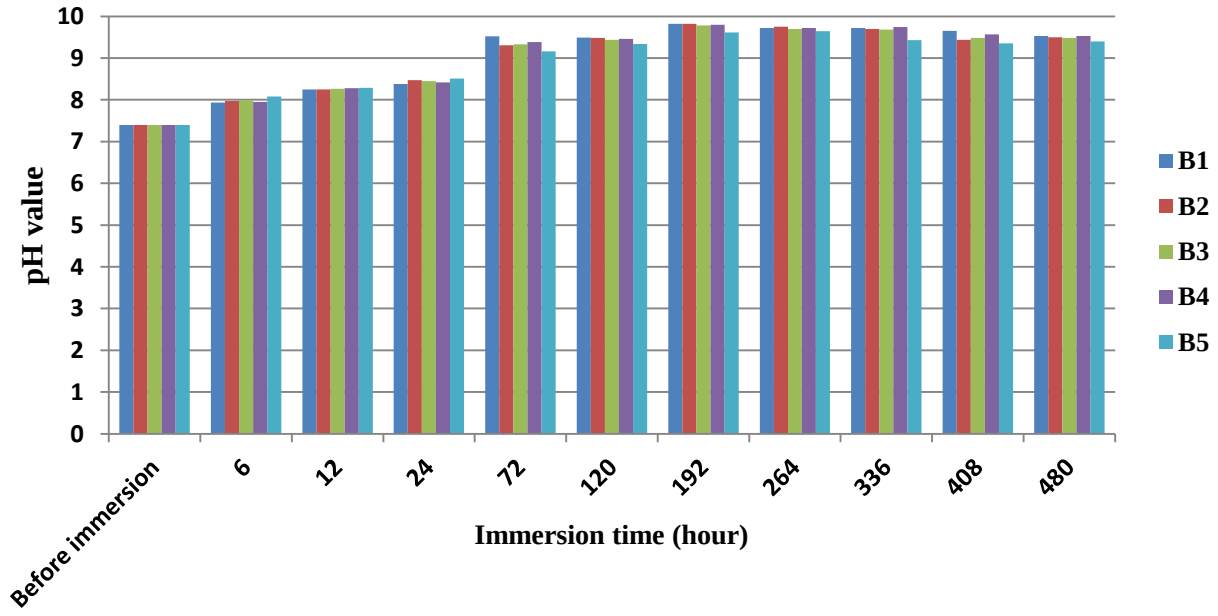

Figure 3.12 pH values of more quickly solidified cast commercial pure magnesium samples (B_1 to B_5) during 480 hour immersion in SBF.

Figure 3.12 indicates that the behaviour of pH changes in the more quickly solidified cast commercial pure magnesium (B_1 to B_5) is almost similar to the behaviour of pH changes in A samples (A_1 to A_5). The pH value of the samples increased with increased immersion time and afterwards started to fall and reached to an approximate stability. The increase in pH for the samples continued up to 192 hour immersion and then reduction and stability of pH happened. The pH value of all the samples went above 9 at 72 hour immersion.

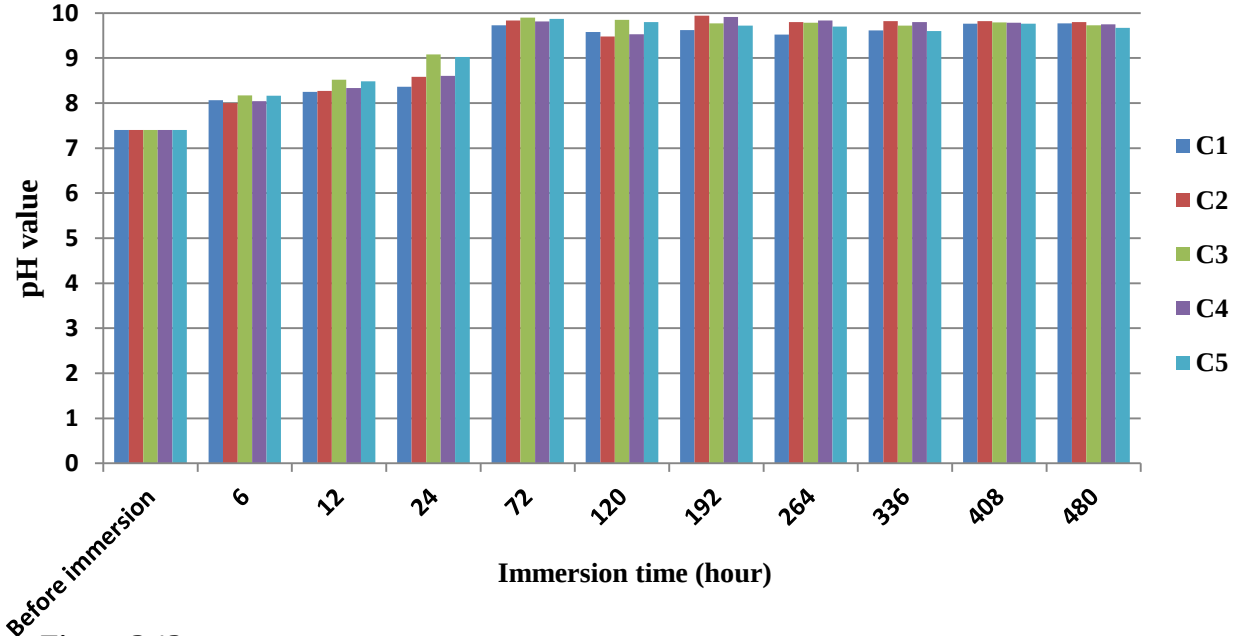

Figure 3.13 pH values of more slowly solidified cast commercial pure magnesium samples (C_1 to C_5) during 480 hour immersion in SBF.

Figure 3.13 showed that the increase in pH and then reduction and approximate stability in pH values happened for the more slowly solidified cast commercial pure magnesium samples (C_1 to C_5), same as A and B types of samples. But there is a fluctuation in the behaviour of this type of sample, which was not visible for other types of samples (A, B, D and E). After increase in pH values of samples, which occurred up to 72 hour immersion, and reduction of pH value after 72 hour immersion, a second increase in pH value happened in all the samples except C_5 and then the pH value of the samples stabilized roughly till the end. Increase of pH value to more than 9 for all the samples happened at 72 hour immersion except C_3, which occurred at 24 hour immersion in SBF. Also, the increase of pH value from 24 to 72 hours was severe in all the samples.

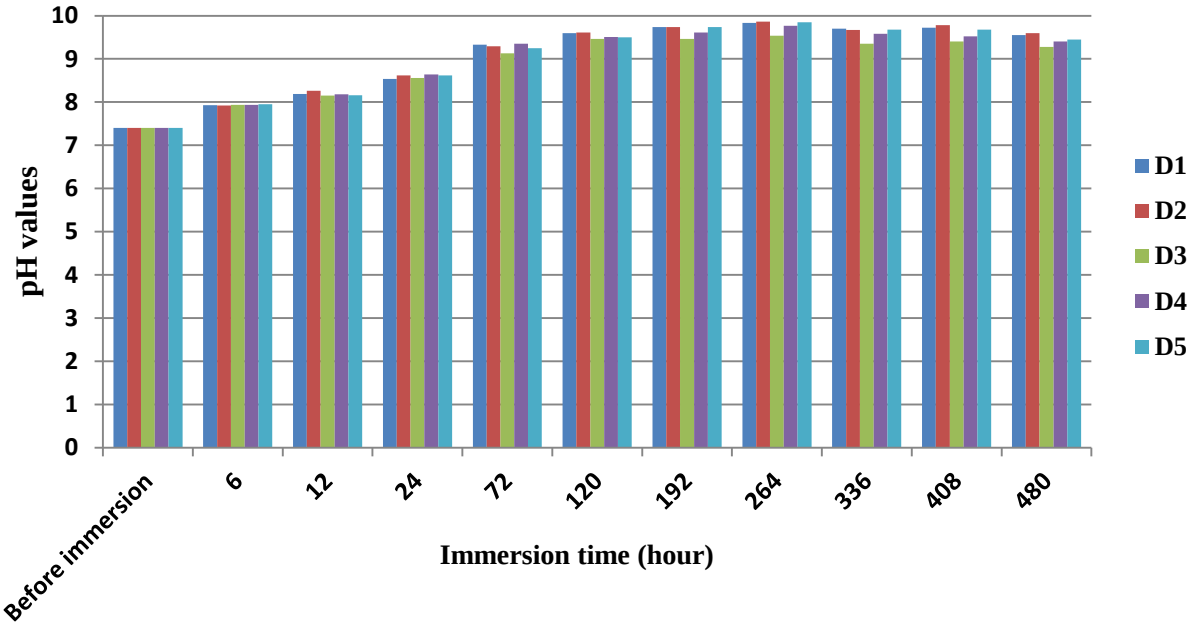

Figure 3.14 pH values of extruded commercial pure magnesium samples (D_1 to D_5) during 480 hour immersion in SBF.

Figure 3.14 indicated that the increase in pH and then reduction and approximate stability in pH values happened for the extruded commercial pure magnesium samples, the same as A, B and C types of samples. The pH values increased up to 264 hour immersion and then started to decrease and stabilize after 264 hour immersion. The pH values went above 9 at 72 hour immersion in SBF.

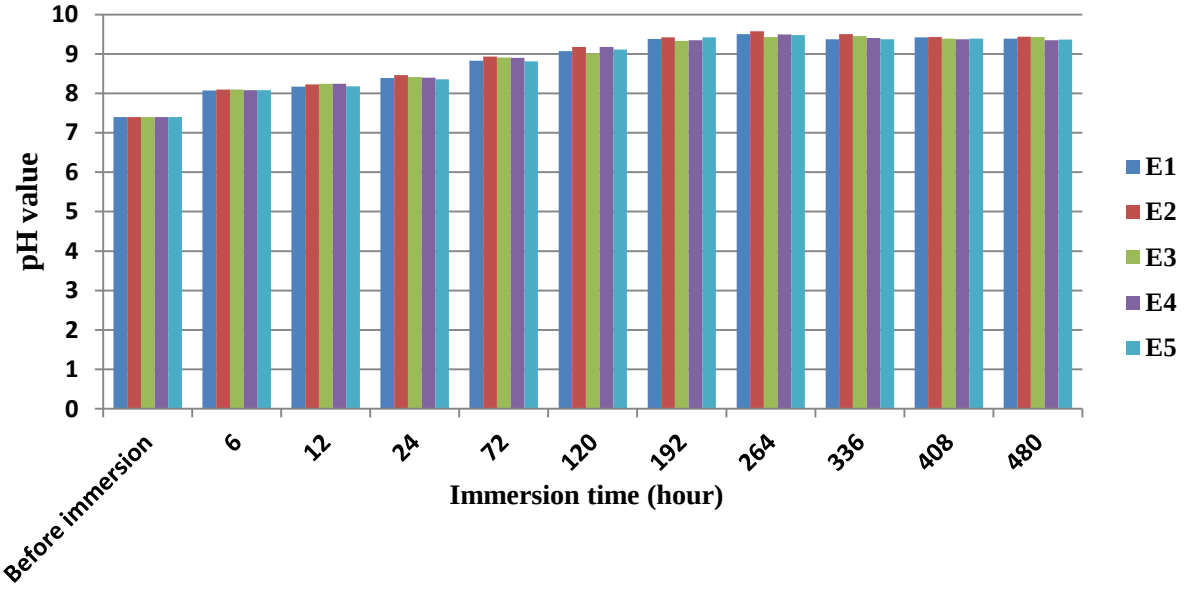

Figure 3.15 pH values of extruded super pure magnesium samples (E_1 to E_5) during 480 hour immersion in SBF.

The increase in pH and then reduction and approximate stability in pH values happened for the extruded supper pure magnesium samples (Figure 3.15), the same as previous types of samples. The increase of pH happened up to 264 hour immersion and then the pH values started to reduce and stabilize after 264 hour immersion, the same as D samples (Figure 3.14). In addition, the pH values for all the samples went very slightly above 9 at 120 hour immersion. In addition, a very similar behaviour in the pH changes of the samples in every time interval was observed for this type of sample.

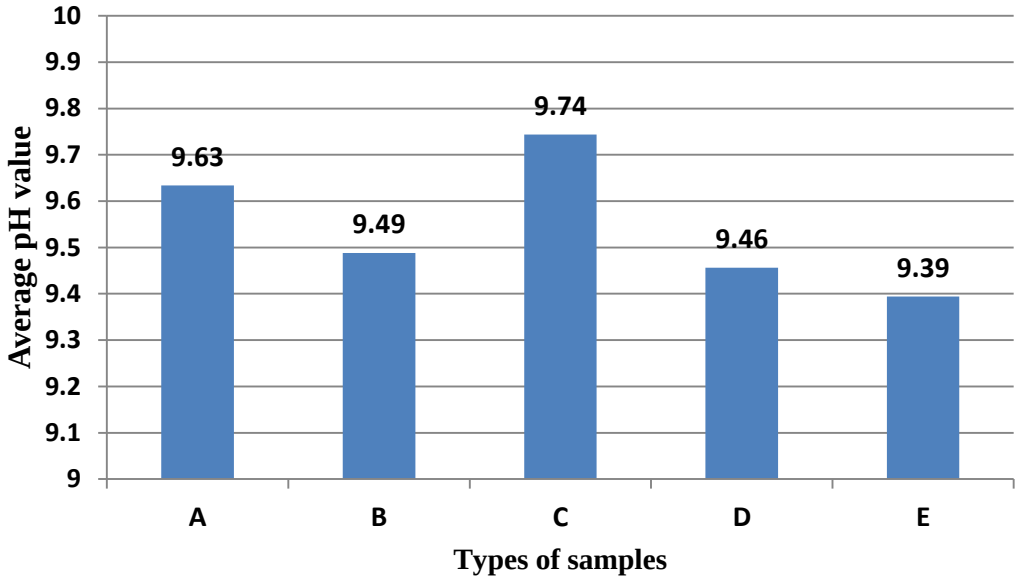

Figure 3.16 Average pH values of various types of samples (A, B, C, D and E) after 480 hour immersion in SBF.

It seems there is a relation between the corrosion performance of the samples and the pH values. Firstly, the pH values after 480 hour immersion in SBF is completely based on the weight loss of the samples. The average weight loss for A, B, C, D and E after 480 hour immersion was about 26.93, 22.80, 66.66, 3.58 and 2.56 wt%, respectively (Figure 3.9). Furthermore, the average pH value for A, B, C, D and E after 480 hour immersion was about 9.63, 9.49, 9.74, 9.46 and 9.39, respectively (Figure 3.16). This indicated that samples with higher weight loss (lower corrosion resistance) have more increase in pH after 480 hour immersion in SBF. As was mentioned in the literature review, hydroxide ions (OH^-) will be released within the solution during magnesium alloy corrosion and the pH value will then be increased [66]. Hence, increase in weight loss would lead to a greater release of hydroxide ions and a greater increase in pH value.

Secondly, the average pH value for sample C with highest weight loss (lowest corrosion resistance) (Figure 3.9) went above 9 at 72 hour immersion (Figure 3.13). But, the pH value of sample E with lowest weight loss (highest corrosion resistance) (Figure 3.9) went above 9 at 120 hour immersion (Figure 3.15). This indicated that the increase of pH to above 9 occurs sooner in the samples with higher weight loss (lower corrosion resistance).

Thirdly, the reduction and approximate stability of pH (Figures 3.11 to 3.15) showed that the corrosion rate of magnesium specimens can become very slow after a while, with increased immersion time. Since the release of hydroxide ions within the solution and increase in pH should continue, if the corrosion process continues normally. Therefore, researches conducted on magnesium corrosion *in vitro* may not reflect its real corrosion behaviour *in vivo* because of the effect of increase in pH of the solution on the degradation rate of specimens.

3.3 Release of ions during corrosion studied by Ion Chromatography of the solutions

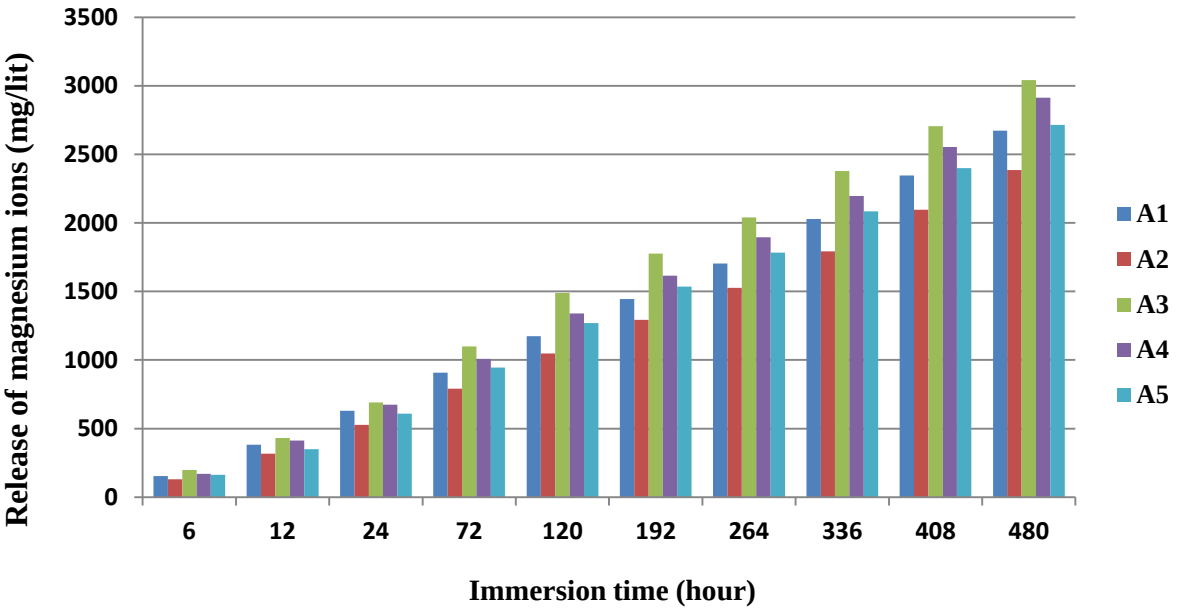

Figure 3.17 Release of magnesium ions for cast commercial pure magnesium ingot samples (A_1 to A_5) during 480 hour immersion in SBF.

In figure 3.17, the release of magnesium ions at different time intervals in cast commercial pure magnesium ingot (A_1 to A_5) can be observed. The release of ions increases with increased immersion time during 480 hour immersion in SBF for all samples.

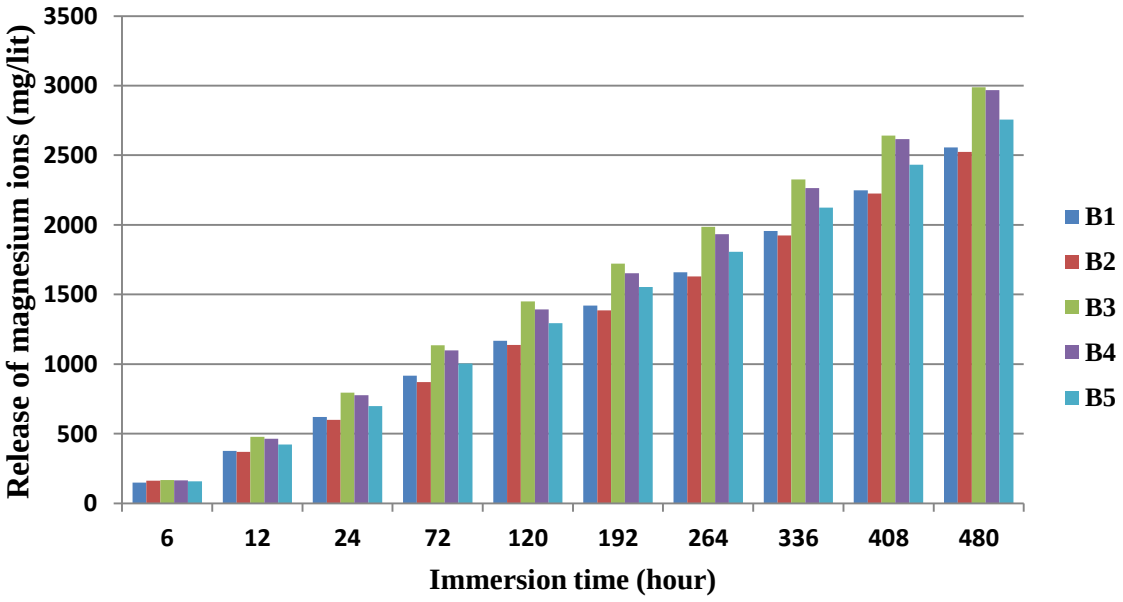

Figure 3.18 Release of magnesium ions for more quickly solidified cast commercial pure magnesium samples (B_1 to B_5) during 480 hour immersion in SBF.

In figure 3.18, increase in magnesium ion release with increased immersion time can be observed for the more quickly solidified cast commercial pure magnesium samples (B_1 to B_5), which was similar to the A samples, during 480 hour immersion in SBF. The trend of increase in magnesium ions release with increased immersion time for all the samples in every time interval maintained, during 480 hour immersion in SBF.

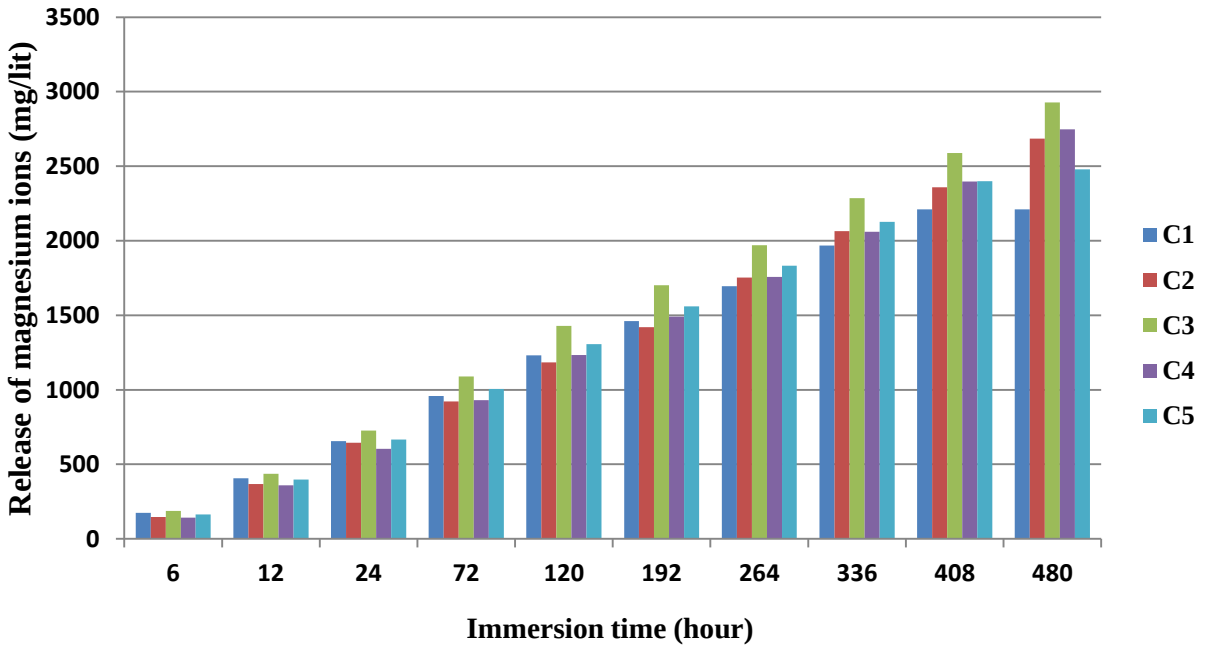

Figure 3.19 Release of magnesium ions for more slowly solidified cast commercial pure magnesium samples (C_1 to C_5) during 480 hour immersion in SBF.

Figure 3.19 indicated that the release of magnesium ions increased with increased immersion time for more slowly solidified cast commercial pure magnesium samples (C_1 to C_5), similar to A and B types of samples. C_5 indicated more release of magnesium ions compared to C_2 and C_4 in the first 336 hours but after that the release of magnesium ions for C_5 became lower than C_2 and C_4. The release of magnesium ions for C_2 was less than C_1 during 192 hour immersion but after that, its release became more than C_1. Also, the release of magnesium ions for C_1 was stable from 408 to 480 hour immersion in SBF because this sample completely dissolved within the solution during 408 hour immersion.

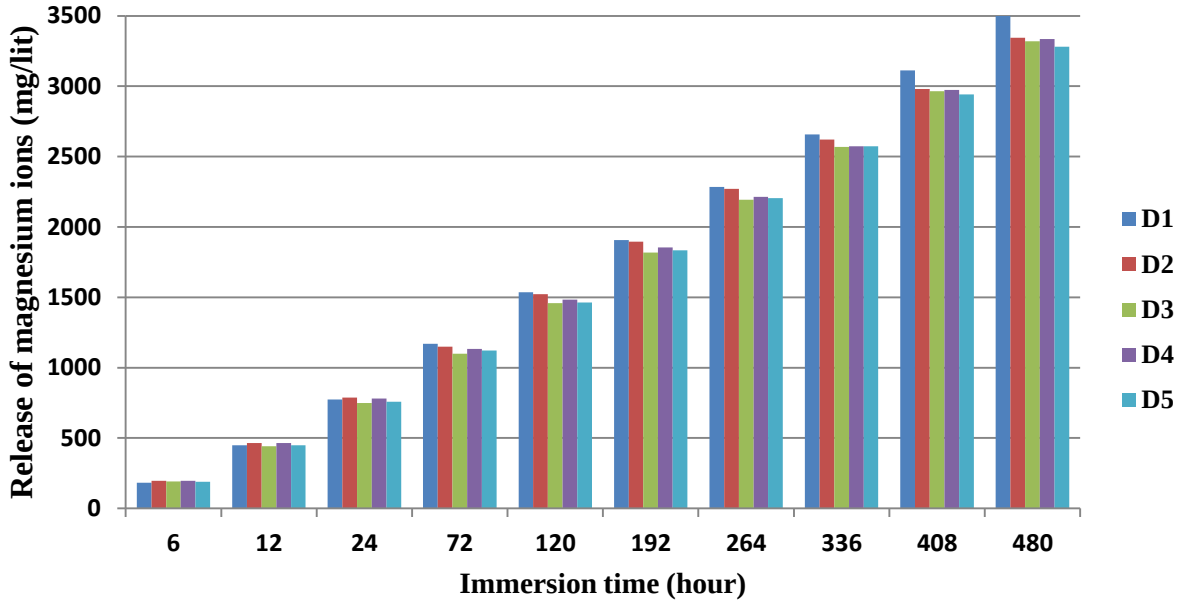

Figure 3.20 Release of magnesium ions for extruded commercial pure magnesium samples (D_1 to D_5) during 480 hour immersion in SBF.

In figure 3.20, the release of magnesium ions increased with increased immersion time for the extruded commercial pure magnesium samples (D_1 to D_5) during 480 hour immersion in SBF, similar to previous types of samples (A, B and C). All the samples approximately showed a similar release of magnesium ions during the whole immersion time at every time interval except D_1, which had more release of magnesium ions after 480 hour immersion in SBF compared to the rest of samples.

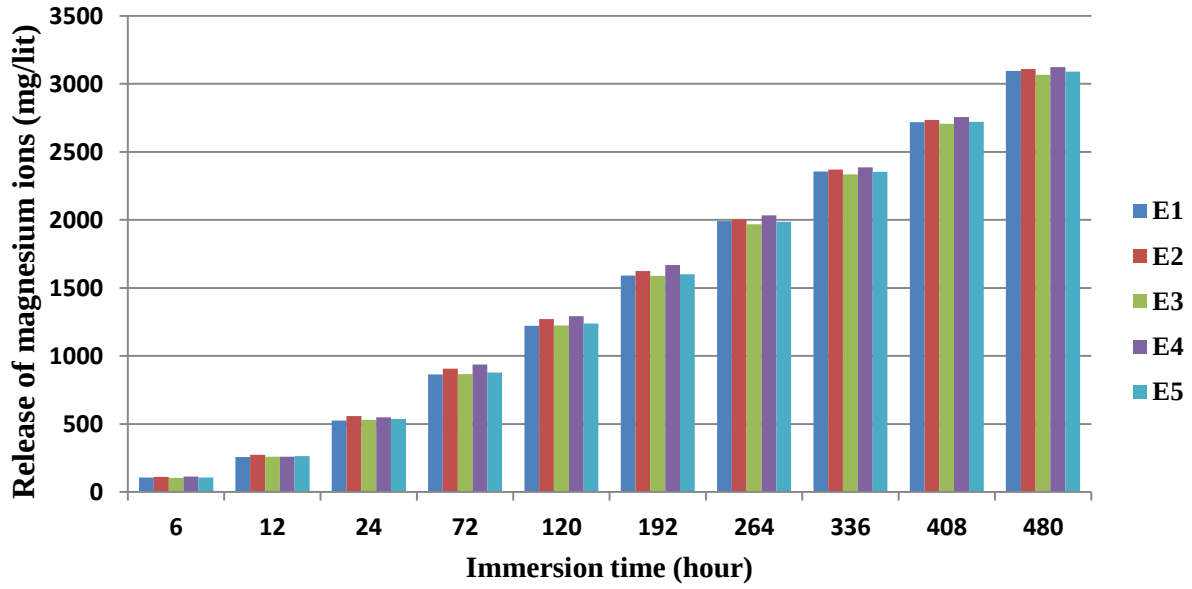

Figure 3.21 Release of magnesium ions for extruded super pure magnesium samples (E_1 to E_5) during 480 hour immersion in SBF.

Increase of magnesium ion release with increased immersion time can be observed for the extruded super pure magnesium samples during 480 hour immersion in SBF, similar to the previous A, B, C and D samples (Figure 3.21). The release of magnesium ions in all the samples (E_1 to E_5) was very similar in every time interval during the 480 hour immersion in SBF.

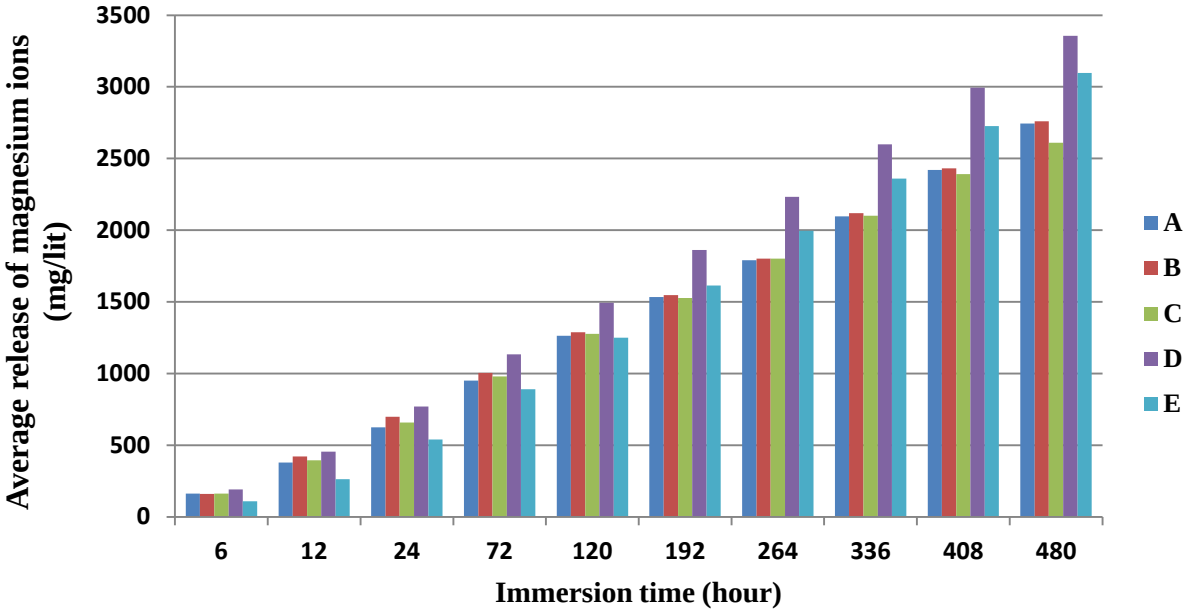

Figure 3.22 Average of magnesium ion release for various types of samples (A, B, C, D and E) during 480 hour immersion in SBF.

Figure 3.22 shows the average of magnesium ion release for A, B, C, D and E in every time interval during 480 hour immersion in SBF. Increase in magnesium release with increased immersion time can be observed during 480 hour immersion in SBF for all types of samples. Figure 3.22 showed the lowest amount of magnesium release for extruded super pure sample (E) in the first 120 hour immersion. But after 120 hour immersion, the release of magnesium ions for E sample increased and became the second highest after extruded commercial pure magnesium (D). D type of sample represented the highest release of ions at every time interval during 480 hour immersion in SBF among all the samples. Also, more slowly solidified cast sample (C) indicated the lowest release of magnesium ions after 480 hour immersion in SBF among all the samples. Among the cast types of samples (A, B and C), the release of magnesium ions for more quickly solidified cast sample (B) was the highest and for more slowly solidified cast sample (C) was the lowest during 480 hour immersion

in SBF. The samples with more weight loss (less corrosion resistance) such as A, B and C indicated less release of ions after 480 hour immersion and the samples with less weight loss (more corrosion resistance) such as B, D and E showed more release of ions after 480 hour immersion (Figures 3.9, 3.22).

Weight loss: E < D < B < A < C

Release of magnesium ions: D > E > B > A > C

This behaviour does not look to be sensible. The samples such as C, which had the highest weight loss among all the samples, should show the highest release of magnesium ions not the lowest one.

3.4 Electron Microscopy of Sample Surfaces

3.4.1 Grain structure

Figures 3-23 to 3.27 indicate the surface morphology and the grain structure of different types of samples (A, B, C, D and E) after etching and before immersion tests. For the extruded super pure magnesium (E), it is difficult to tell the surface structure, whether it shows the grain structure or not (Figure 3.27). On the one side in the figure 3.28, it seems the surface structure shows the grains which are connected by grain boundaries. On the other side in figure 3.29, it seems the surface of the sample has been corroded because of the effect of etchant and there is no grain structure revealed on the surface morphology.

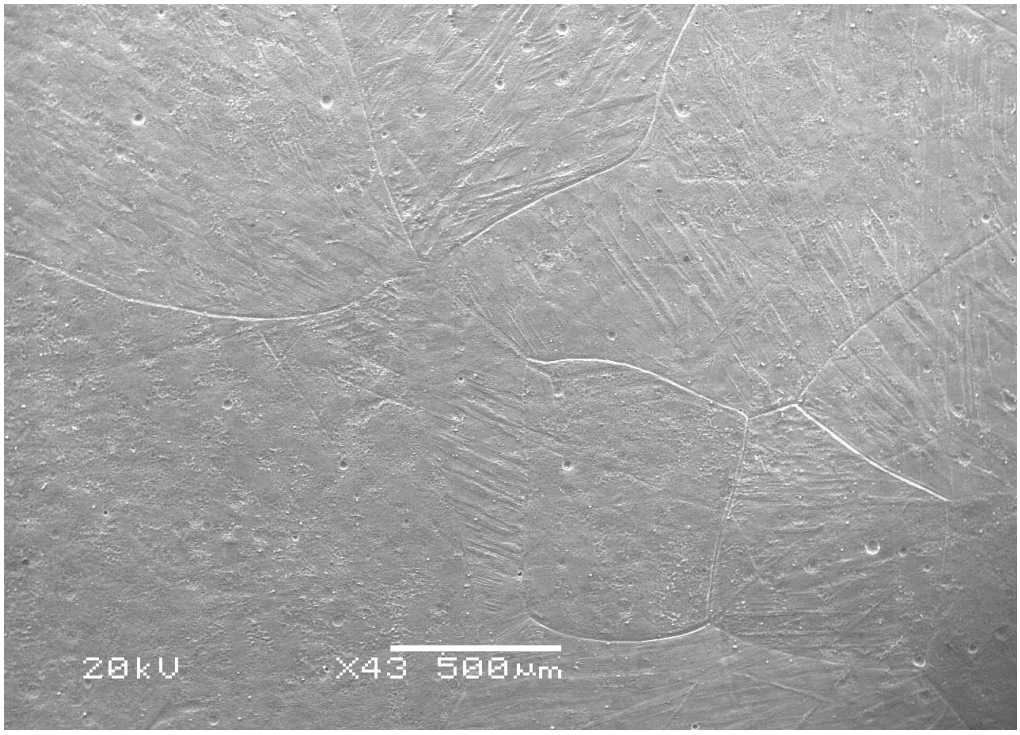

Figure 3.23 SEM morphology and grain structure of cast commercial pure magnesium ingot (A).

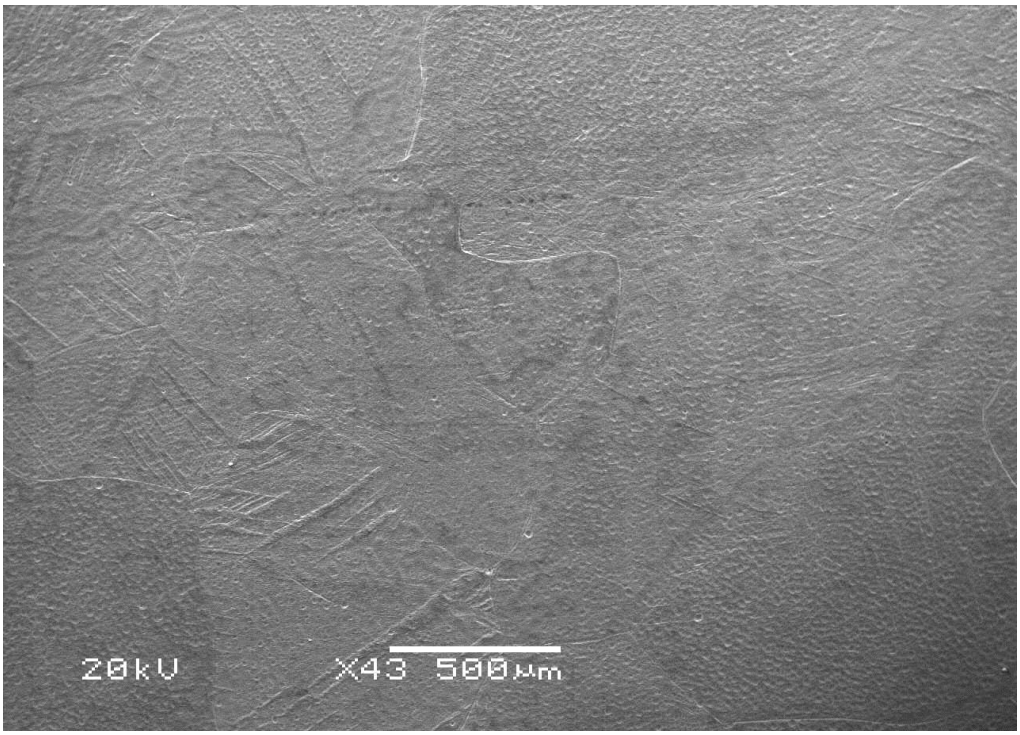

Figure 3.24 SEM morphology and grain structure of more quickly solidified cast commercial pure magnesium (B).

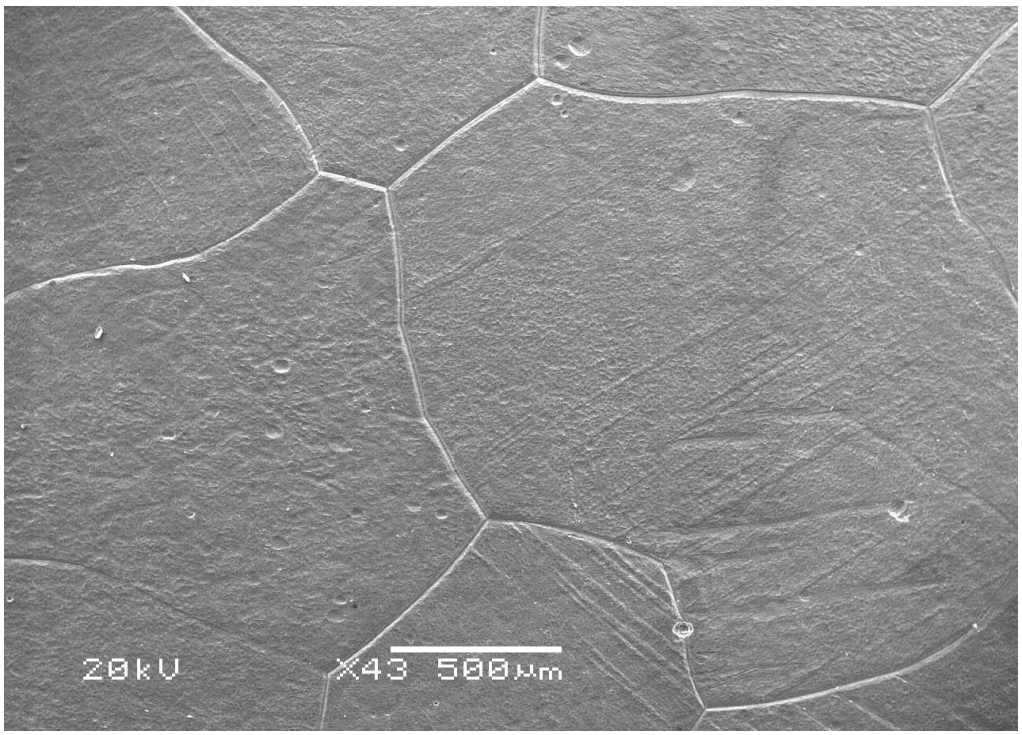

Figure 3.25 SEM morphology and grain structure of more slowly solidified cast commercial pure magnesium (C).

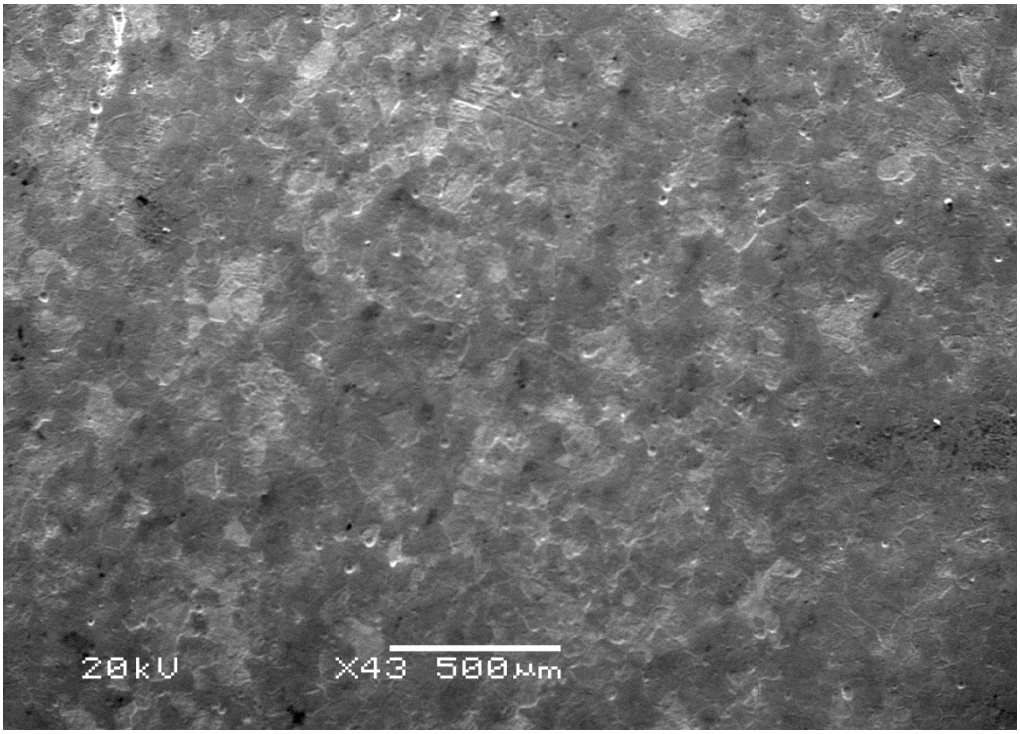

Figure 3.26 SEM morphology and grain structure of extruded commercial pure magnesium (D).

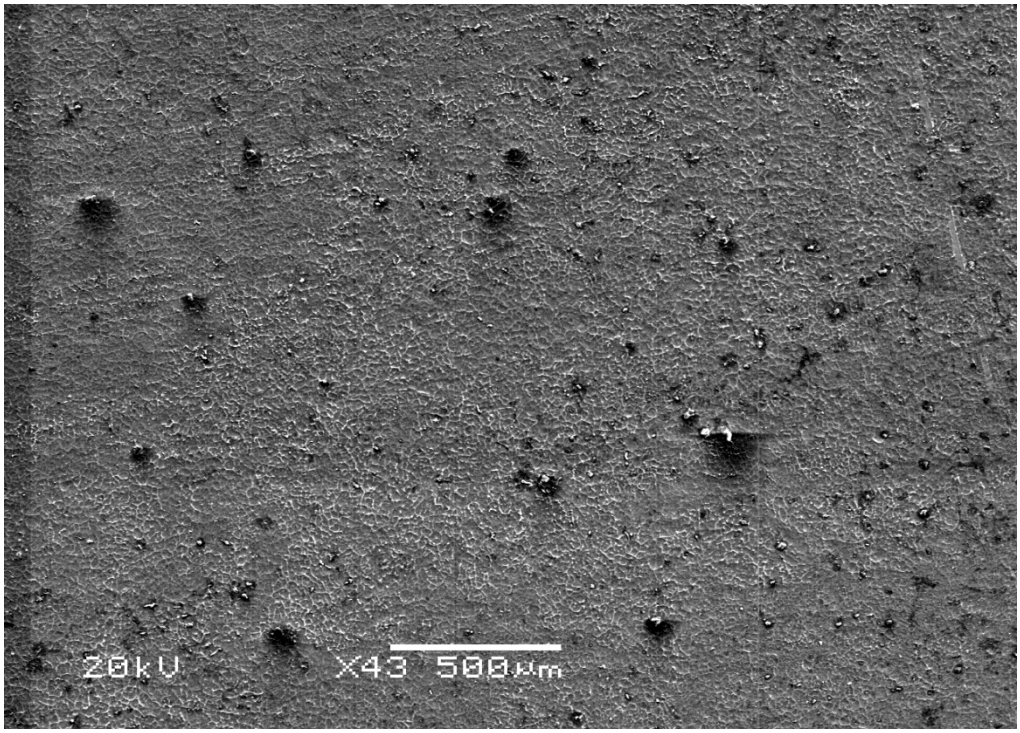

Figure 3.27 SEM morphology of extruded super pure magnesium (E) with lower magnification.

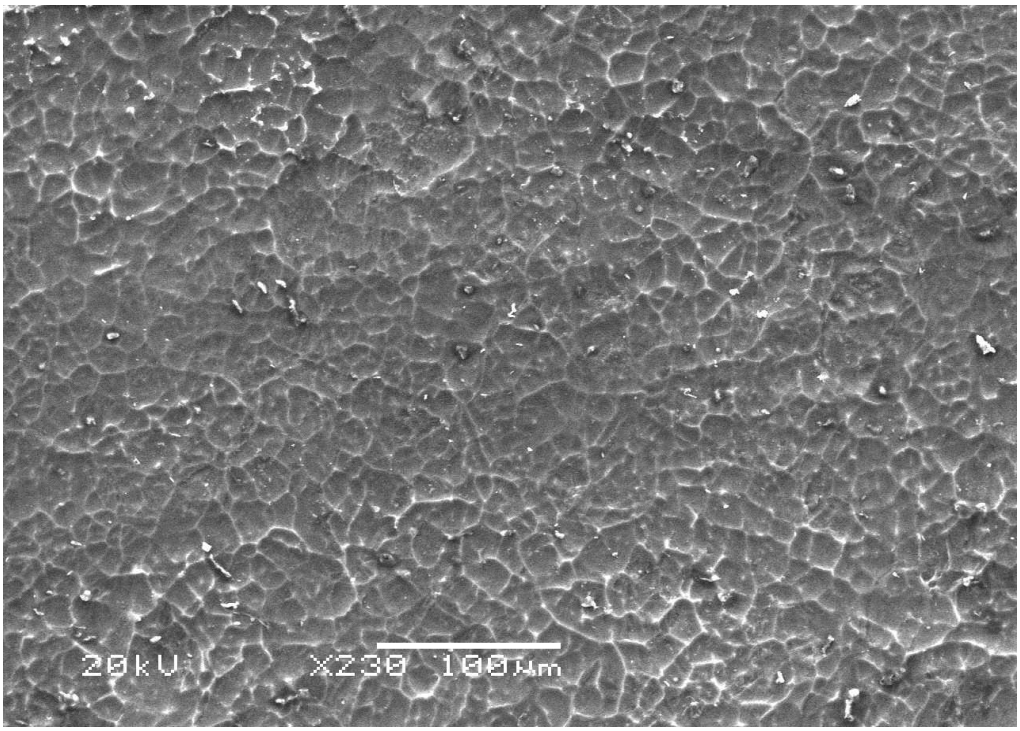

Figure 3.28 SEM morphology of super pure magnesium (E) with higher magnification.

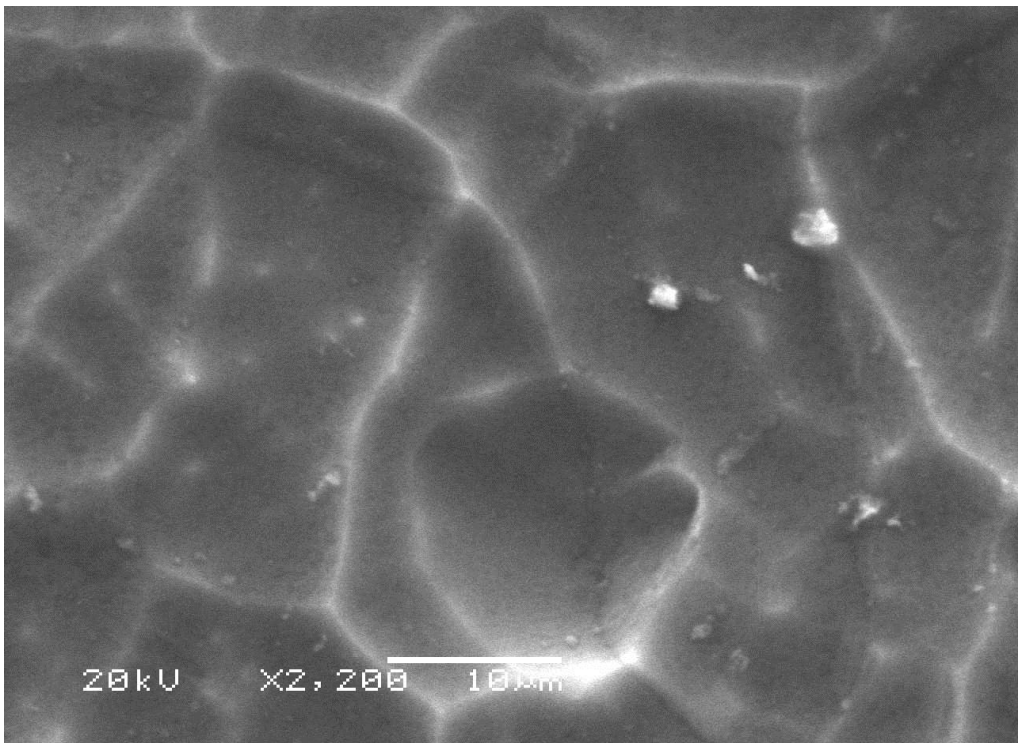

Figure 3.29 SEM morphology of super pure magnesium (E) with high magnification.

If the structure of the extruded super pure magnesium (E) surface represents the grain structure, it is clear that super pure magnesium has the finest grain size of about 20 µm compared to other types of samples (Figures 3.23 to 3.27).

The more slowly solidified cast commercial pure magnesium (C) showed the largest grain size of about 2000 µm among all the types of samples (Figures 3.23 to 3.27). The more quickly solidified cast commercial pure magnesium (B) showed the finest grain size of about 1000µm among the cast samples including cast commercial pure magnesium ingot (A), more quickly solidified cast commercial pure magnesium (B) and more slowly solidified cast commercial pure magnesium (C) (Figures 3.23 to 3.25). Therefore, it can be concluded:

Grain size of samples: C > A > B > D > E

3.4.2 Surface morphology after corrosion

Figures 3.30 to 3.34 indicate the surface morphology of various types of samples (A, B, C, D and E) at different time intervals after immersion in SBF. It is clear that the surface looks more corroded with increased immersion time in all samples. To some extent, there are some similarities to the surface morphology of cast samples (A, B and C) to each other after 480 hour immersion in SBF (Figures 3.30-c, 3.31-c, 3.32-c). Also, there are similarities to the surface morphology of extruded samples (D and E) to each other after 480 hour immersion in SBF (Figures 3.33-b, 3.34-c). However, the surface of extruded samples looks different and less corroded from cast samples after 480 hour immersion in SBF. Also, it seems the surface of super pure extruded sample (E) is more resistant to sever corrosion compared to the rest of samples after 480 hour immersion in SBF (Figures 3.30-c, 3.31-c, 3.32-c, 3.33-b, 3.34-c).

(a)

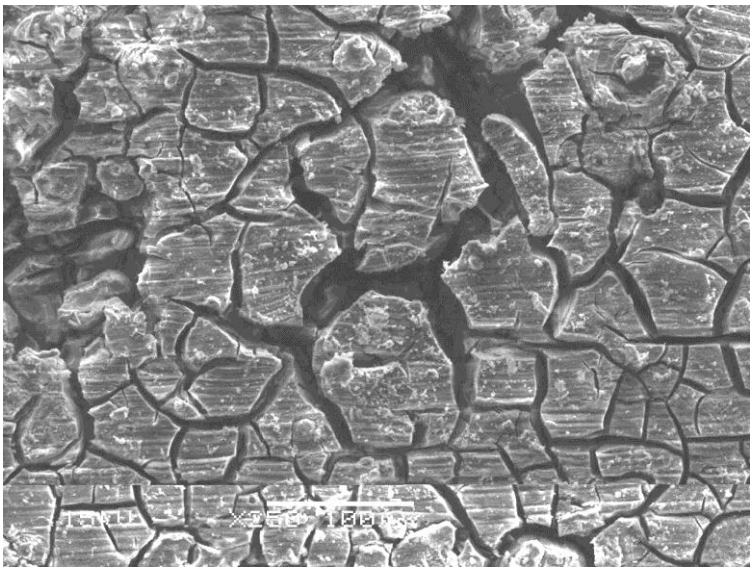

(b)

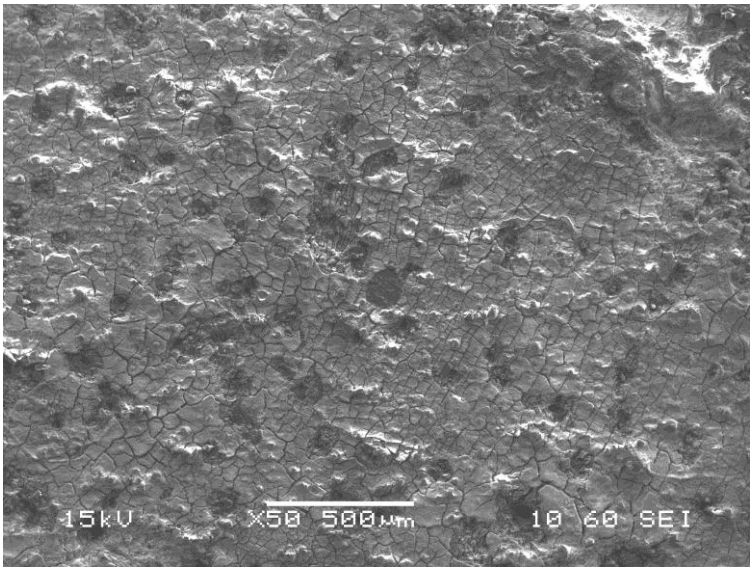

(c)

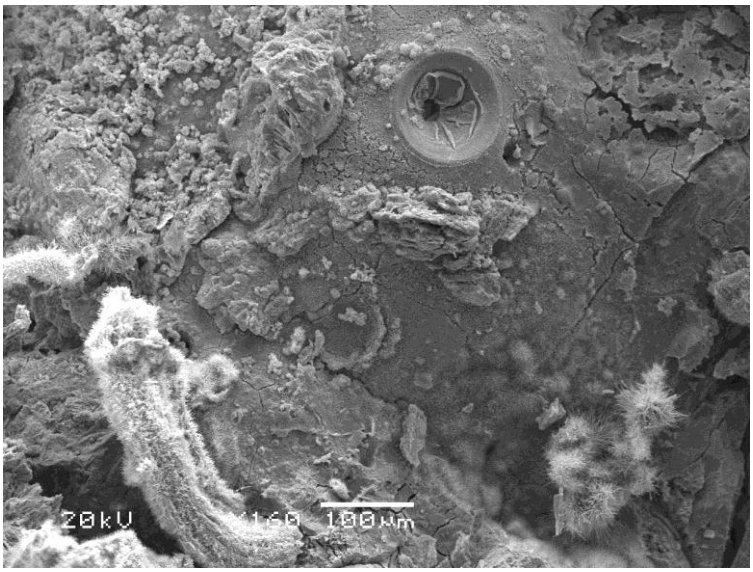

Figure 3.30 Surface morphology of cast commercial pure magnesium ingot (A) after **(a)** 24 hour **(b)** 72 hour **(c)** 480 hour immersion in SBF.

(a)

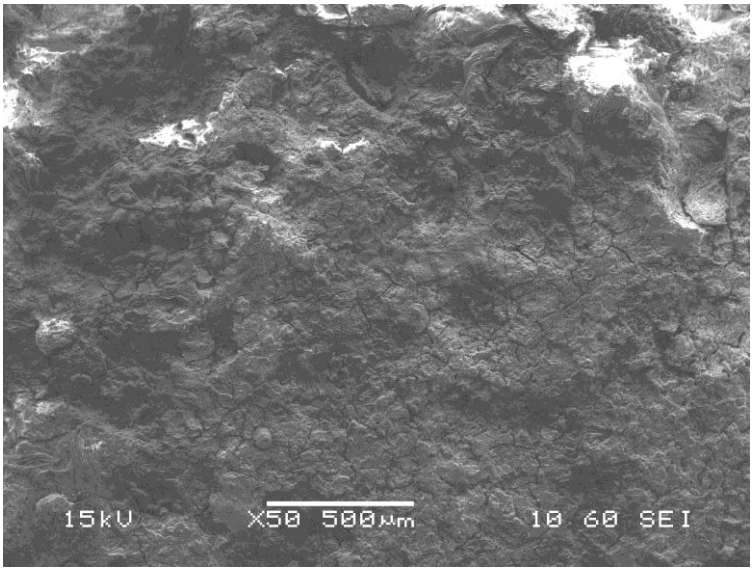

(b)

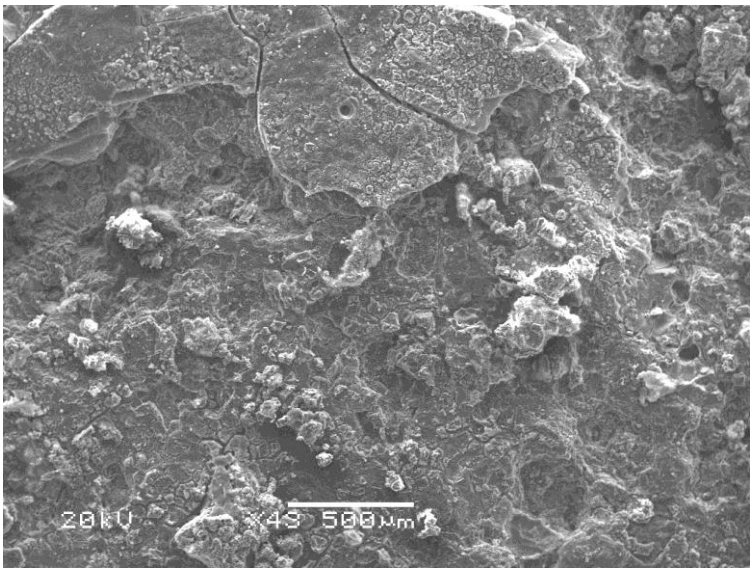

(c)

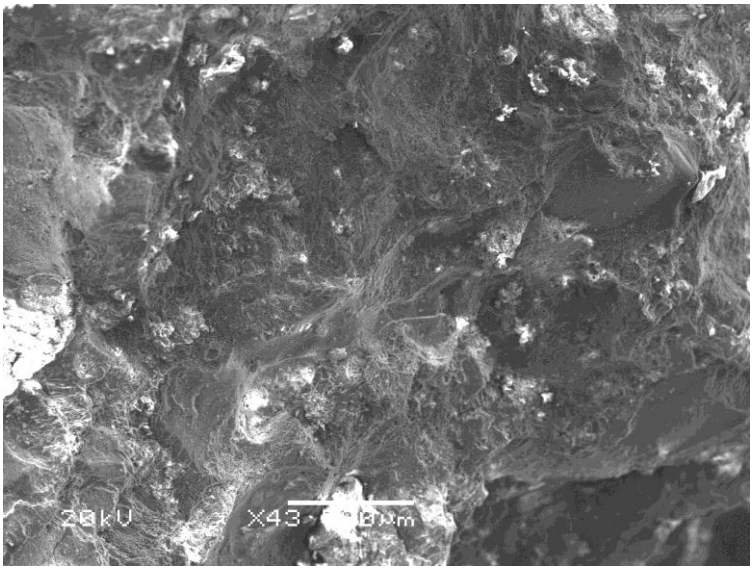

Figure 3.31 Surface morphology of more quickly solidified cast commercial pure magnesium (B) after **(a)** 72 hour **(b)** 264 hour **(c)** 480 hour immersion in SBF.

(a)

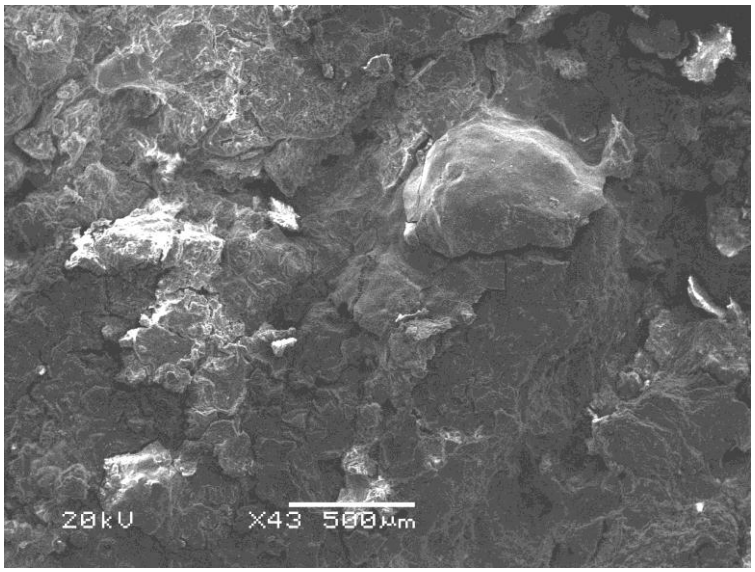

(b)

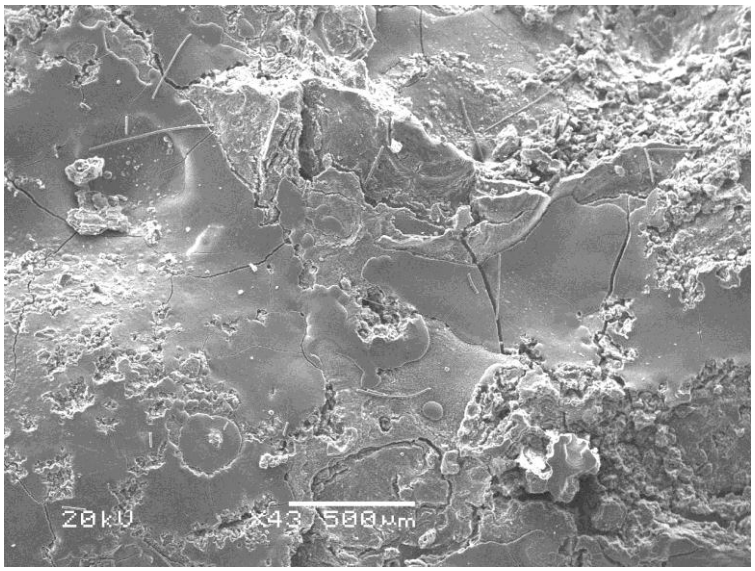

(c)

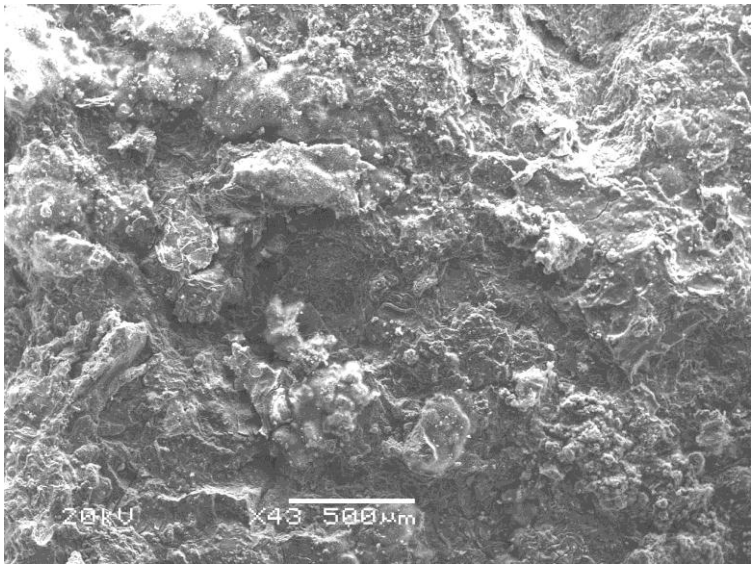

Figure 3.32 Surface morphology of more slowly solidified cast commercial pure magnesium (C) after **(a)** 72 hour **(b)** 264 hour **(c)** 480 hour immersion in SBF.

(a)

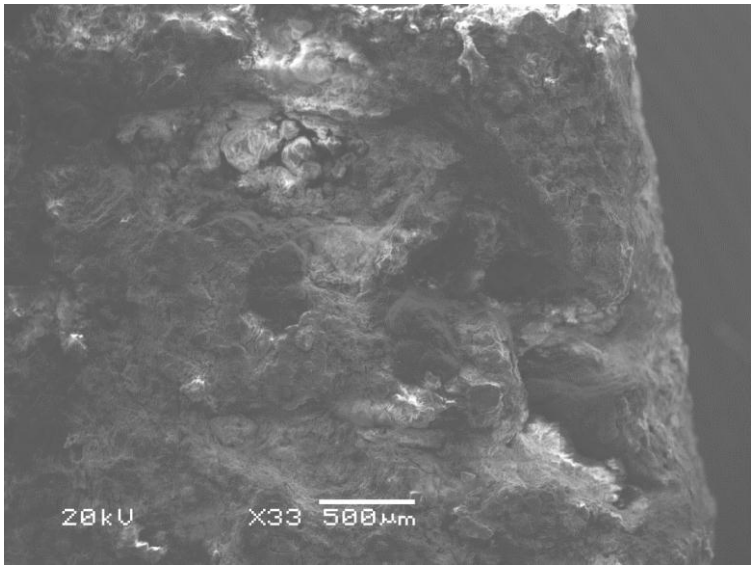

(b)

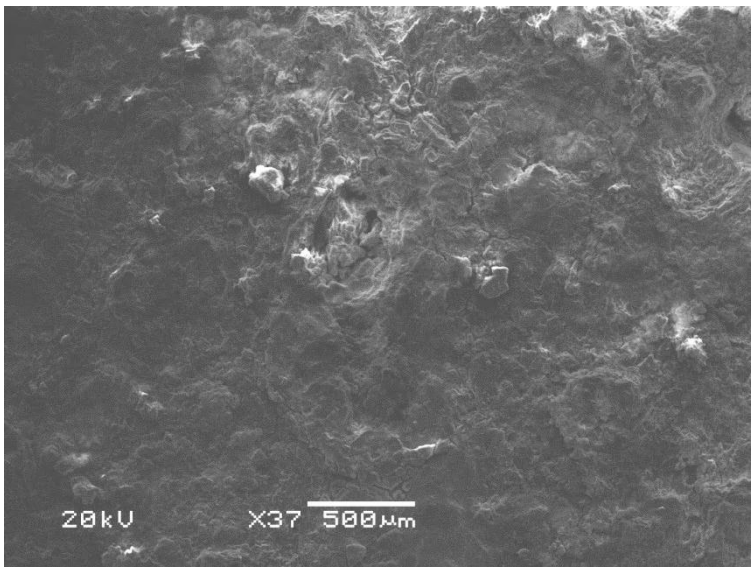

(c)

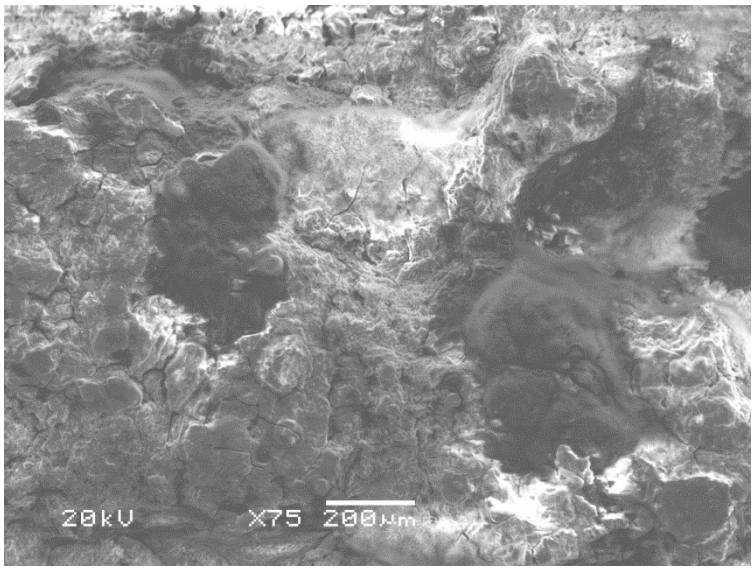

Figure 3.33 Surface morphology of extruded commercial pure magnesium (D) after 480 hour immersion in SBF (a, b and c).

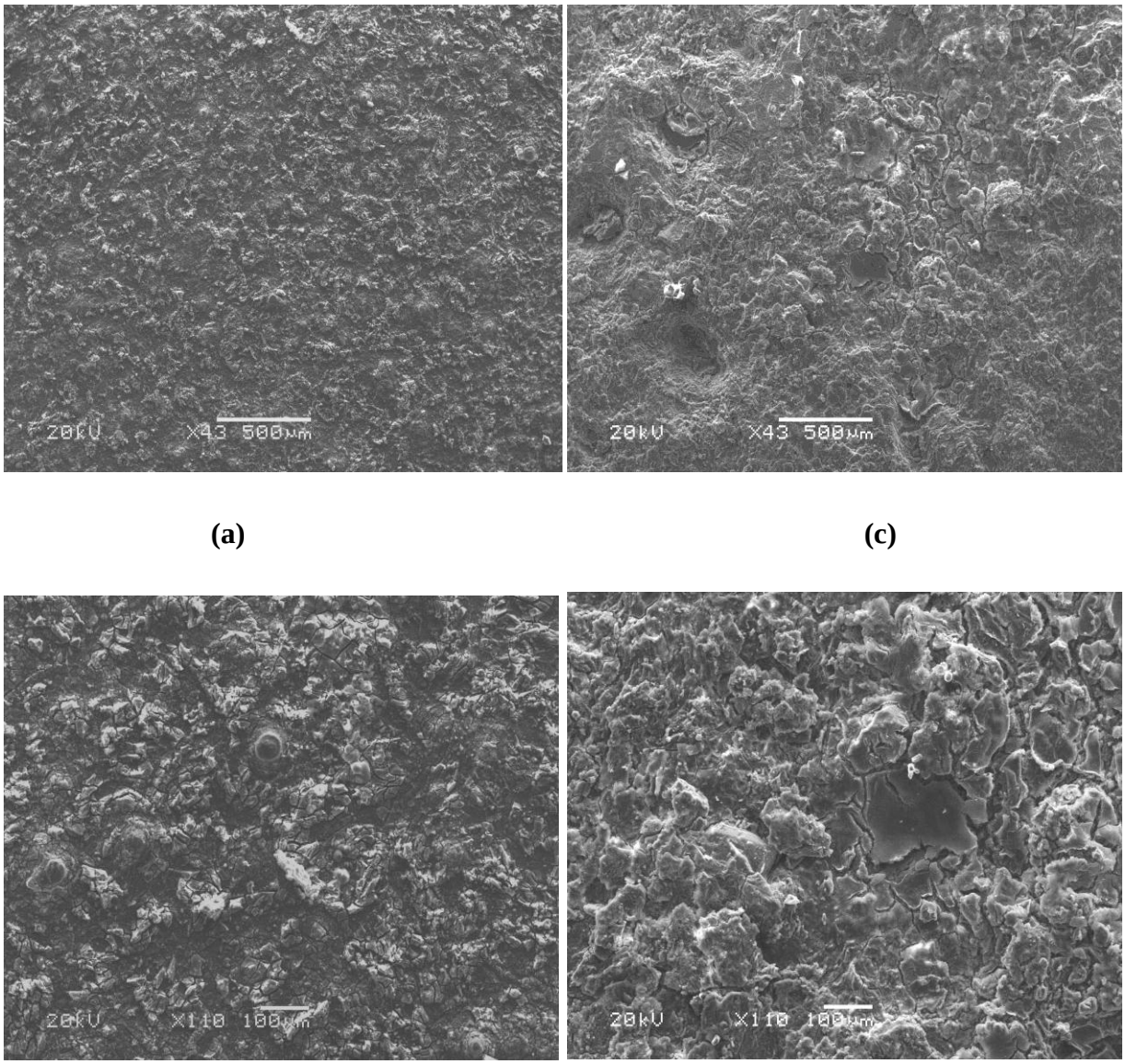

(a) **(c)**

(b) **(d)**

Figure 3.34 Surface morphology of extruded super pure magnesium (E) after **(a), (b)** 72 hour **(c), (d)** 480 hour immersion in SBF.

3.4.3 Corrosion products

Figures 3.35 to 3.44 indicate the main corrosion products formed on the corroded surface of different samples (A, B, C, D and E) after 480 hour immersion in SBF. Deposition of Ca and P, formation of needle-shaped clusters of $MgCl_2$ and formation of Mg $(OH)_2$ was observed for all the cast samples (Figures 3.35 to 3.40). Y. Wong et al. reported formation of the same corrosion products on the surface of ingot pure magnesium after immersion in SBF [66]. C. B. Baliga and P. Tsakiropoulos observed formation of such morphology of Mg $(OH)_2$ in figures 3.35-b, 3.37-b and 3.39-b, in Mg-16Al alloy after immersion in 3% NaCl solution [67]. The extruded commercial pure magnesium (D) showed deposition of Ca and P and formation of $MgCl_2$ on its surface, but formation of Mg $(OH)_2$ was not observed on the surface of sample D (Figure 3.41). In addition, for extruded super pure magnesium (E), only deposition of Ca and P observed and no morphology related to Mg $(OH)_2$ and $MgCl_2$ was observed (Figure 3.43). Furthermore, the presence of an unknown film layer was observed on super pure extruded sample (E) after 480 hour immersion in SBF (Figure 3.43-b-1). The EDX (Energy Dispersive X-ray spectroscopy) results on this film indicated magnesium and oxygen in the composition of this film (Figure 3.44-b-1) which was the same as the EDX results on the magnesium surface without the presence of this film on the surface (Figure 3.44-b-2).

(a)

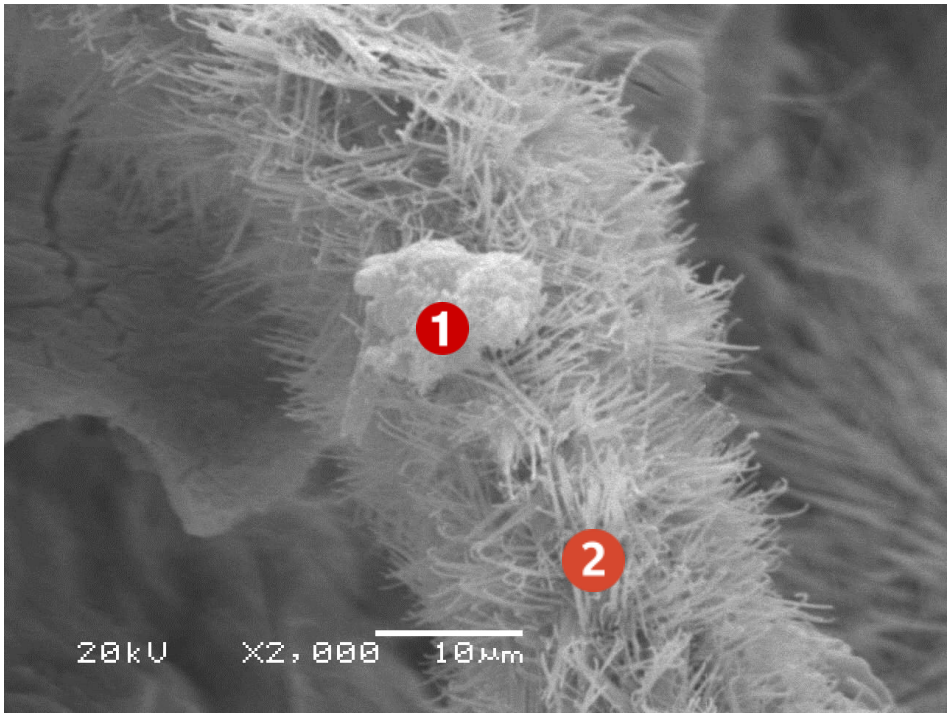

(b)

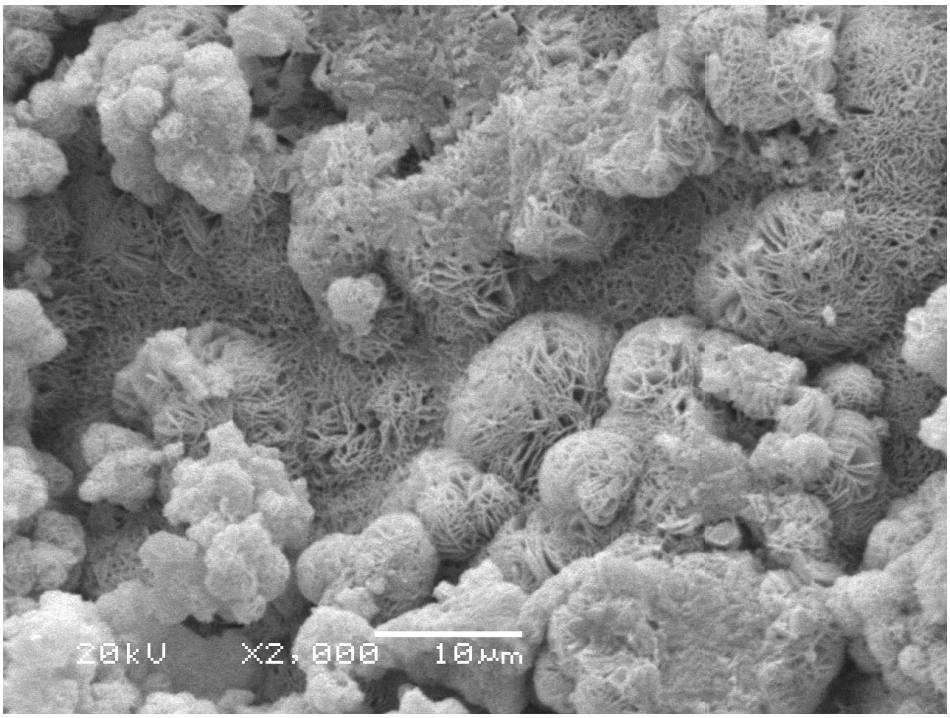

Figure 3.35 SEM analysis of corrosion products for cast commercial pure magnesium ingot (A) after 480 hour immersion in SBF: **(a) 1:** Deposition of Ca and P **2:** $MgCl_2$ **(b)** Mg $(OH)_2$.

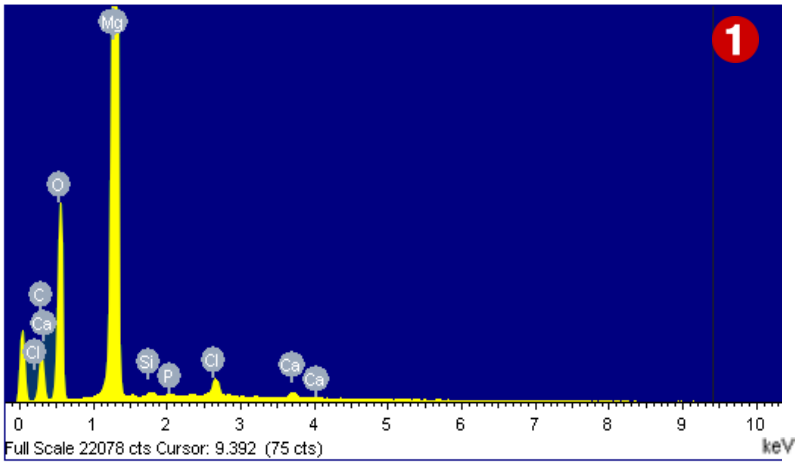

Element	Weight%	Atomic%
O K	40.15	50.91
Mg K	56.48	47.13
Si K	0.41	0.29
P K	0.26	0.17
Cl K	1.95	1.12
Ca K	0.75	0.38
Totals	100.00	

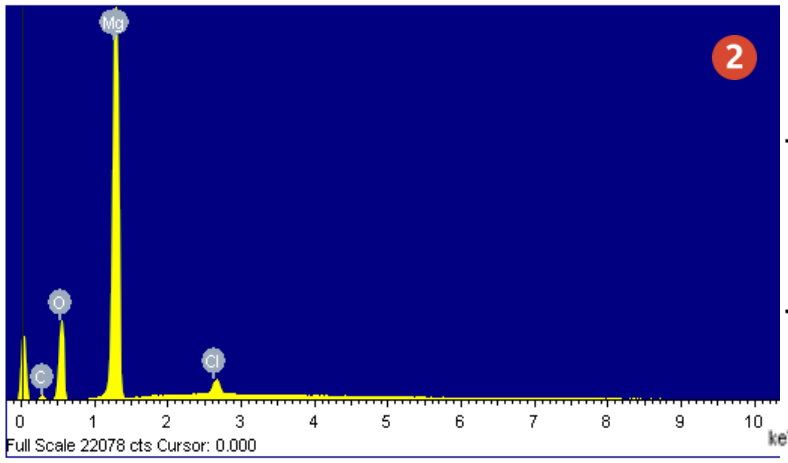

Element	Weight%	Atomic%
O K	36.35	46.92
Mg K	59.95	50.92
Cl K	3.70	2.16
Totals	100.00	

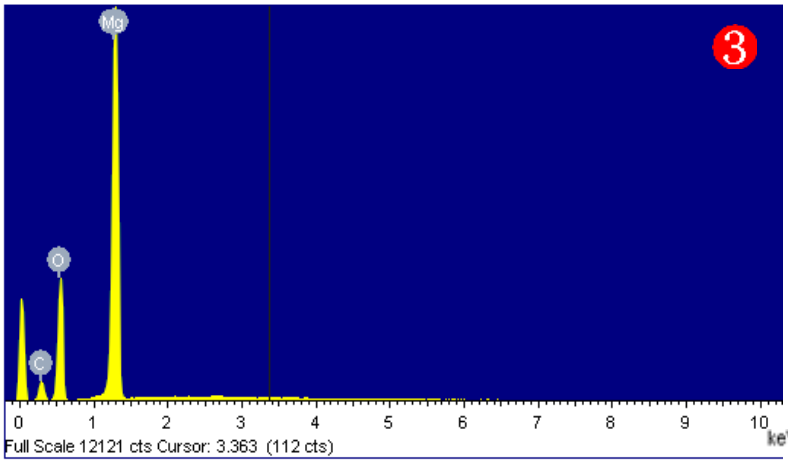

Element	Weight%	Atomic%
O K	44.14	54.56
Mg K	55.86	45.44
Totals	100.00	

Figure 3.36 EDX analysis of corrosion products for cast commercial pure magnesium ingot (A) after 480 hour immersion in SBF: **1)** Deposition of Ca and P **2)** $MgCl_2$ **3)** Mg $(OH)_2$.

(a)

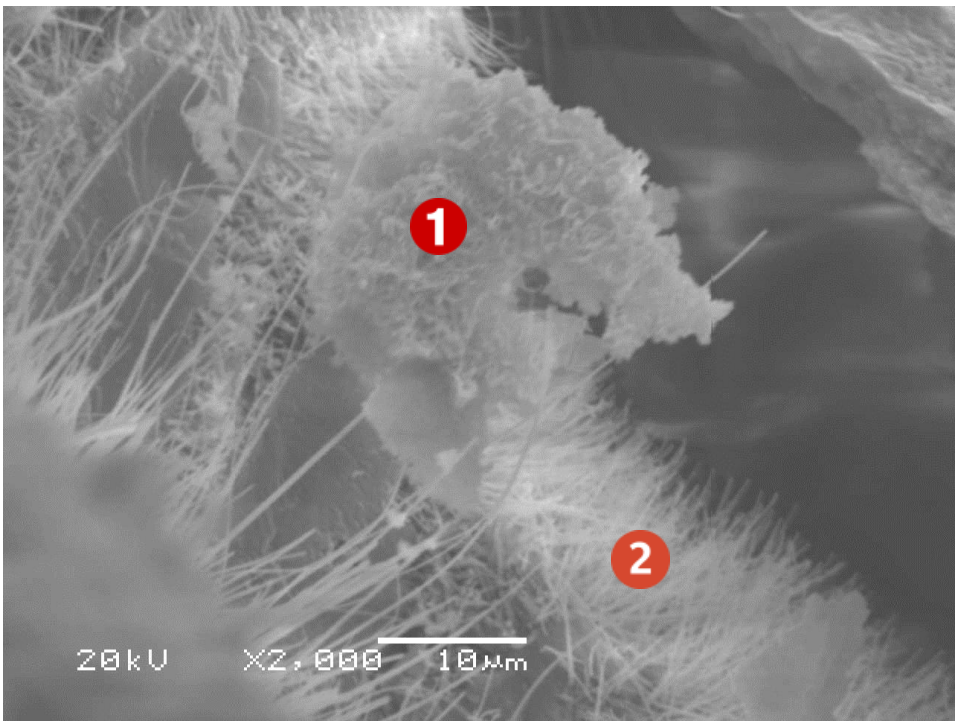

(b)

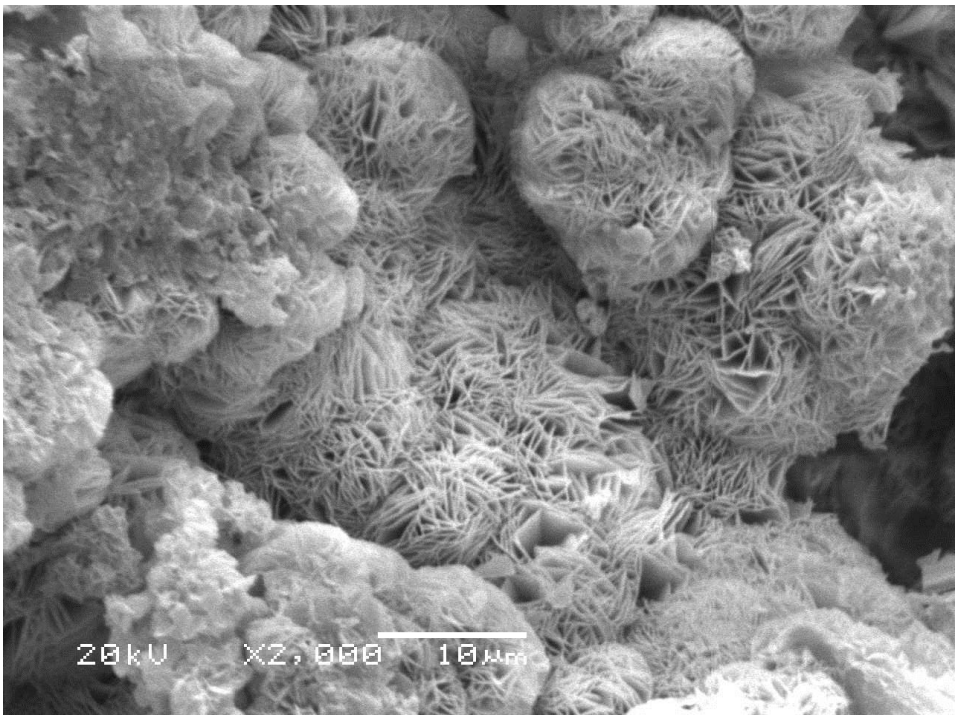

Figure 3.37 SEM analysis of corrosion products for more quickly solidified cast commercial pure magnesium (B) after 480 hour immersion in SBF: **(a) 1:** Deposition of Ca and P **2:** $MgCl_2$ **(b)** Mg $(OH)_2$.

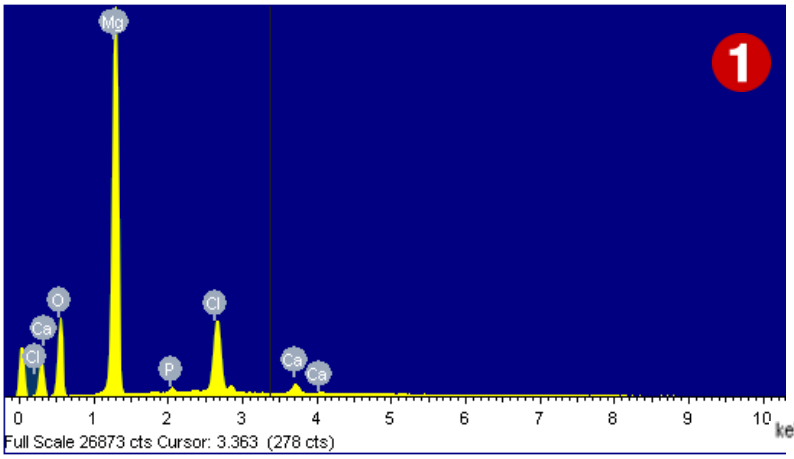

Element	Weight%	Atomic%
O K	36.59	48.91
Mg K	46.69	41.06
P K	0.95	0.65
Cl K	13.75	8.30
Ca K	2.02	1.08
Totals	100.00	

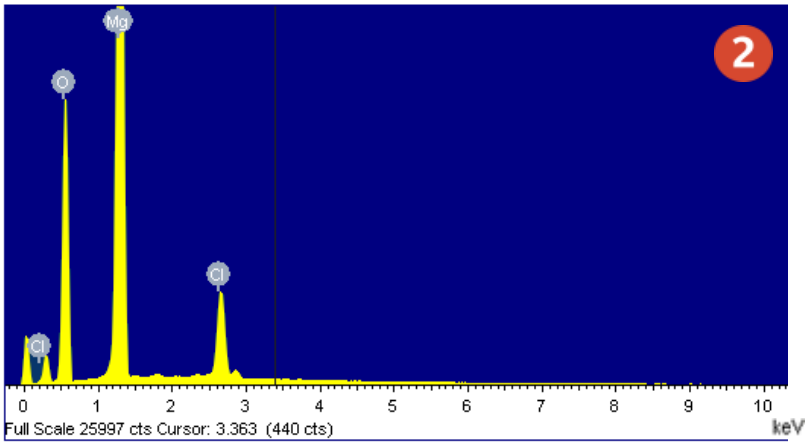

Element	Weight%	Atomic%
O K	44.44	55.91
Mg K	48.26	39.95
Cl K	7.30	4.14
Totals	100.00	

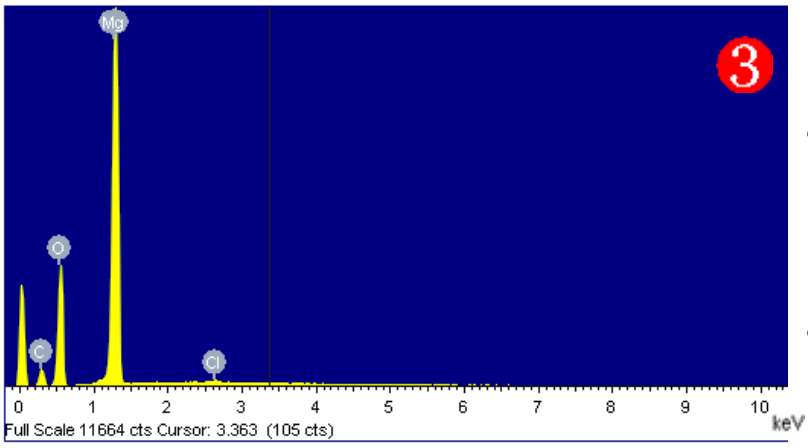

Element	Weight%	Atomic%
O K	44.46	54.93
Mg K	55.16	44.85
Cl K	0.38	0.21
Totals	100.00	

Figure 3.38 EDX analysis of corrosion products for more quickly solidified cast commercial pure magnesium (B) after 480 hour immersion in SBF: **1)** Deposition of Ca and P **2)** $MgCl_2$ **3)** Mg $(OH)_2$.

(a)

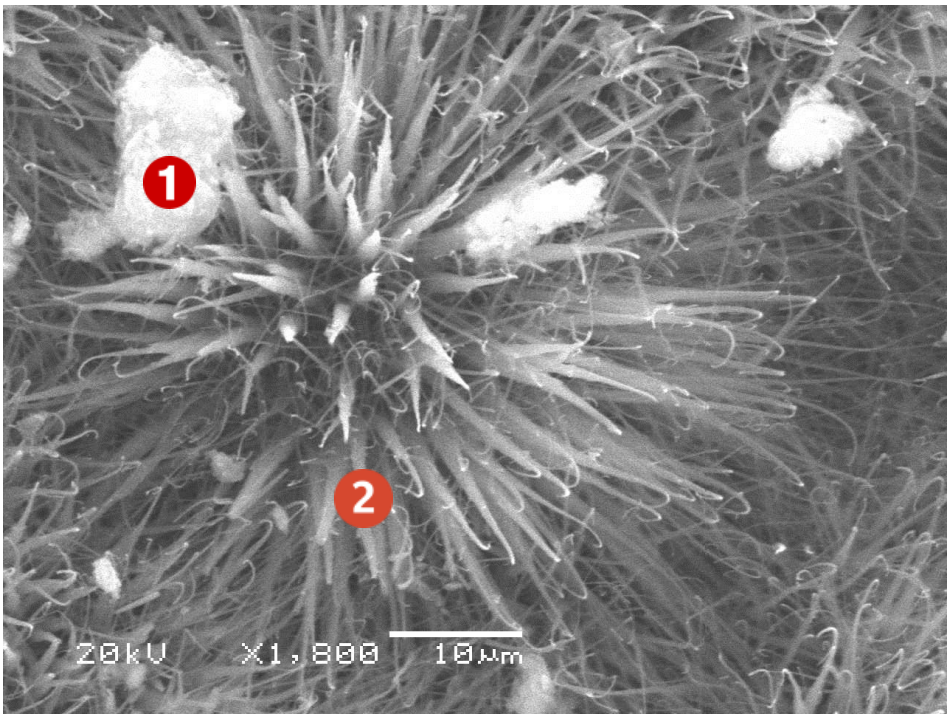

(b)

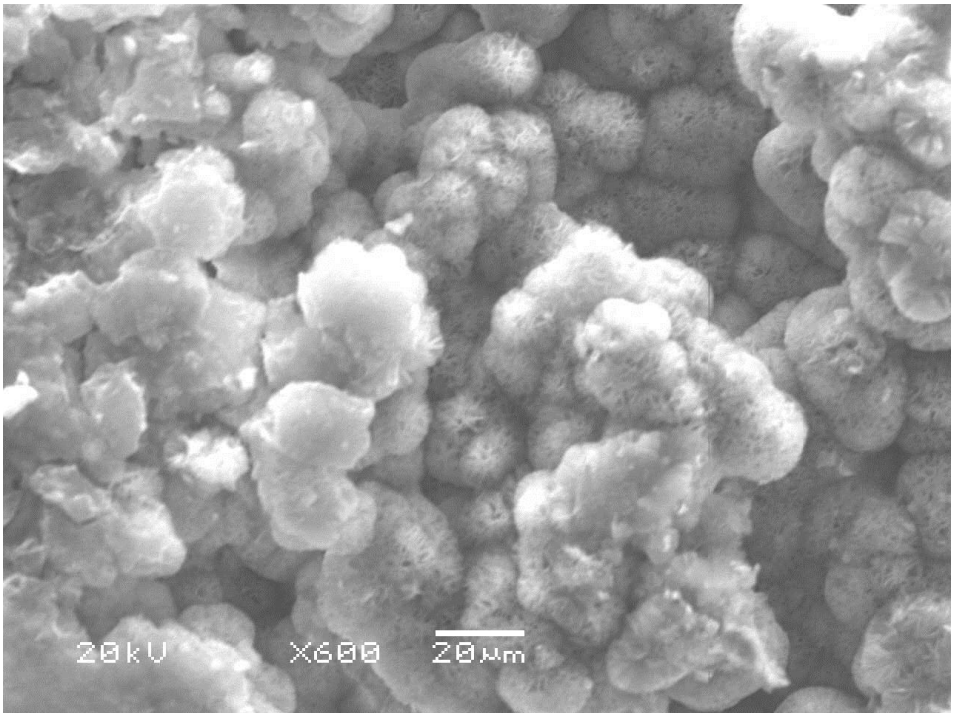

Figure 3.39 SEM analysis of corrosion products for more slowly solidified cast commercial pure magnesium (C) after 480 hour immersion in SBF: **(a) 1:** Deposition of Ca and P **2:** $MgCl_2$ **(b)** Mg $(OH)_2$.

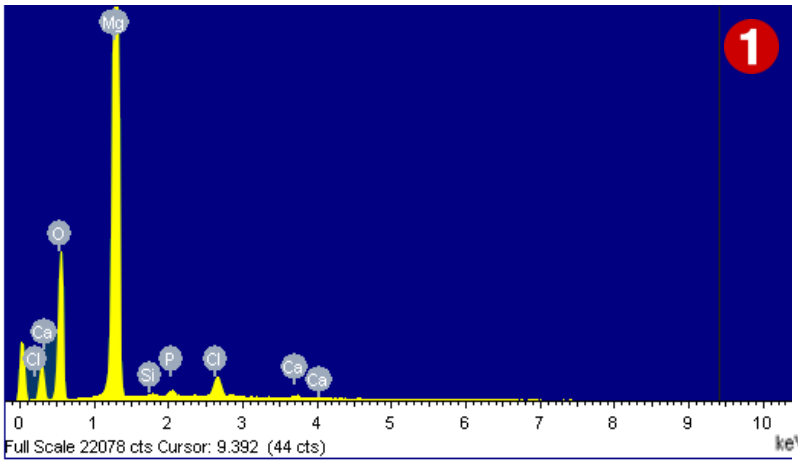

Element	Weight%	Atomic%
O K	39.70	50.58
Mg K	55.65	46.66
Si K	0.36	0.26
P K	0.85	0.56
Cl K	2.99	1.72
Ca K	0.44	0.22
Totals	100.00	

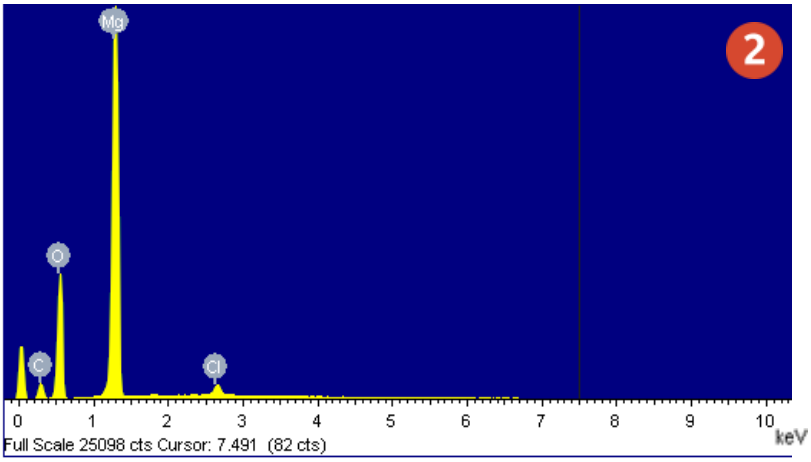

Element	Weight%	Atomic%
O K	44.25	54.96
Mg K	53.67	43.87
Cl K	2.07	1.16
Totals	100.00	

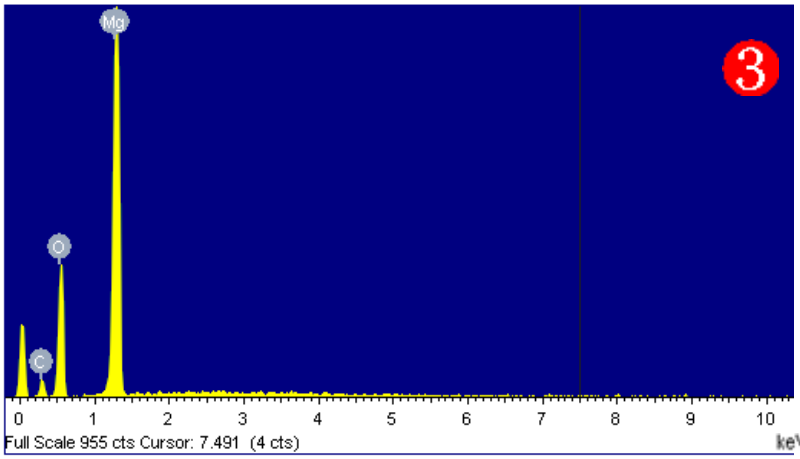

Element	Weight%	Atomic%
O K	45.21	55.63
Mg K	54.79	44.37
Totals	100.00	

Figure 3.40 EDX analysis of corrosion products for more slowly solidified cast commercial pure magnesium (C) after 480 hour immersion in SBF: **1)** Deposition of Ca and P **2)** $MgCl_2$ **3)** Mg $(OH)_2$.

(a)

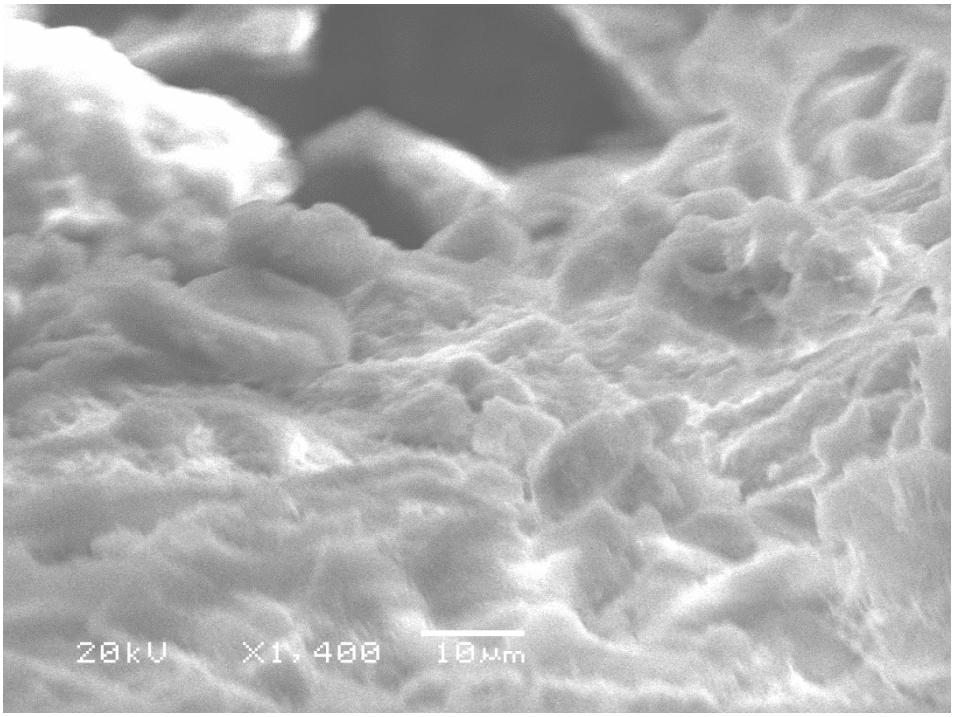

(b)

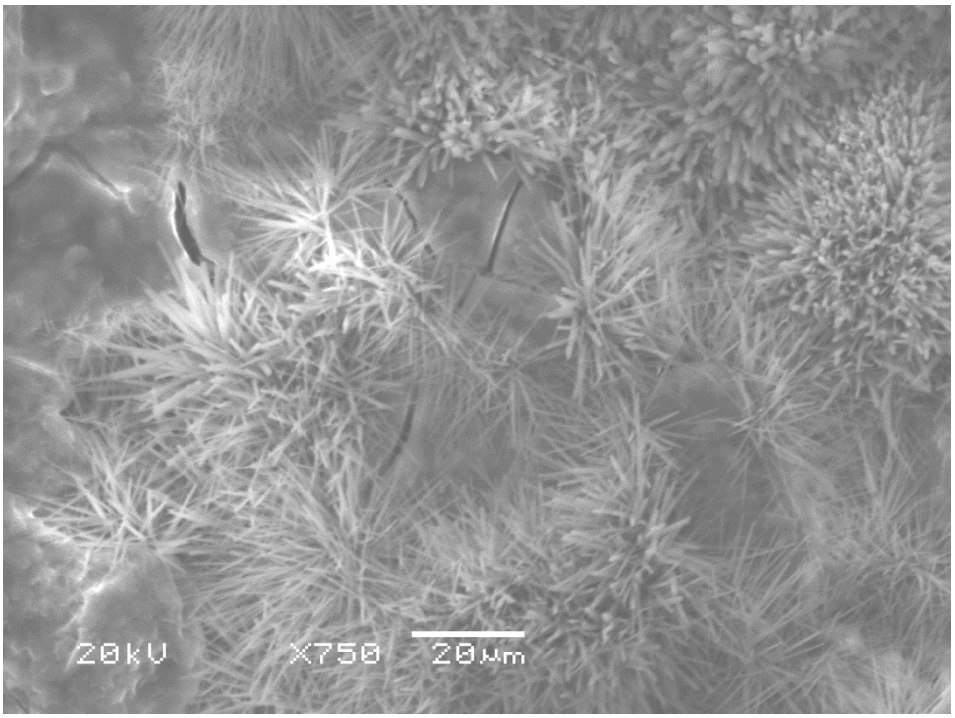

Figure 3.41 SEM analysis of corrosion products for extruded commercial pure magnesium (D) after 480 hour immersion in SBF: **(a)** Deposition of Ca and P **(b)** $MgCl_2$.

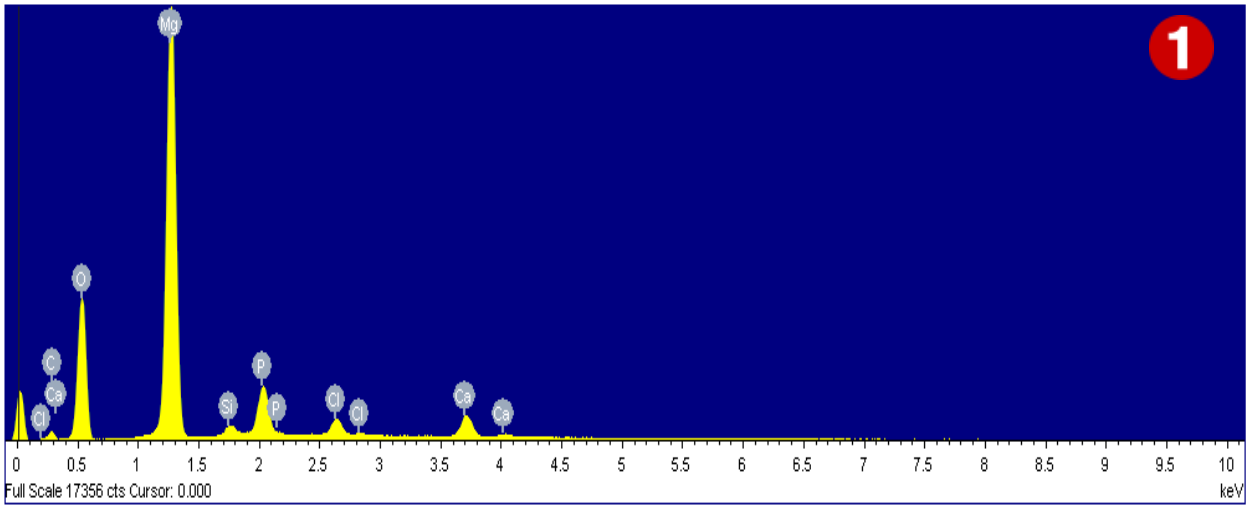

Element	Weight%	Atomic%
C K	9.52	15.02
O K	42.15	49.92
Mg K	36.13	28.15
Si K	0.97	0.65
P K	5.88	3.60
Cl K	2.05	1.10
Ca K	3.29	1.56
Totals	100.00	

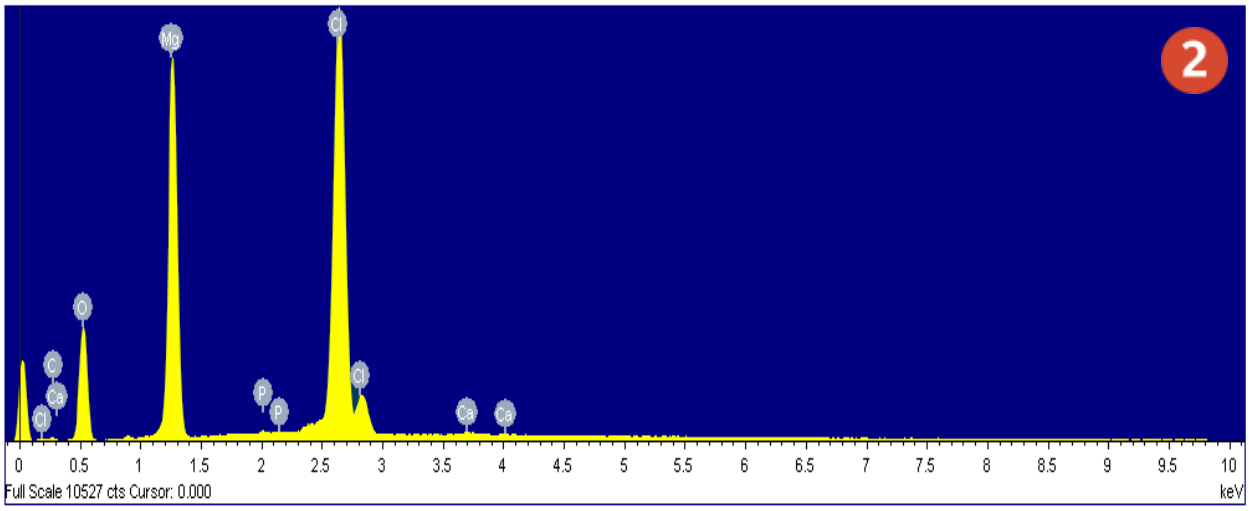

Element	Weight%	Atomic%
C K	4.33	7.86
O K	35.53	48.44
Mg K	23.76	21.32
P K	0.17	0.12
Cl K	35.93	22.10
Ca K	0.28	0.15
Totals	100.00	

Figure 3.42 EDX analysis of corrosion products for extruded commercial pure magnesium (D) after 480 hour immersion in SBF: **1)** Deposition of Ca and P **2)** $MgCl_2$.

(a)

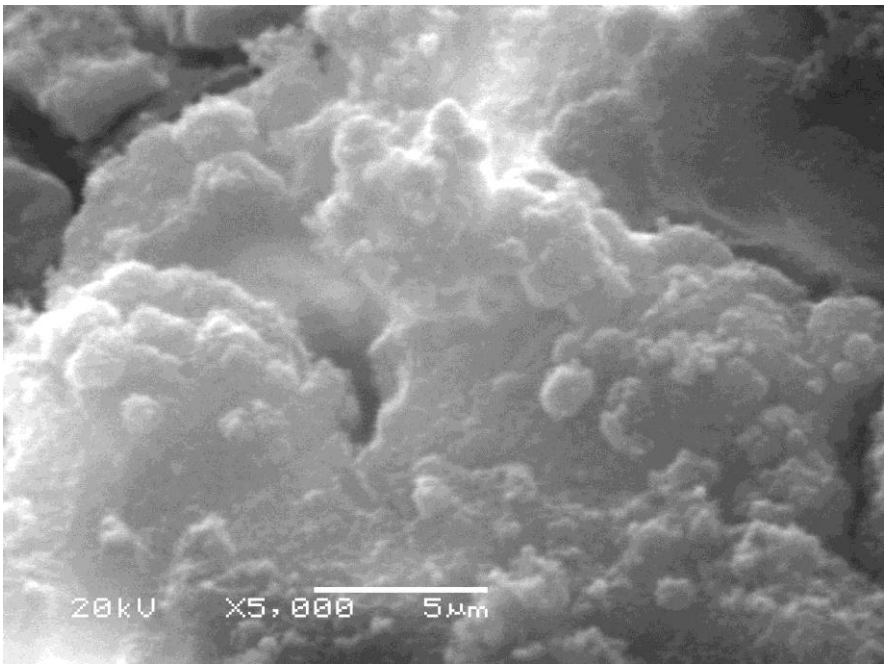

(b)

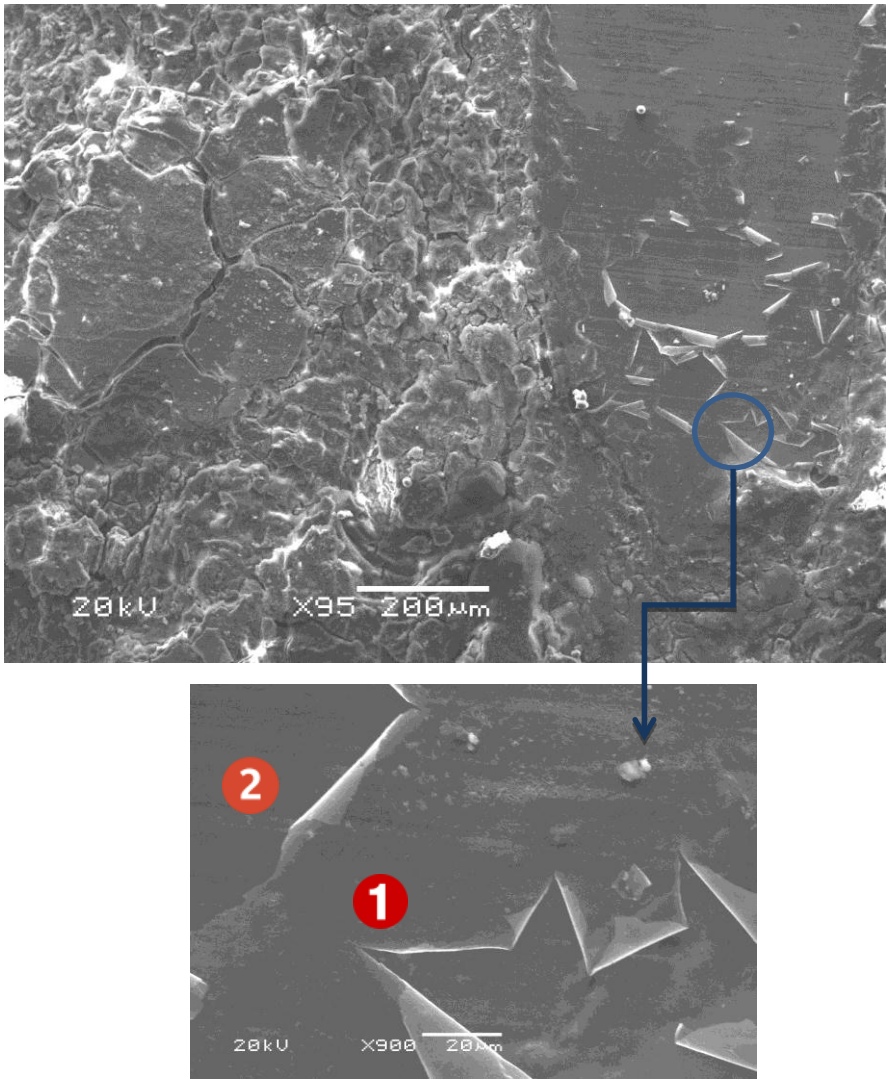

Figure 3.43 SEM analysis of corrosion products for extruded super pure magnesium (E) after 480 hour immersion in SBF: **(a)** deposition of Ca and P **(b) 1:** unknown film **2:** sample surface next to the unknown film layer.

(a)

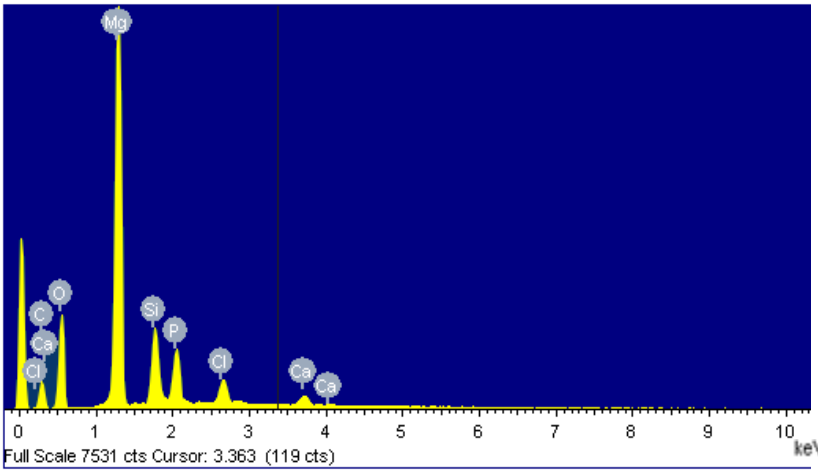

Element	Weight%	Atomic%
O K	36.21	48.42
Mg K	39.32	34.61
Si K	10.02	7.63
P K	8.61	5.94
Cl K	3.99	2.41
Ca K	1.86	0.99
Totals	100.00	

(b)

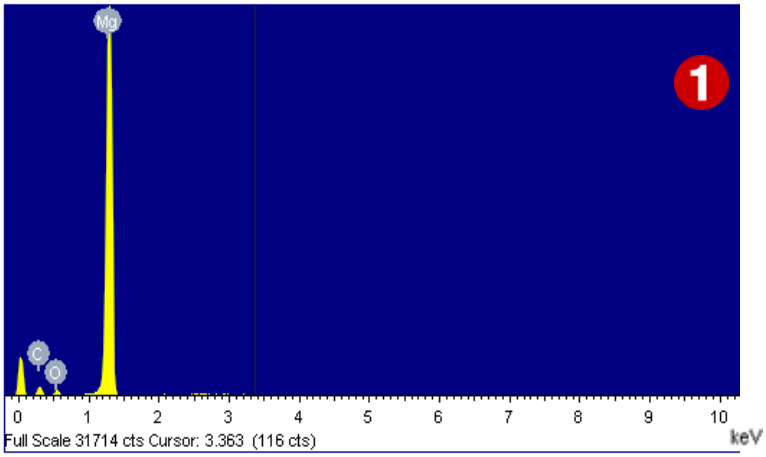

Element	Weight%	Atomic%
O K	6.09	8.97
Mg K	93.91	91.03
Totals	100.00	

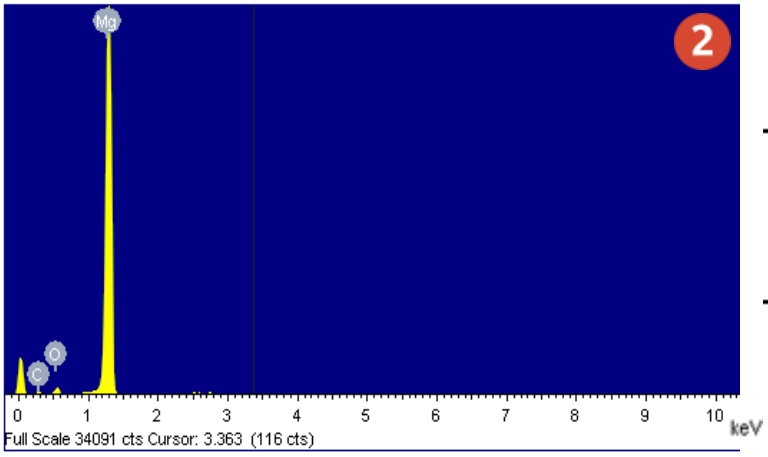

Element	Weight%	Atomic%
O K	6.89	10.10
Mg K	93.11	89.90
Totals	100.00	

Figure 3.44 EDX analysis of corrosion products for extruded super pure magnesium (E) after 480 hour immersion in SBF: **(a)** deposition of Ca and P **(b) 1:** unknown film **2:** sample surface next to the unknown film layer.

3.5 XRD Diffraction of Samples

5 samples from each type of sample were characterized by XRD (X-ray Diffraction) at different time intervals after immersion in SBF. The outcomes of the results for each type of sample were the same. Figures 3.45 to 3.49 show the X-ray diffraction results for various samples before and after immersion in SBF at different time intervals. Magnesium, as the only phase, was observed in all the samples (A, B, C, D and E) before immersion in SBF (Figures 3.45 to 3.49). Magnesium and Mg $(OH)_2$ were determined for all the cast samples, cast commercial pure magnesium ingot (A), more quickly solidified cast commercial pure magnesium (B) and more slowly solidified cast commercial pure magnesium (C), at different time intervals after immersion in SBF (Figures 3.45 to 3.47). For extruded samples including extruded commercial pure magnesium (D) and extruded super pure magnesium (E), magnesium was observed at different time intervals after immersion in SBF. But the presence of Mg $(OH)_2$ was only observed for extruded commercial pure magnesium (D) after 480 hour immersion in SBF, and for extruded super pure magnesium (E), the presence of Mg $(OH)_2$ was not observed at any time intervals after immersion in SBF (Figures 3.48 and 3.49).

In addition, Glancing Angle XRD on the surface of extruded super pure magnesium (E) was attempted after 1440 hour immersion in SBF. The results showed the presence of some phases other than magnesium on the surface. The presence of Mg, $CaCO_3$ and $CaCO_3.H_2O$ were confidently determined (Figure 3.50).

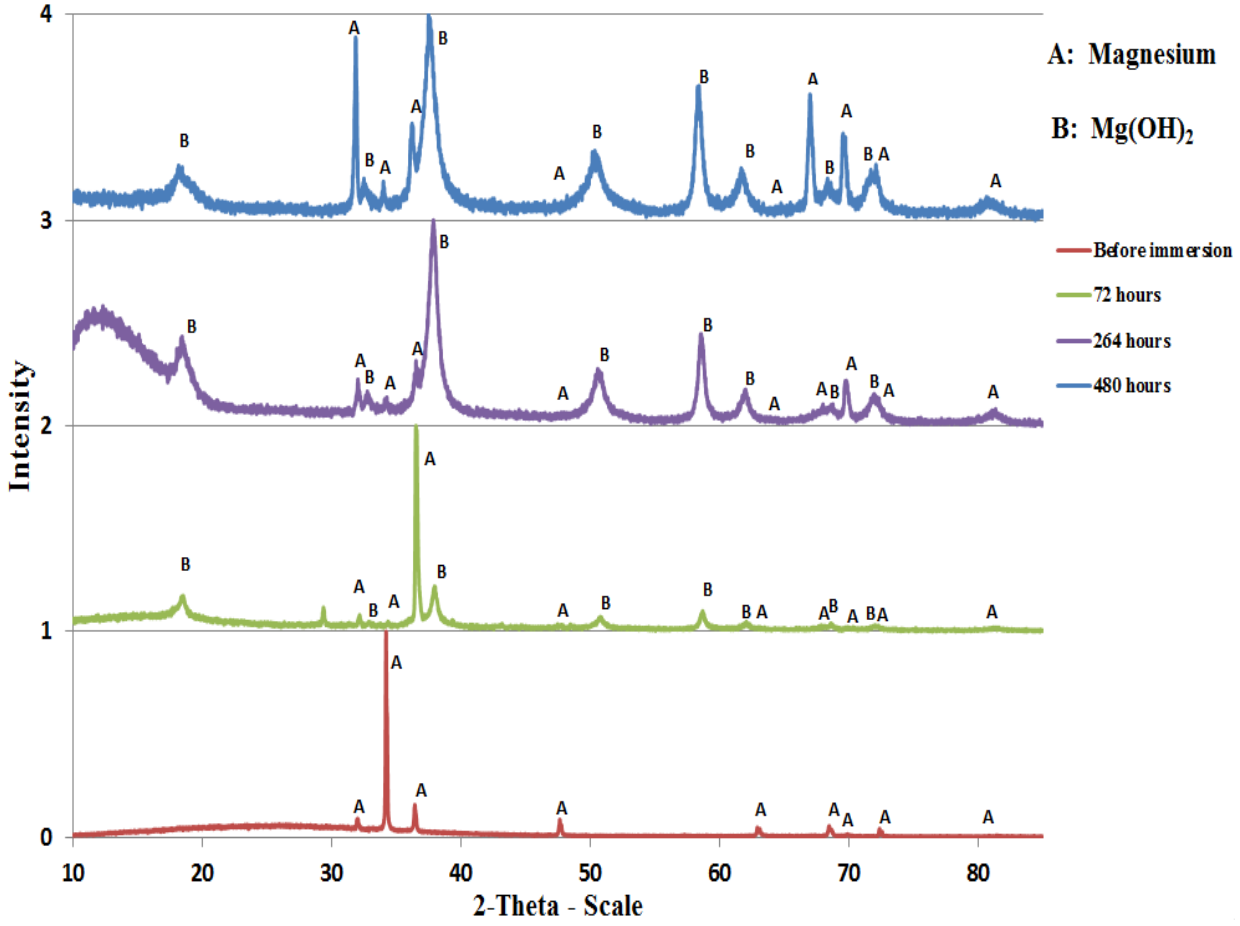

Figure 3.45 XRD diffraction of cast commercial pure magnesium ingot (A) before and after immersion in SBF at different time intervals.

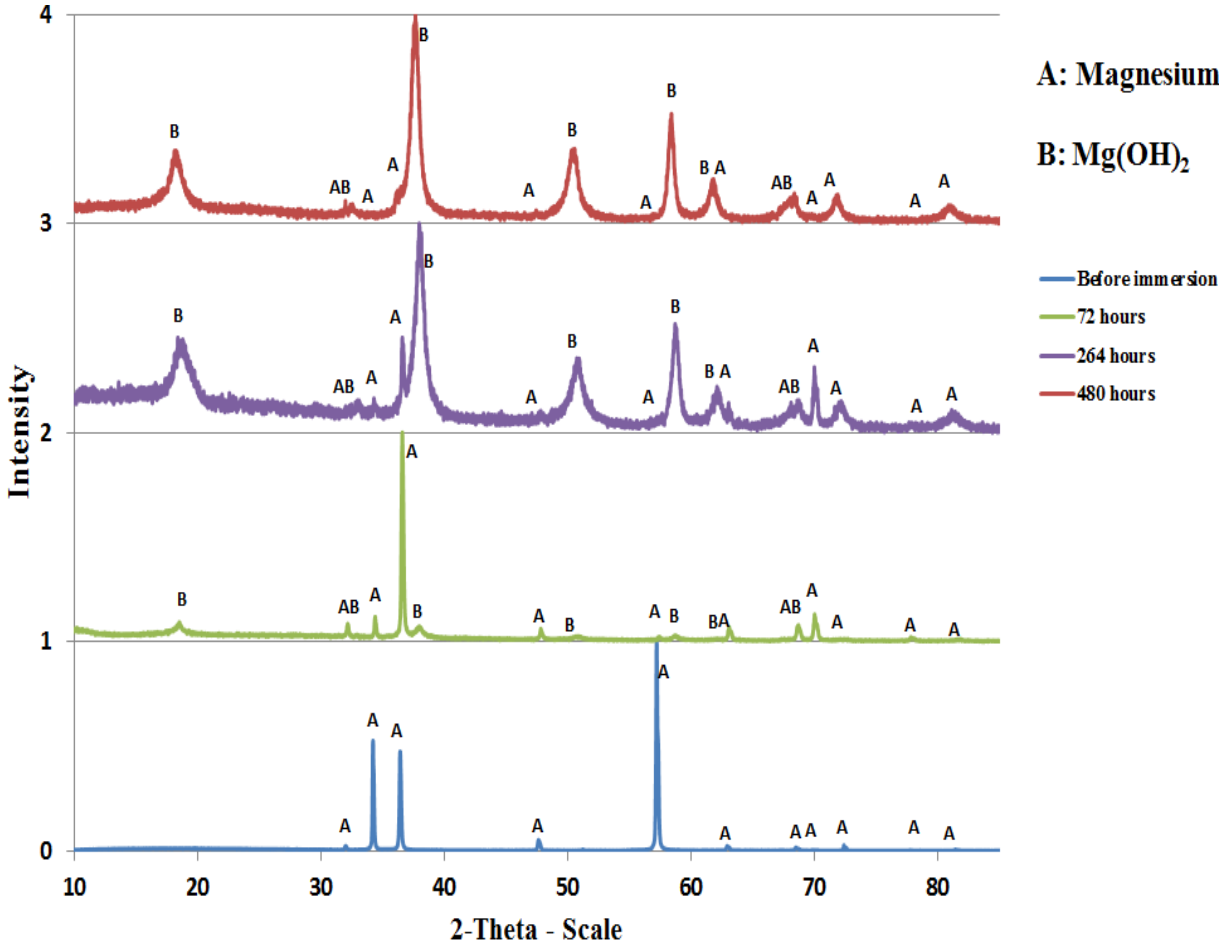

Figure 3.46 XRD diffraction of more quickly solidified cast commercial pure magnesium (B) before and after immersion in SBF at different time intervals.

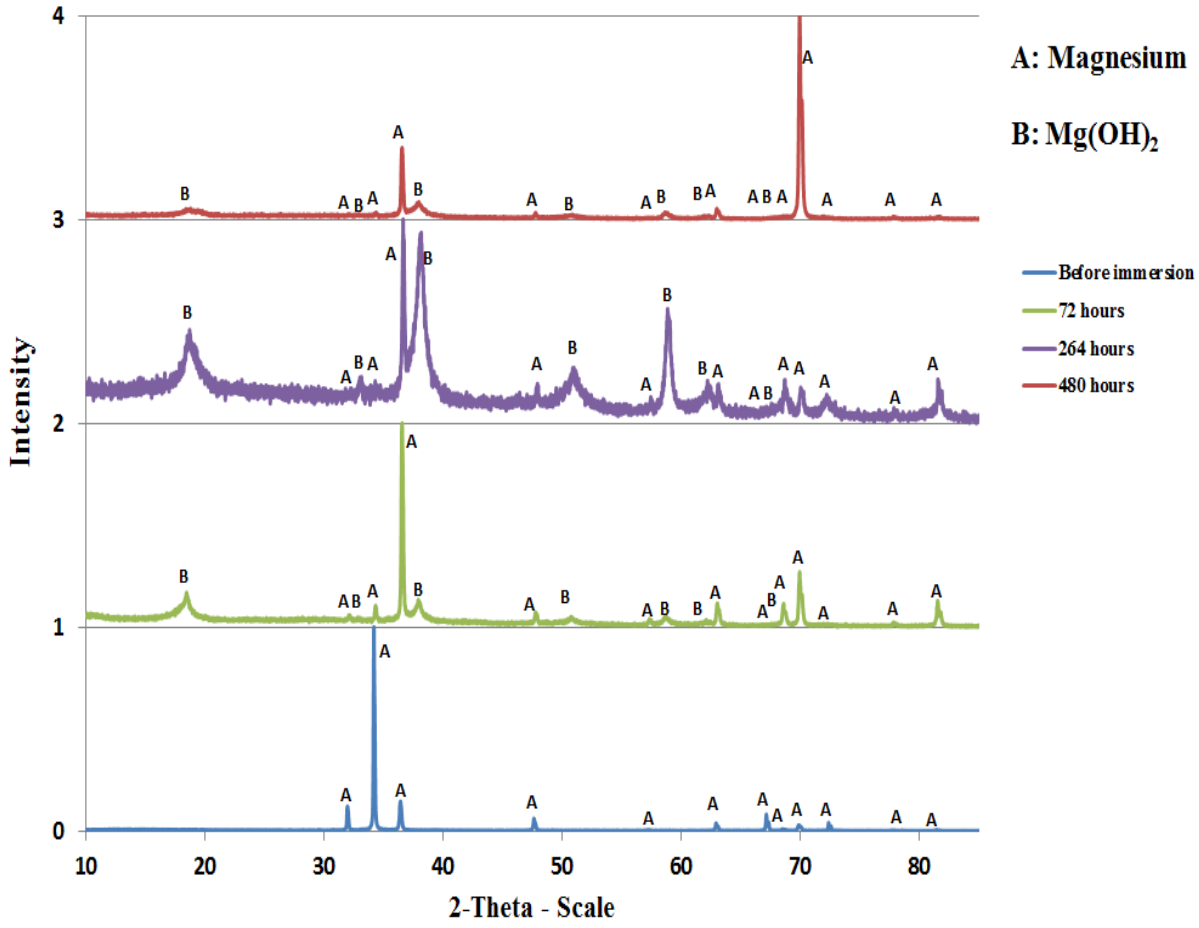

Figure 3.47 XRD diffraction of more slowly solidified cast commercial pure magnesium (C) before and after immersion in SBF at different time intervals.

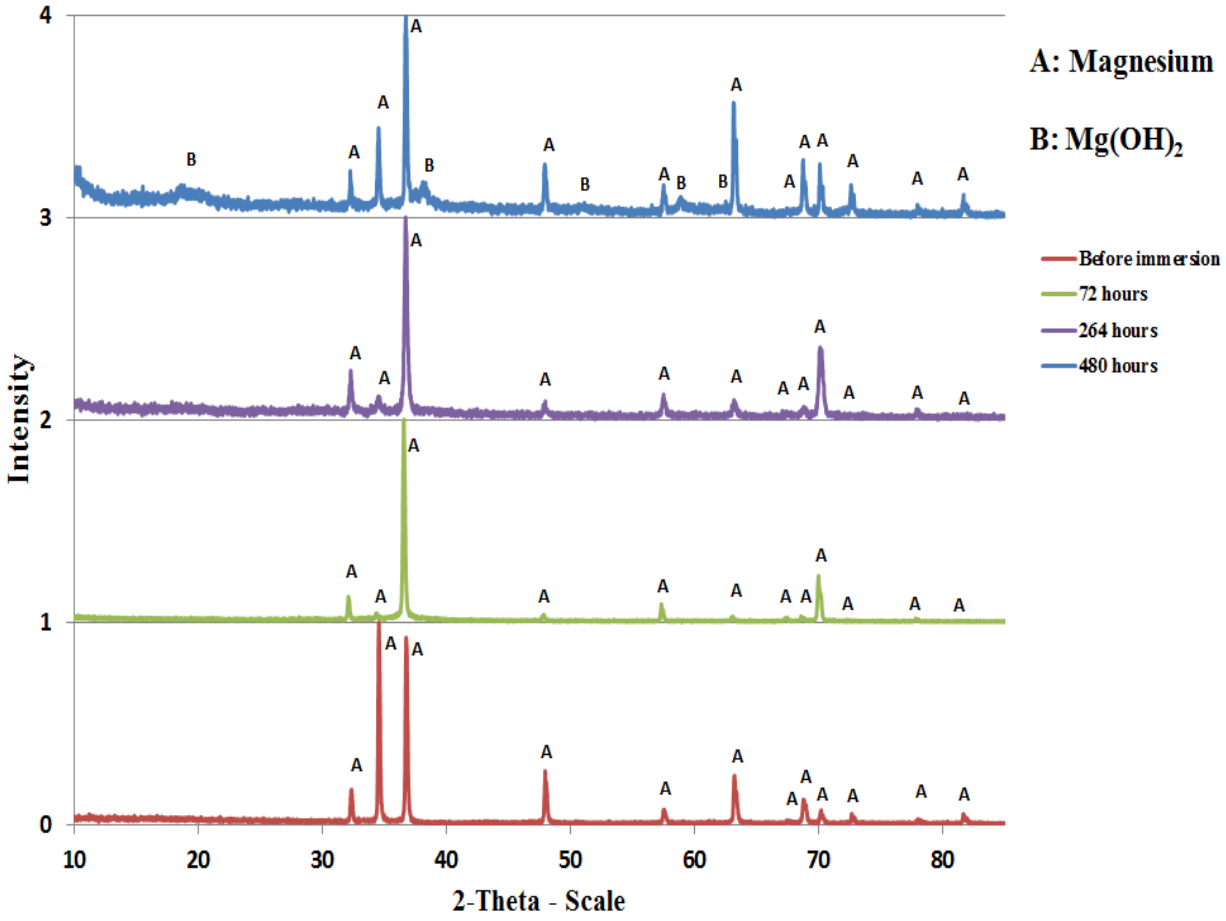

Figure 3.48 XRD diffraction of extruded commercial pure magnesium (D) before and after immersion in SBF at different time intervals.

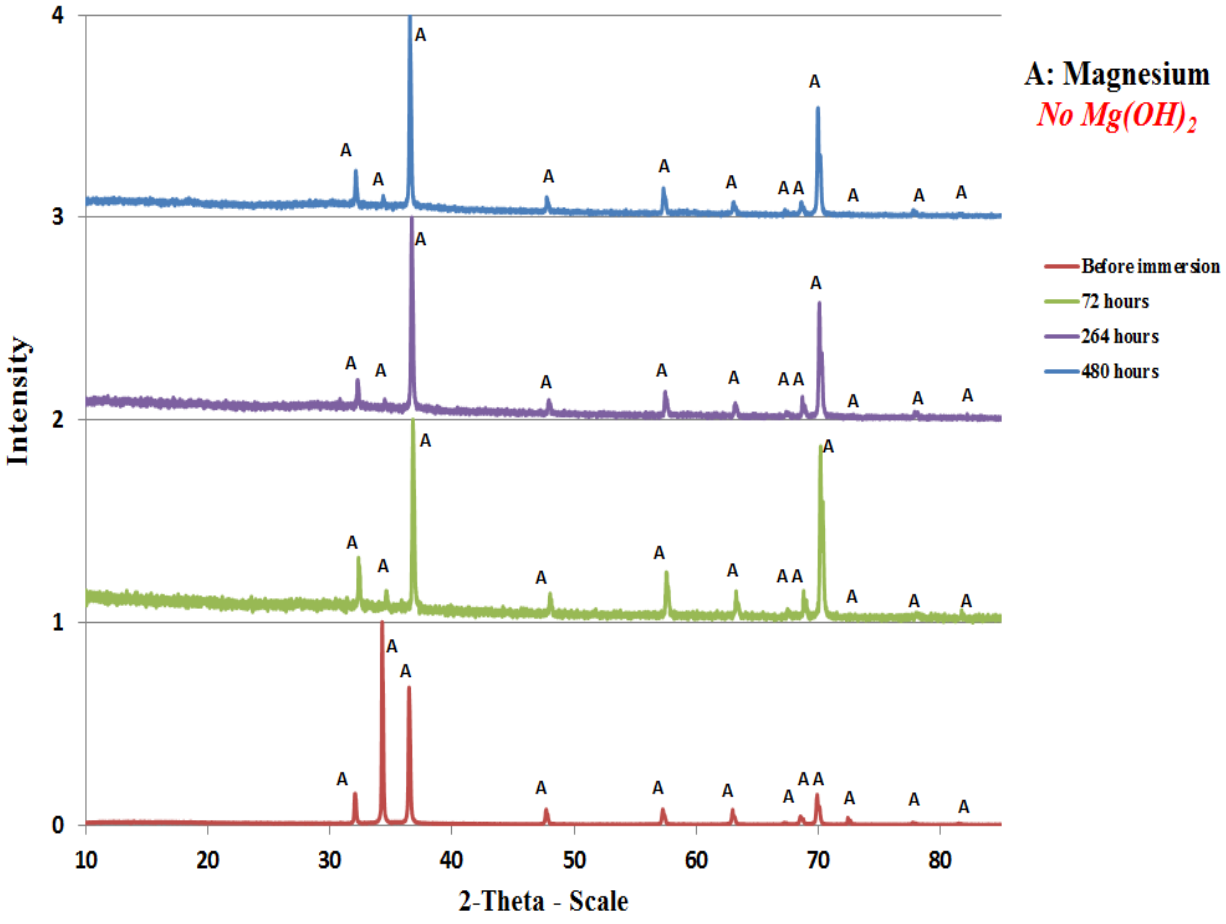

Figure 3.49 XRD diffraction of extruded super pure magnesium (E) before and after immersion in SBF at different time intervals.

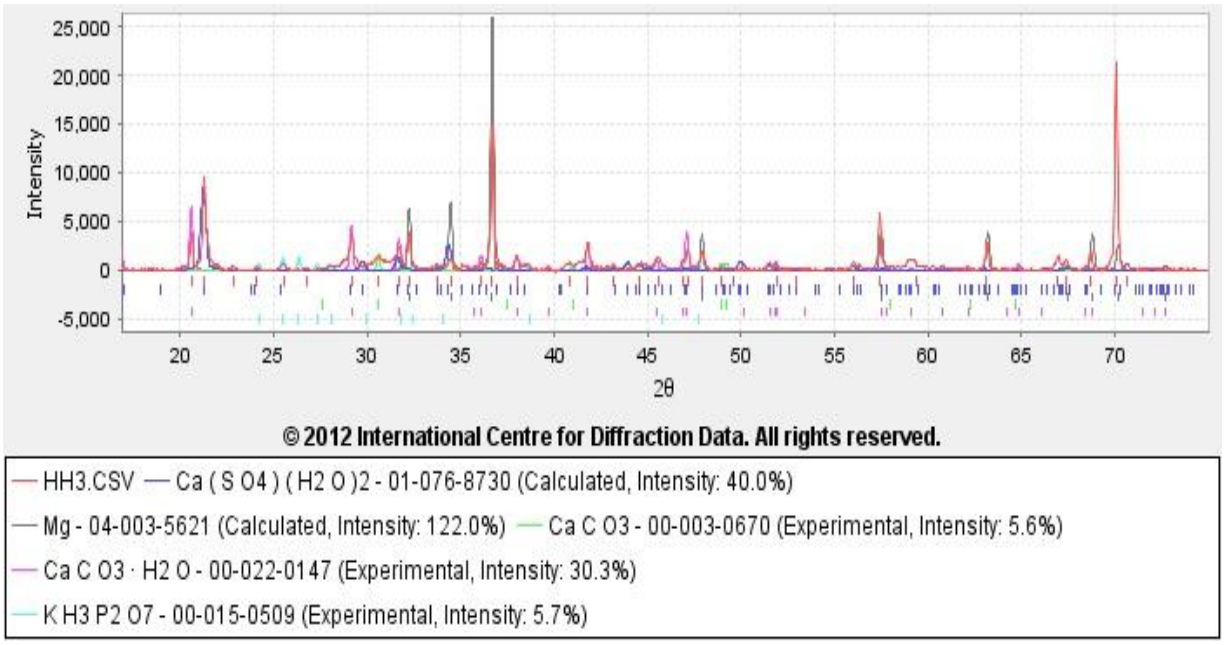

Figure 3.50 Glancing Angle XRD diffraction of extruded super pure magnesium (E) after 1440 hour immersion in SBF.

CHAPTER 4: Discussion

4.1 Corrosion behaviour of the samples

As was shown in figure 3.9, the order of the weight loss of the samples and their corrosion resistance was as follows:

Weight loss of samples: E < D < B < A < C

and

Corrosion resistance: E > D > B > A > C

The reason for this order in the corrosion behaviour of the various types of samples can stem from factors such as their intermetallic content and their distribution, the grain size and the presence of casting defects including porosity.

4.1.1 Intermetallics and their distribution

Although previous research has shown that intermetallics and their distribution play an important role in determining the corrosion behaviour of magnesium alloys [1, 3, 8, 49, 50], the corrosion behaviour of these samples was found to be independent of the intermetallics and their distribution because no large amounts of intermetallics were found due to the high purity of the alloys (Figures 3.30 to 3.40). In addition, the distribution of the few intermetallics found in these samples, was discontinuous. The solidification rate during casting and subsequent plastic deformation, are factors which affect the continuity of intermetallics considerably [50, 53, 57]. Increase in solidification rate leads to a more continuous distribution of intermetallics and higher corrosion resistance in magnesium alloys [50]. Plastic deformation lowers the continuity of intermetallics and reduces the corrosion of magnesium alloys [53, 57]. But, in these samples, where the amount of impurities or alloying elements is low, it does not affect the continuity of the intermetallics, whether the solidification rate is quick or slow

during casting. Also, when the amount of impurities or alloying elements is low, the continuity of the intermetallics will not be affected by plastic deformation either; because a low amount of impurities or alloying elements is not capable of forming considerable amount of intermetallics to form a continuous structure. For instance, Song indicated that an addition of 5% aluminium to a magnesium matrix led to a discontinuous distribution of β phase ($Mg_{17}Al_{12}$) and reduction of corrosion performance whereas an addition of 10% aluminium to magnesium resulted in a continuous distribution of β and improved the corrosion performance of the alloy [49].

Hence the distribution of intermetallics would always be discontinuous in commercial pure magnesium (A, B, C, D) and super pure magnesium (E). Regarding super pure magnesium (E), the possibility of formation of intermetallics is, of course, much lower compared to the commercial pure magnesium samples (A, B, C and D) because, on the one hand, the purity is higher and on the other hand, there is no iron present as an impurity in the composition of the super pure magnesium (99.95 wt% Mg; 0.02% Al, 0.02% Mn, 0.01 Si). The maximum solid solubility of iron in magnesium is very low (0.00043 at%), which increases the possibility of formation of α-Fe as an intermetallic [68], even if there is low amount of Fe as an impurity.

4.1.2 Grain size

To some extent, grain refining improves the corrosion behaviour of magnesium alloys [49, 54] because, in casting, refining the grains of magnesium alloys obtained by increase in solidification rate and the increase in solidification rate improves the segregation and leading to more continuous distribution of intermetallics which improves the corrosion performance [1, 49, 50, 54-56]. But, refining the grains of magnesium alloys via plastic deformation is different and reduces the corrosion resistance of magnesium alloys owing to the rearrangements of intermetallics caused by recrystallization [53, 57].

In fact, it is not grain size that affects the distribution of the intermetallics and the corrosion performance of magnesium alloys, it is the solidification rate and segregation or subsequent plastic deformation which can affect the continuity of intermetallics and the corrosion performance of

magnesium alloys. But as was mentioned before, the intermetallics and their distribution is not the main reason for such a difference in the corrosion behaviour of the samples (A, B, C, D and E). Hence, the difference in corrosion behaviour of the samples not only cannot be related to the intermetallics but also is not dependent on the grain size.

4.1.3 Porosity in casting

The main reason for such a difference in the corrosion behaviour of the samples (A, B, C, D and E) originates from the presence of porosity within the specimens.

In the cast samples (A, B and C), the corrosion performance was reduced with increased grain size. The more slowly solidified cast commercial pure magnesium (C) had the largest grain size among the cast samples (Figures 3.23 to 3.25) and showed the highest weight loss and lowest corrosion resistance among the cast samples after 480 hour immersion in SBF (Figure 3.9). The more quickly solidified cast commercial purity magnesium (B) had the finest grain size among the cast samples (Figures 3.23 to 3.25) and showed the lowest weight loss and highest corrosion resistance among the cast samples after 480 hour immersion in SBF (Figure 3.9). The cast commercial pure magnesium ingot (A) had a medium grain size among the cast samples (Figures 3.23 to 3.25) and showed a medium weight loss and corrosion resistance among the cast samples after 480 hour immersion in SBF (Figure 3.9). This does not mean the corrosion performance of the cast samples was related to the grain size. In fact, the difference in solidification rate led to such a corrosion performance in the cast samples (A, B and C). The increase in solidification rate during casting led to less and finer porosity in more quickly solidified sample (Figure 4.1- c), whereas, a decrease in solidification rate resulted in the formation of more and larger porosity in more slowly solidified sample (Figure 4.1-b). The presence of more porosity within the specimen makes the exposure area larger and consequently leads to more severe corrosion rate [49, 50].

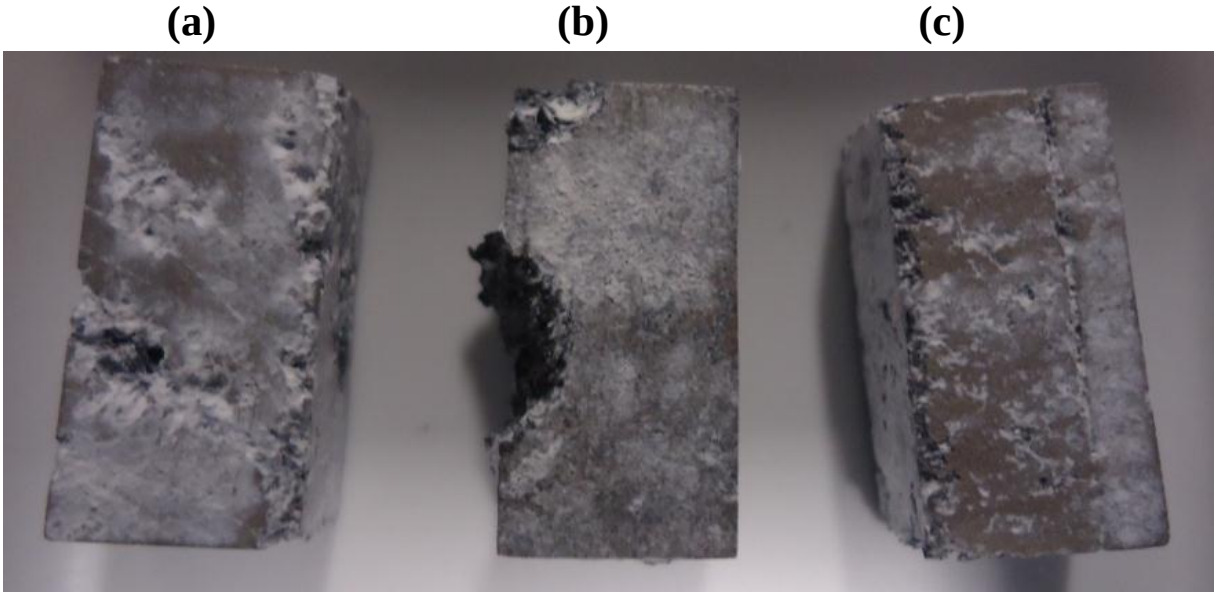

Figure 4.1 Presence of porosity in the cast samples after 72 hour immersion in SBF: **(a)** cast commercial pure magnesium ingot **(b)** more slowly solidified cast commercial pure magnesium **(c)** more quickly solidified cast commercial pure magnesium.

Regarding the extruded samples (D and E), since plastic deformation eliminates most of the casting defects, including porosity [59-61], the extruded samples showed a higher corrosion resistance compared to the cast samples (A, B and C). The weight loss of extruded samples (D and E) was about 7 to 20 times lower, compared to the cast samples (A, B and C), which indicated a higher corrosion resistance for the extruded samples (Figure 3.9). In addition, super pure sample (E) had a lower weight loss and higher corrosion resistance compared to the commercial purity sample (D) (Figure 3.9). This could be related to the higher purity of the E sample and no presence of Fe content in this sample. On the other hand, it can also be related to the finer grain size in this sample (E) compared to the D sample (Figures 3.26, 3.27). The Finer grain size in the super pure sample (E) was induced by plastic deformation and can eliminate more porosity within the sample compared to the commercial pure sample (D).

The important point is that the reduction in the grain size due to plastic deformation showed negative effects on corrosion behaviour of magnesium alloys and made it worse because of an increase in discontinuity of intermetallics [53, 57]. But, according to the results shown here, refining the grains by plastic deformation leads to an improvement of corrosion performance in the pure form of magnesium because there are no considerable amount of intermetallics to be affected by plastic deformation and in

fact plastic deformation only leads to reduction in porosity which increases the corrosion performance of the specimen.

4.2 An increase in weight with increased immersion time

An abnormal behaviour, an increase in weight with increased immersion time, occurred above a pH value of 9 for the cast samples (A_1, A_4 and B_5) and the super pure extruded samples (E_1, E_2 and E_5) (Figure 3.10 and Tables 4.1, 4.2).

There was no considerable loss in weight of the cast samples (A_1, A_4 and B_5) and the super pure extruded samples (E_1, E_2 and E_5) during 480 hour immersion in SBF (Table 4.1), which indicates a high corrosion resistance for these samples.

The highlighted points in table 4.1 show the start time of increase in weight of the samples and the highlighted points in table 4.2 are the pH values at those moments. The pH values increased to more than 9 during corrosion in SBF (Table 4.2), and an increase of pH to more than 9 caused more stability for the magnesium hydroxide formed on the corroded surface and made it more protective [10, 12]. Therefore, the combination of high corrosion resistance and increase in the stability of magnesium hydroxide layer led to an increase in weight with increased immersion time in the cast samples (A_1, A_4 and B_5). The same occurred for super pure extruded samples (E_1, E_2 and E_5) because this abnormal behaviour was also observed above pH 9 for these samples, although here a different film layer occurred on the surface, ($CaCO_3$), (See figure 3.50).

Table 4.1 The weight percentage of the samples, all of which had an increase in weight with increased immersion time, at different time intervals during immersion in SBF.

Sample / Time (h)	A_1	A_4	B_5	E_1	E_2	E_5
6	99.60	99.59	99.56	99.73	99.74	99.68
12	99.20	99.17	99.28	99.58	99.55	99.48
24	98.94	98.89	98.72	99.27	99.18	99.15
72	98.39	98.31	98.09	98.59	98.52	98.49
120	**98.00**	**97.83**	97.74	98.15	98.16	98.09
192	98.10	98.04	97.59	97.90	97.92	97.83
264	98.19	98.24	97.58	97.76	97.78	97.70
336	98.35	98.32	**97.58**	97.60	97.69	97.60
408	98.61	98.44	97.64	97.54	97.62	97.48
480	98.69	98.97	97.72	97.45	97.53	97.43
720	-	-	-	**97.37**	**97.46**	-
830	-	-	-	97.61	97.66	-
1368	-	-	-	-	-	**96.93**
1608	-	-	-	-	-	97.44

Table 4.2 pH values of the samples, all of which had an increase in weight with increased immersion time, at different time intervals during immersion in SBF.

Sample / Time (h)	A_1	A_4	B_5	E_1	E_2	E_5
6	8	8.04	8.08	8.07	8.1	8.08
12	8.14	8.15	8.29	8.17	8.23	8.18
24	8.21	8.23	8.51	8.39	8.46	8.36
72	8.76	8.84	9.16	8.83	8.93	8.81
120	9.11	9.13	9.34	9.07	9.18	9.11
192	9.45	9.53	9.61	9.38	9.42	9.42
264	9.74	9.76	9.64	9.5	9.57	9.48
336	9.72	9.77	9.43	9.37	9.5	9.37
408	9.67	9.72	9.35	9.42	9.43	9.39
480	9.56	9.65	9.4	9.39	9.44	9.36
720	-	-	-	9.32	9.36	-
1368	-	-	-	-	-	9.21

4.2.1 The difference between the abnormal behaviour (an increase in weight with increased immersion time) of cast samples (A_1, A_4 and B_5) and extruded super pure samples (E_1, E_2 and E_5)

Figure 3.10 shows that the increase in weight with increased immersion time happened earlier for the cast samples compared to the extruded samples. Also, the increase in weight with increased immersion time was greater in the cast samples compared to the extruded samples.

The weight loss of cast commercial pure magnesium ingot (A_1 and A_4), more quickly solidified cast commercial pure magnesium (B_5) and extruded super pure magnesium (E_1, E_2 and E_5), all of which had an increase in weight with increased immersion time, was not considerable during 480 hour immersion in SBF (Table 4.1), which indicated a high corrosion resistance for all of these 6 samples. Therefore, the reason for the difference between the abnormal behaviour of cast samples and extruded samples cannot be related to the corrosion performance of the samples, but this difference could stem from two different corrosion mechanisms in the cast samples (A_1, A_4 and B_5) and the extruded samples (E_1, E_2 and E_5). Unlike the cast samples, formation of magnesium hydroxide, which is an important part of the corrosion mechanism in magnesium alloys [10, 12, 13, 17-19], did not occur on the surface of super pure extruded sample (E) (Figure 3.49) and formation of phases, including $CaCO_3$, was observed instead of Mg $(OH)_2$ on the surface of sample (E) (Figure 3.50).

4.3 Greater uniformity of corrosion for extruded samples

The XRD (X-ray Diffraction) results indicated the presence of a magnesium hydroxide layer on the surface of all cast samples (A, B and C) and extruded commercial pure magnesium samples (D) during immersion in SBF (Figures 3.45 to 3.48). But the presence of Mg $(OH)_2$ was not observed on the surface of extruded super pure magnesium (E) at any time during immersion in SBF (Figure 3.49). The presence of white precipitates of Mg $(OH)_2$ not only was not observed on the surface of extruded super pure magnesium (Figure 3.49) but also was not observed within the solution (Figure 4.3-e). These results indicated that formation of magnesium hydroxide, which is an important part of the corrosion mechanism in magnesium alloys [10, 12, 13, 17-19] did not occur in the case of super pure

extruded sample (E). In addition, deposition of Mg $(OH)_2$ occurred very late on the surface of extruded commercial pure magnesium (D) compared to cast samples (A, B and C). The presence of Mg $(OH)_2$ was observed after 72 hour immersion in SBF for cast samples (Figures 3.45 to 3.47), whereas, for sample D it was observed only after 480 hour immersion in SBF (Figure 3.48) and the amount was much less compared to the cast samples (Figure 4.2 - a to d). Furthermore, the presence of white precipitates of Mg $(OH)_2$ within the extruded commercial pure magnesium (D) solution was not observed either (Figure 4.3-d).

Extrusion was therefore capable of eliminating or reducing the formation of magnesium hydroxide during corrosion of pure magnesium in SBF. In other words, extrusion can improve the uniformity of corrosion in pure magnesium samples by the reduction of a passive layer (magnesium hydroxide) on the surface. The formation of a passive layer on the specimen surface during corrosion is essential in order to cause pitting corrosion, which is the common type of localized corrosion in magnesium alloys [16, 17].

But Glancing Angle XRD indicated the formation of phases, including $CaCO_3$, on the surface of the super pure extruded sample (E) instead of Mg $(OH)_2$ (Figure 3.50), suggesting another type of passive layer. The $CaCO_3$ on the surface of super pure sample (E) did not seem to be similar to the Mg $(OH)_2$ on the surface of the rest of the samples (A, B, C and D) because Mg $(OH)_2$ formed as white precipitates but $CaCO_3$ was not in the form of precipitates on the surface of extruded super pure magnesium (E) (Figure 4.2). Hence, breakdown of passivity cannot occur in the same way as Mg $(OH)_2$ and it seems the breakdown of passivity for $CaCO_3$ was not as strong as Mg $(OH)_2$. Figure 4.2 indicates a higher uniformity in corrosion behaviour of extruded samples compared to cast samples. Also, the super pure sample indicated the most uniformity compared to all the rest of samples.

(a)

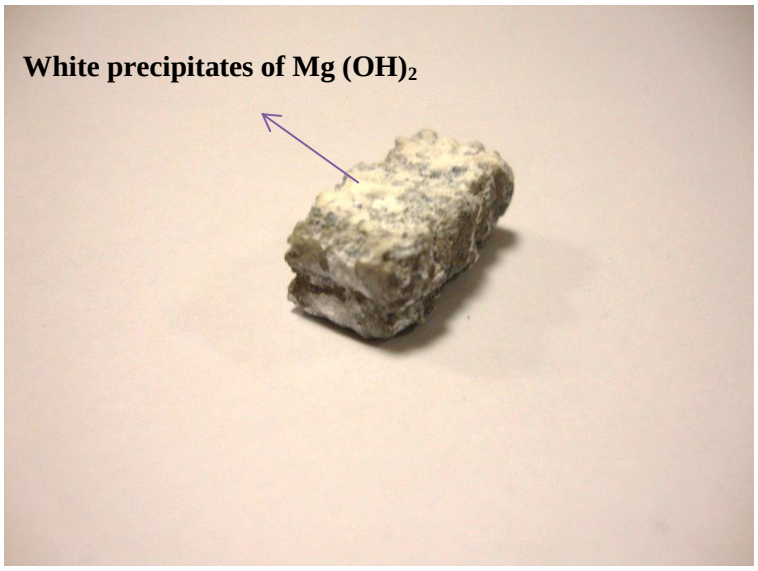
White precipitates of Mg (OH)2

(b)

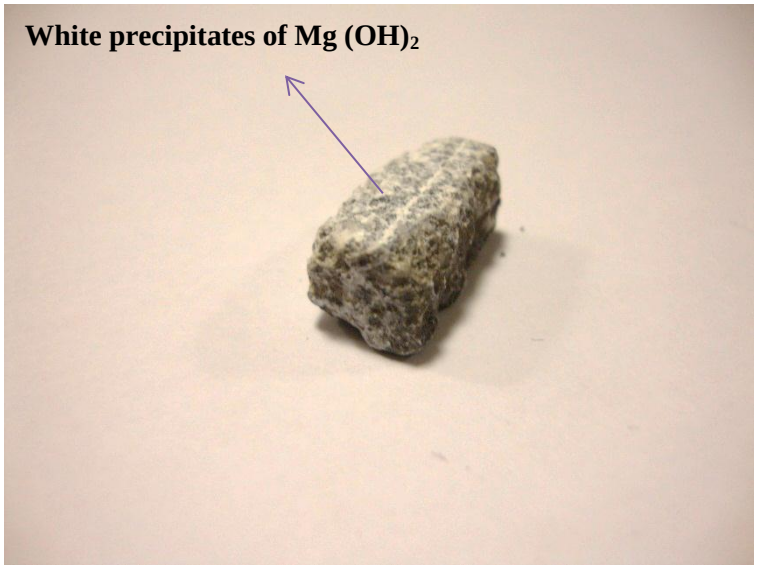
White precipitates of Mg (OH)2

(c)

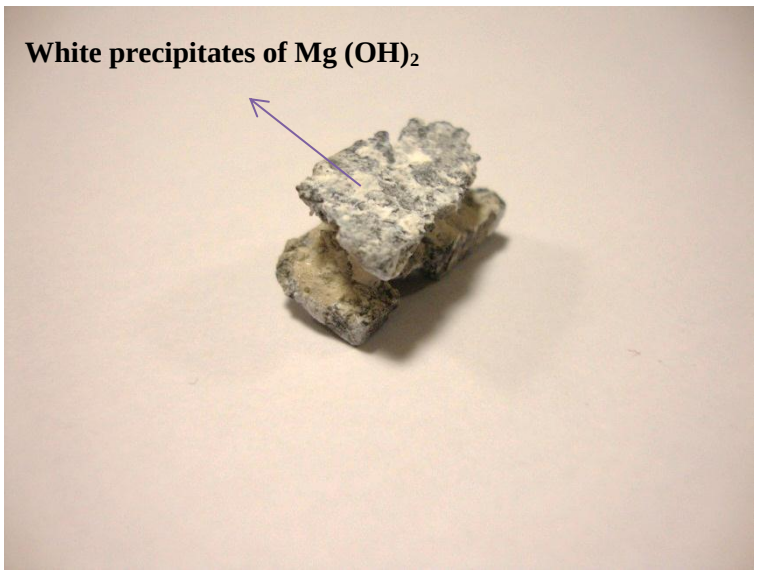
White precipitates of Mg (OH)2

(d)

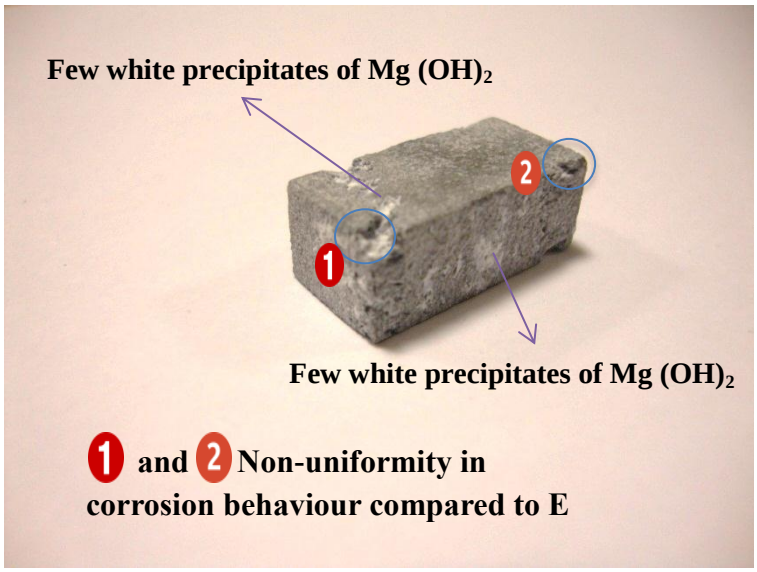

(e)

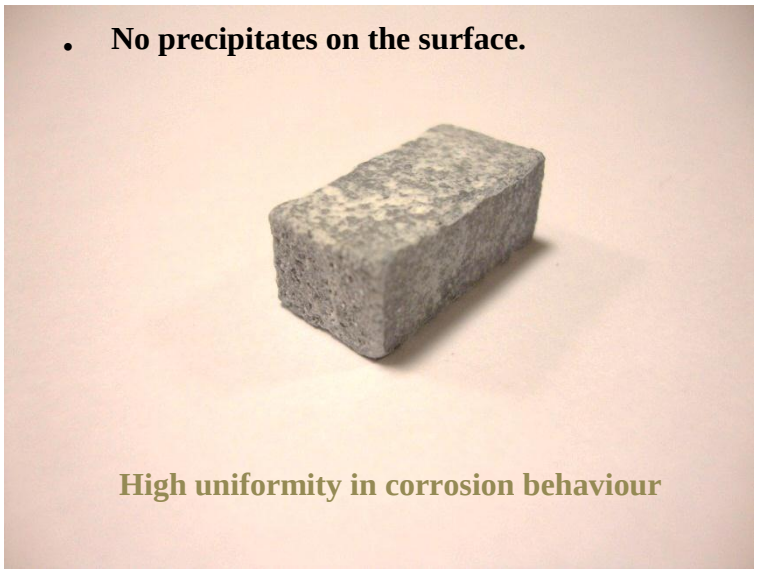

Figure 4.2 Various types of samples: **(a)** cast commercial pure magnesium ingot **(b)** More quickly solidified cast commercial pure magnesium **(c)** More slowly solidified cast commercial pure magnesium **(d)** Extruded commercial pure magnesium **(e)** Extruded super pure magnesium after 480 hour immersion in SBF.

(a)

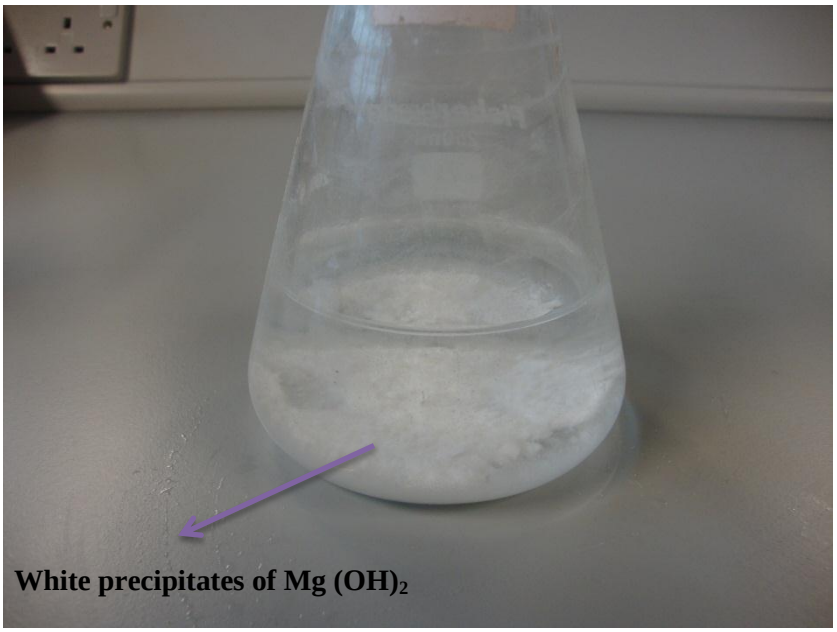
White precipitates of Mg (OH)2

(b)

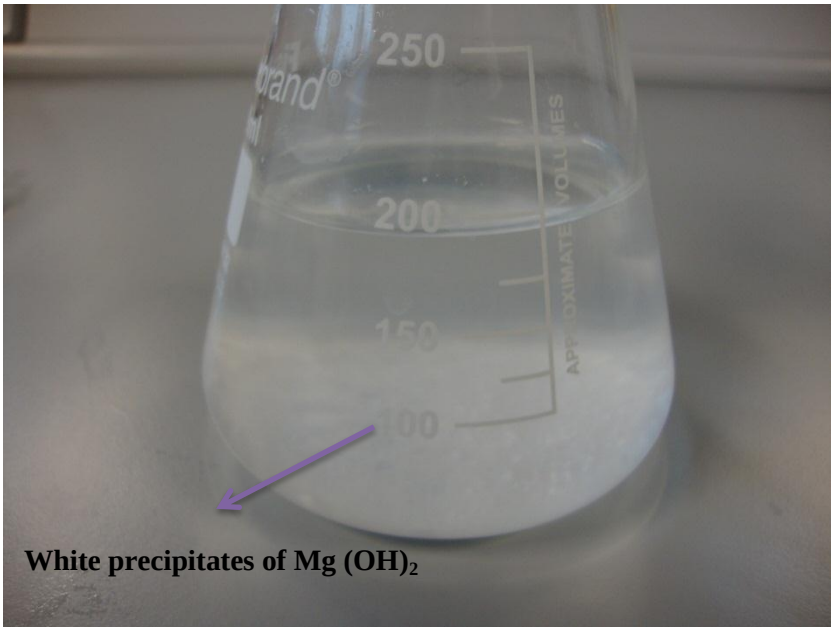
250
200
150
White precipitates of Mg (OH)2

(c)

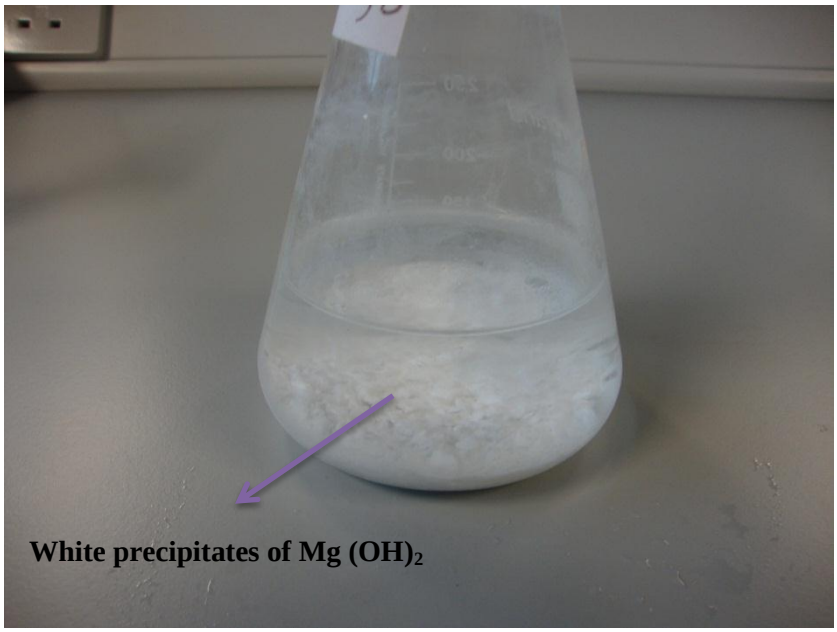
White precipitates of Mg (OH)2

(d)

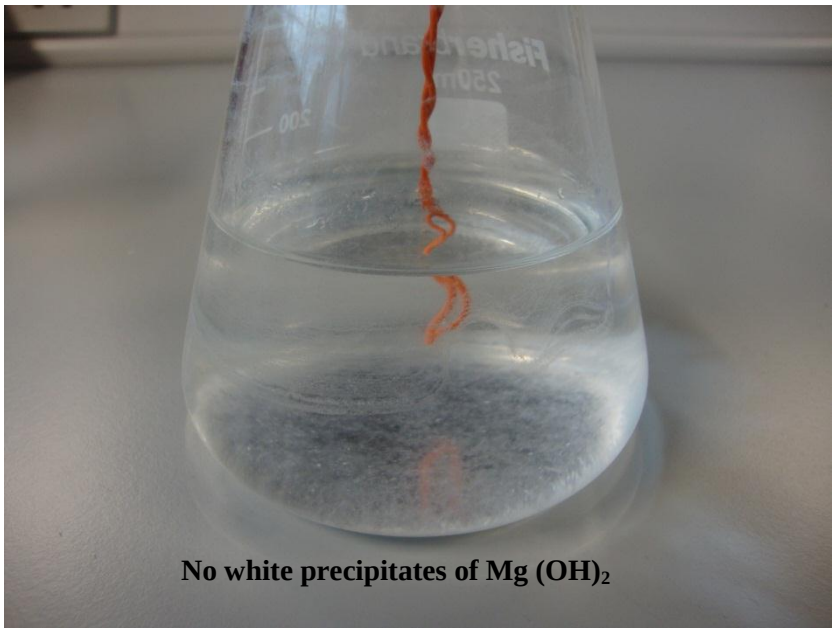

(e)

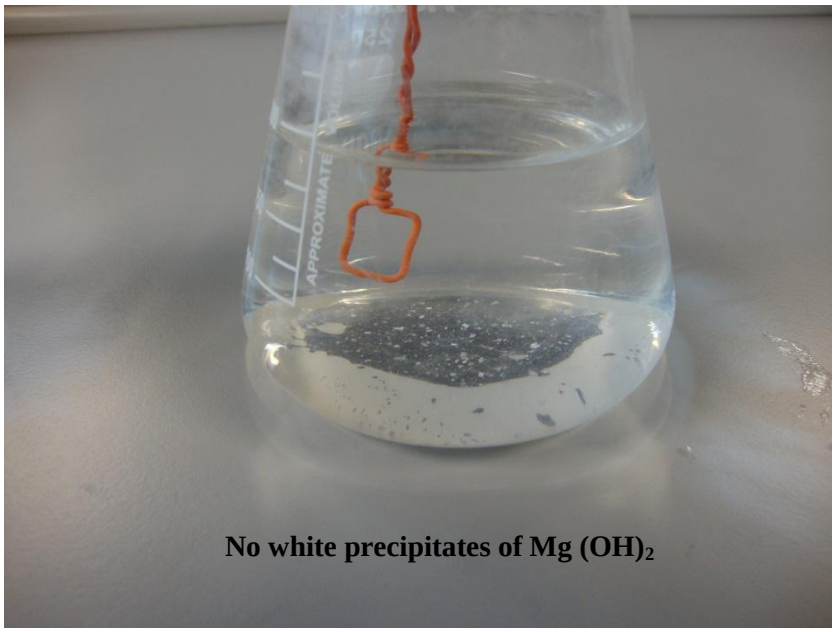

Figure 4.3 SBF solution for various types of samples: **(a)** cast commercial pure magnesium ingot **(b)** More quickly solidified cast commercial pure magnesium **(c)** More slowly solidified cast commercial pure magnesium **(d)** Extruded commercial pure magnesium **(e)** Extruded super pure magnesium after 480 hour immersion.

4.4 The effect of pH on the corrosion behaviour of magnesium

Increase in pH value *in vitro* (Table 4.2) and its effect on the passivity of formed layers on the surface of magnesium, which resulted in an increase in weight with increased immersion time (Figure 3.10), can lead to reflection of results which are not completely comparable with the *in vivo* results because there is no increase in the pH value *in vivo* and the pH value is almost constant in the human body [69], except at the first stages of implantation which the pH is variable and can drop to 5.5 [70]. Therefore, some researches tried to keep the pH constant *in vitro*, whether via changing the solution periodically [2, 71] or addition of buffers [72, 73], but none of these procedures does not seem to be efficient.

Changing the solution means changing the medium of the experiment and is not a correct procedure in order to keep the pH constant. Increase in pH *in vitro* occurs very quickly after a few hours of immersion in SBF [71] (Table 4.2). Hence, replacing the solution means running the experiments in a variable pH. For example, the pH value *in vitro* rises from 7.4 to 8.8 during corrosion and then it drops from 8.8 to 7.4 on changing the solution.

On the other hand, addition of buffers such as tris into the solution, in order to keep the pH constant, led to an increase in the corrosion rate of commercial pure magnesium [72].

But it seems there is a problem if the pH of the solution maintained constant *in vitro*. On the one hand, the corrosion rate of magnesium alloys *in vivo* has been reported to be slower than *in vitro* [74-76]. On the other hand, the pH of the solution increases during corrosion of magnesium *in vitro* and leads to a decrease in corrosion rate [66]. This indicates that, in spite of a reduction in corrosion rate *in vitro*, the corrosion rate is still higher *in vitro* compared to *in vivo*. Therefore, the corrosion rate measured in a constant pH condition could be further away from the expected corrosion rate in the human body, compared to when the corrosion rate is measured with an increased pH *in vitro*.

However, in spite of a reduction in corrosion rate *in vitro*, why is the corrosion rate *in vitro* still higher than *in vivo*?

The reason could be related to the blood circulation and accumulation of chloride ions. *In vivo*, the blood circulation prevents the accumulation of chloride ions on the specimen surface whereas there is no circulation of the solution *in vitro*. Therefore, the corrosion ions can accumulate on the surface of the specimen *in vitro* and increase the corrosion rate. It is very important to have a combination of constant pH and circulation of solution in order to obtain the results to be compared to *in vivo* results.

4.5 Release of magnesium ions

Figure 3.9 indicated less weight loss for the extruded samples (D and E) compared to the cast samples (A, B and C). But ion chromatography of solutions showed more release of ions for the extruded samples which was strange (Figure 3.22). The reason could be related to the formation of magnesium hydroxide precipitates. For cast samples (A, B and C), magnesium hydroxide partly precipitated on the surface of the samples (Figure 4.2 - a to c) and partly entered into the solution (Figure 4.3 - a to c). But, for extruded samples (D and E), only few precipitates of Mg $(OH)_2$ observed on the surface of extruded commercial pure magnesium (D) (Figure 4.2 - d). Therefore, for cast samples, a high amount of magnesium ions were stuck within the white precipitates of Mg $(OH)_2$ and could not enter into the solution. Therefore, it was not possible to measure the release of all the magnesium ions by ion chromatography for cast samples. Regarding the extruded samples (D and E), all the magnesium ions entered into the solution and measured by ion chromatography and that is why more release of magnesium ions observed for extruded samples.

4.6 Summary

The corrosion behaviour of samples was found to be independent of the intermetallics, their distribution and the grain size. The main reason for such a difference in the corrosion behaviour of the samples (A, B, C, D and E) was related to the presence of porosity within the specimens. Since plastic deformation eliminates most of the casting defects including porosity, the extruded samples showed a higher corrosion resistance compared to the cast samples (A, B and C).

Regarding the cast samples (A, B and C), increase in solidification rate during casting led to less and finer porosity (B), whereas, a decrease in solidification rate resulted in more and larger porosity (C). The presence of more porosity within the specimen (C) made the exposure area larger and led to more severe corrosion.

Extrusion is not only capable of eliminating or reducing the porosity but also is capable of eliminating or reducing the formation of magnesium hydroxide during corrosion of pure magnesium in SBF. Therefore, extrusion can improve the uniformity of corrosion in pure magnesium in both ways. That is why higher uniformity in corrosion behaviour of the extruded samples (D and E) was observed compared to the cast samples (A, B and C).

In spite of reduction of corrosion rate in vitro owing to increased pH, corrosion rate is still higher *in vitro* compared to *in vivo,* which might be related to the accumulation of corrosive ions on the sample surface *in vitro.* Therefore, corrosion behaviour in the constant pH condition could be a value further away from the expected corrosion rate in the human body compared to increased pH *in vitro*. Furthermore, Increase in pH value *in vitro* and its effect on the passivity of formed layers on the surface of magnesium, which resulted in an increase in weight with increased immersion time in some samples (A_1, A_4, B_5, E_1, E_2 and E_5), can lead to reflection of results which are not completely comparable with the *in vivo* results. Therefore, it is very important to have a combination of constant pH and circulation of solution in order to obtain the results which are completely comparable to *in vivo* results.

For cast samples (A, B and C), a high amount of magnesium ions were stuck within the white precipitates of Mg $(OH)_2$ and could not enter into the solution. Hence, it was not possible to measure the release of all the magnesium ions inside their solutions by ion chromatography. That is why less release of magnesium ions observed for the cast samples (A, B and C), in spite of the fact that they had lower corrosion resistance compared to the extruded samples (D and E).

CHAPTER 5: Conclusions

The corrosion behaviour of 5 types of samples; cast commercial pure magnesium ingot (A), more quickly solidified cast commercial pure magnesium (B), more slowly solidified cast commercial pure magnesium (C), extruded commercial pure magnesium (D) and extruded super pure magnesium (E), was studied in immersion tests during 480 hour immersion in SBF. Weight loss, pH changes and the release of magnesium ions was measured. Furthermore, SEM, EDX and XRD were conducted on the surface of the specimens in order to characterize the corrosion products. The following conclusions were drawn:

1) Extruded super pure magnesium (E) had the lowest weight loss of about 2.56 wt% after 480 hour immersion (3 weeks) in SBF and also had the highest reproducibility amongst all the samples at every time interval during the 480 hour immersion. Furthermore, it showed the highest uniformity in corrosion behaviour after 480 hour immersion in SBF.

2) The corrosion behaviour of samples was found to be independent of the intermetallics and their distribution.

3) The extruded samples (D and E) showed a higher corrosion resistance compared to the cast samples (A, B and C). The main reason for such a difference in the corrosion behaviour of the samples originated from the presence of porosity within the specimens. Refining the grains of pure magnesium by plastic deformation led to elimination of porosity which is in favour of corrosion performance of the specimen.

4) The presence of more and larger porosity within the specimen makes the exposure area larger and consequently leads to more severe corrosion.

5) Formation of magnesium hydroxide, which is an important part of the corrosion mechanism in magnesium alloys, did not occur for super pure extruded sample (E). Also, formation of magnesium hydroxide occurred very late for commercial purity extruded sample (D). This meant that the extruded samples E and D had the most uniform corrosion, respectively, due to the absence of magnesium hydroxide.

6) During the *in vitro* experiment there was an increase in pH. In spite of the reduction of corrosion rate *in vitro,* because of this increased pH, the corrosion rate was still higher *in vitro* compared to *in vivo,* which might be related to the accumulation of corrosive ions on the sample surface *in vitro.* Therefore, the corrosion rate in a constant pH condition could be further away from the expected corrosion rate in the human body than the corrosion rate associated with an increased pH *in vitro*.

7) It is very important to have a combination of constant pH and circulation of solution in order to obtain results which are completely comparable to *in vivo* results.

CHAPTER 6: Future work

The effect of casting, solidification rate and extrusion was studied on the corrosion behaviour of commercial pure magnesium (> 99.5 wt% Mg) but the corrosion behaviour of super pure magnesium with higher purity (99.95 wt% Mg; 0.02% Al, 0.02% Mn, 0.01 Si) was only studied in extruded form. The corrosion behaviour of samples was mainly related to the porosity and not the intermetallics but the effect of casting and solidification rate on the corrosion performance of super pure magnesium can be studied in order to observe whether higher purity in super pure magnesium can play a key role in the corrosion behaviour or not.

A considerable corrosion resistance and uniformity of corrosion was achieved for extruded super pure sample (E) and the role of plastic deformation was very remarkable for this achievement but plastic deformation imposes high costs on the industry. Therefore, it would be worthy to change the casting design instead of doing plastic deformation in order to reduce porosity and have the favourable corrosion performance, reproducibility and uniformity of corrosion. For instance, instead of doing gravity die-casting which the melt will be injected into the mould from the top, the injection of melt into the mould could be applied from the bottom of the mould.

Also, other corrosion measurements can be applied in order to study the corrosion behaviour of magnesium samples such as hydrogen evolution test and electrochemical tests including Tafel and Electrochemical Impedance Spectroscopic (EIS) experiments. However, electrochemical tests does not seem to be quite useful for measuring the corrosion behaviour of magnesium because of the abnormal electrochemical behaviour of magnesium and the Negative Difference Effect (NDE) in this metal. In addition, it would be useful to investigate the mechanical properties of all the samples because it can be find out whether super pure extruded sample (E) is capable of indicating the highest mechanical integrity or not among all the samples as it presented the highest corrosion resistance, reproducibility and uniformity among them.

References

1. Alvarez-Lopez, M., M. Dolore Pereda, *J.A. del Valle, M. Fernandez-Lorenzo, M.C. Garcia-Alonso,* O.A. Ruano and M.L. Escudero, *Corrosion behaviour of AZ31 magnesium alloy with different grain sizes in simulated biological fluids.* Acta Biomater, 2010. **6**(5): p. 1763-71.

2. Song, Y., D. Shan, R. Chen, F. Zhang and E-H. Han, *Biodegradable behaviors of AZ31 magnesium alloy in simulated body fluid.* Materials Science and Engineering: C, 2009. **29**(3): p. 1039-1045.

3. Wen, Z., C. Wu, C. Dai and F. Yang, *Corrosion behaviors of Mg and its alloys with different Al contents in a modified simulated body fluid.* Journal of Alloys and Compounds, 2009. **488**(1): p. 392-399.

4. Staiger, M.P., A. M. Pietak, J. Huadmai and G. Dias, *Magnesium and its alloys as orthopedic biomaterials: a review.* Biomaterials, 2006. **27**(9): p. 1728-34.

5. Xin, Y., T. Hu, and P.K. Chu, *In vitro studies of biomedical magnesium alloys in a simulated physiological environment: a review.* Acta Biomater, 2011. **7**(4): p. 1452-9.

6. Candan, S., M. Unal, E. Koc, Y. Turen and E. Candan, *Effects of titanium addition on mechanical and corrosion behaviours of AZ91 magnesium alloy.* Journal of Alloys and Compounds, 2011. **509**(5): p. 1958-1963.

7. Li, Z., X. Gu, S. Lou and Y. Zheng, *The development of binary Mg-Ca alloys for use as biodegradable materials within bone.* Biomaterials, 2008. **29**(10): p. 1329-44.

8. Kannan, M.B., *Influence of microstructure on the in-vitro degradation behaviour of magnesium alloys.* Materials Letters, 2010. **64**(6): p. 739-742.

9. Song, Y., E-H. Han, D. Shan, C. D. Yim and B. S. You, *The role of second phases in the corrosion behavior of Mg–5Zn alloy.* Corrosion Science, 2012. **60**: p. 238-245.

10. Song, G. and A. Atrens, *Corrosion Mechanisms of Magnesium Alloys.* Advanced Engineering Materials, 1999. **1**(1): p. 11-33.

11. Eliezer, D. and H. Alves, *Corrosion and Oxidation Of Magnesium Alloys*, in *Handbook of Materials Selection*, M. Kutz, Editor 2002, John Wiley & Sons: New York. p. 267-291.

12. Makar, G.L. and J. Kruger, *Corrosion of magnesium.* International Materials Reviews, 1993. **38**(3): p. 138-153.

13. Song, G. and A. Atrens, *Understanding Magnesium Corrosion.* Advanced Engineering Materials, 2003. **5**(12): p. 837-858.

14. Song, Y., D. Shan, R. Chen and E-H. Han, *Effect of second phases on the corrosion behaviour of wrought Mg–Zn–Y–Zr alloy.* Corrosion Science, 2010. **52**(5): p. 1830-1837.

15. Avner, S.H., *Corrosion of Metals*, in *Introduction to Physical Metallurgy*, R. Buchanan and M.W. Breskin, Editors. 1974, McGraw-Hill: New York. p. 583-603.

16. Strehblow, H.-H., *mechanisms of pitting corrosion* in *Corrosion Mechanisms in Theory and Practice*, p. Marcus and j. oudar, Editors. 1995, Marcel Dekker, Inc.: New York. p. 201-237.

17. Zeng, R.-c., Z. Jin, H. Wei-jiu, W. Dietzel, K. U. Kainer, C. Blawert and K. Wei, *Review of studies on corrosion of magnesium alloys.* Transactions of Nonferrous Metals Society of China, 2006. **16**: p. s763-s771.

18. Song, G. and A. Atrens, *Recent Insights into the Mechanism of Magnesium Corrosion and Research Suggestions.* Advanced Engineering Materials, 2007. **9**(3): p. 177-183.

19. Ghali, E., W. Dietzel, and K.-U. Kainer, *General and Localized Corrosion of Magnesium Alloys: A Critical Review.* Journal of Materials Engineering and Performance, 2004. **13**(1): p. 7-23.

20. Fruhwirth, O., G. W. Herzog, I. Hollerer and A. Rachetti, *Dissolution and hydration kinetics of MgO.* Surface Technology, 1985. **24**: p. 301-317.

21. Ackerman, H., et al., *Corrosion*, in *ASM Handbook*, J.D. Destefani, et al., Editors. 1987, ASM International: United States of America. p. 1432 pages, 2400 illustrations, over 600 tables, ISBN 0-87170-007-7.

22. Bobby Kannan, M., W. Dietzel, R.K. Singh Raman and P. Lyon, *Hydrogen-induced-cracking in magnesium alloy under cathodic polarization.* Scripta Materialia, 2007. **57**(7): p. 579-581.

23. Bobby Kannan, M., W. Dietzel, C. Blawert, A. Atrens and P. Lyon, *Stress corrosion cracking of rare-earth containing magnesium alloys ZE41, QE22 and Elektron 21 (EV31A) compared with AZ80.* Materials Science and Engineering: A, 2008. **480**(1-2): p. 529-539.

24. Song, R.G., C. Blawert, W. Dietzel and A. Atrens, *A study on stress corrosion cracking and hydrogen embrittlement of AZ31 magnesium alloy.* Materials Science and Engineering: A, 2005. **399**(1-2): p. 308-317.

25. Ben-Hamu, G., D. Eliezer, W. Dietzel and K.S. Shin, *Stress corrosion cracking of new Mg–Zn–Mn wrought alloys containing Si.* Corrosion Science, 2008. **50**(5): p. 1505-1517.

26. Bobby Kannan, M. and R.K. Singh Raman, *Evaluating the stress corrosion cracking susceptibility of Mg–Al–Zn alloy in modified-simulated body fluid for orthopaedic implant application.* Scripta Materialia, 2008. **59**(2): p. 175-178.

27. Choudhary, L. and R.K. Raman, *Magnesium alloys as body implants: fracture mechanism under dynamic and static loadings in a physiological environment.* Acta Biomater, 2012. **8**(2): p. 916-23.

28. Kannan, M.B. and R.K. Raman, *In vitro degradation and mechanical integrity of calcium-containing magnesium alloys in modified-simulated body fluid.* Biomaterials, 2008. **29**(15): p. 2306-14.

29. Xin, Y., K. Huo, H. Tao, G. Tang and P. K. Chu, *Influence of aggressive ions on the degradation behavior of biomedical magnesium alloy in physiological environment.* Acta Biomater, 2008. **4**(6): p. 2008-15.

30. Bombara, G. and M. cavallini, *STRESS CORROSION CRACKING OF BONE IMPLANTS.* Corrosion Science, 1977. **17**: p. 77-85.

31. Teoh, S.H., *Fatigue of biomaterials: a review.* International Journal of Fatigue, 2000. **22**: p. 825-837.

32. Akahori, T., M. Niinomi, K-I Fukunaga and I. Inagaki, *Effects of Microstructure on the Short Fatigue Crack Initiation and Propagation Characteristics of Biomedical α/β Titanium Alloys.* Metallurgical and Materials Transactions A, 2000. **31A**: p. 1949-1958.

33. Gu, X.N., W.R. Zhou, Y.F. Zheng, Y. Cheng, S.C. Wei, S.P. Zhong, T.F. Xi and L.J. Chen, Corrosion *fatigue behaviors of two biomedical Mg alloys - AZ91D and WE43 - In simulated body fluid.* Acta Biomater, 2010. **6**(12): p. 4605-13.

34. Bhuiyan, M.S., Y. Mutoh, T. Murai and S. Iwakami, *Corrosion fatigue behavior of extruded magnesium alloy AZ80-T5 in a 5% NaCl environment.* Engineering Fracture Mechanics, 2010. **77**(10): p. 1567-1576.

35. Witte, F., N. Hort, C. Vogt, S. Cohen, K. U. Kainer, R. Willumeit and F. Feyerabend, *Degradable biomaterials based on magnesium corrosion.* Current Opinion in Solid State and Materials Science, 2008. **12**(5-6): p. 63-72.

36. El-Rahman, S., *Neuropathology of aluminum toxicity in rats (glutamate and GABA impairment).* Pharmacological Research, 2003. **47**(3): p. 189-194.

37. Ku, C.-H., D. P. Pioletti, M. Browne and P. J. Gregson, *Effect of different Ti–6Al–4V surface treatments on osteoblasts behaviour.* Biomaterials, 2002. **23**: p. 1447-1454.

38. Zhang, S., X. Zhang, C. Zhao, J. Li, Y. Song, C. Xie, H. Tao, Y. Zhang, Y. He, Y. Jiang and Y. Bian, Re*search on an Mg-Zn alloy as a degradable biomaterial.* Acta Biomater, 2010. **6**(2): p. 626-40.

39. Song, G., *Control of biodegradation of biocompatable magnesium alloys.* Corrosion Science, 2007. **49**(4): p. 1696-1701.

40. Wan, Y., G. Xiong, H. Luo, F. He, Y. Huang and X. Zhou, *Preparation and characterization of a new biomedical magnesium–calcium alloy.* Materials & Design, 2008. **29**(10): p. 2034-2037.

41. Wu, G., Y. Fan, H. Gao, C. Zhai and Y. P. Zhu, *The effect of Ca and rare earth elements on the microstructure, mechanical properties and corrosion behavior of AZ91D.* Materials Science and Engineering: A, 2005. **408**(1-2): p. 255-263.

42. Qudong, W., C. Wenzhou, Z. Xiaoqin, L. Yizhen, D. Wenjiang, Z. Yanping and X. Xiaoping, *Effects of Ca addition on the microstructure and mechanical properties of AZ91magnesium alloy.* Materials science, 2001. **36**: p. 3035-3040.

43. Zhou, W., N.N. Aung, and Y. Sun, *Effect of antimony, bismuth and calcium addition on corrosion and electrochemical behaviour of AZ91 magnesium alloy.* Corrosion Science, 2009. **51**(2): p. 403-408.

44. Neite, G., et al., *Magnesium-Based Alloys*, in *Materials Science and Technology*, R.W. Cahn, P. Haasen, and E.J. Kramer, Editors. 1996, VCH Publishers Inc.: Weinheim: New York. p. 113-212.

45. Zhang, S., J. Li, Y. Song, C. Zhao, X. Zhang, C. Xie, Y. Zhang, H. Tao, Y. He, Y. Jiang and Y. Bian, In vitro degradation, hemolysis and MC3T3-*E1 cell adhesion of biodegradable Mg–Zn alloy.* Materials Science and Engineering: C, 2009. **29**(6): p. 1907-1912.

46. Nakamura, Y., Y. Tsumura, Y. Tonogai, T. Shibata and Y. Ito, *Differences in Behavior among the Chlorides of Seven Rare Earth Elements Administered Intravenously to Rats.* Fundamental and Applied Toxicology, 1997. **37**: p. 106-116.

47. Yang, W., Z. Ping, L. Jiesheng and X. Yanfang, *Effect of Long-Term Intake of Y3+ in Drinking Water on Gene Expression in Brains of Rats.* Journal of Rare Earths, 2006. **24**(3): p. 369-373.

48. Xu, L., G. Yu, E. Zhang, F. Pan and K. Yang, *In vivo corrosion behavior of Mg-Mn-Zn alloy for bone implant application.* J Biomed Mater Res A, 2007. **83**(3): p. 703-11.

49. Song, G., *Recent Progress in Corrosion and Protection of Magnesium Alloys.* Advanced Engineering Materials, 2005. **7**(7): p. 563-586.

50. Song, G., A. Atrens, and M. Dargusch, *Influence of microstructure on the corrosion of diecast AZ91D.* Corrosion Science, 1999. **41**: p. 249-273.

51. Song, G., A. Atrens, X. Wu and B. Zhang, *Corrosion Behaviour of AZ21, AZ501 and AZ91 in Sodium Chloride.* Corrosion Science, 1998. **40**(10): p. 1769-1791.

52. Song, G., A.L. Bowles, and D.H. StJohn, *Corrosion resistance of aged die cast magnesium alloy AZ91D.* Materials Science and Engineering: A, 2004. **366**(1): p. 74-86.

53. Ben-Haroush, M., G. Ben-Hamu, D. Eliezer and L. Wagner, *The relation between microstructure and corrosion behavior of AZ80 Mg alloy following different extrusion temperatures.* Corrosion Science, 2008. **50**(6): p. 1766-1778.

54. Song, G. and D. StJohn, *The effect of zirconium grain refinement on the corrosion behaviour of magnesium-rare earth alloy MEZ.* Journal of Light Metals, 2002. **2**: p. 1-16.

55. Ambat, R., N.N. Aung, and W. Zhou, *Evaluation of microstructural effects on corrosion behaviour of AZ91D magnesium alloy.* Corrosion Science, 2000. **42**: p. 1433-1455.

56. Ballerini, G., U. Bardi, R. Bignucolo and G. Ceraolo, *About some corrosion mechanisms of AZ91D magnesium alloy.* Corrosion Science, 2005. **47**(9): p. 2173-2184.

57. Kutniy, K.V., I.I. Papirov, M.A. Tikhonovsky, A.I. Pikalov, S.V. Sivtzov, L.A. Pirozhenko, V.S. Shokurov and V.A. Shkuropatenko, *Influence of grain size on mechanical and corrosion properties of magnesium alloy for medical implants.* Materialwissenschaft und Werkstofftechnik, 2009. **40**(4): p. 242-246.

58. Sun, H.-f., C.-j. Li, and W.-b. Fang, *Corrosion behavior of extrusion-drawn pure Mg wire immersed in simulated body fluid.* Transactions of Nonferrous Metals Society of China, 2011. **21**: p. s258-s261.

59. Song, S.X., J.A. Horton, N.J. Kim and T.G. Nieh, *Deformation behavior of a twin-roll-cast Mg–6Zn–0.5Mn–0.3Cu–0.02Zr alloy at intermediate temperatures.* Scripta Materialia, 2007. **56**(5): p. 393-395.

60. Wang, C.Y., X.J. Wang, H. Chang, K. Wu and M.Y. Zheng, *Processing maps for hot working of ZK60 magnesium alloy.* Materials Science and Engineering: A, 2007. **464**(1-2): p. 52-58.

61. GALIYEV, A., R. KAIBYSHEV, and G. GOTTSTEIN, *Correlation of Plastic Deformation and Dynamic Recrystallization in Magnesium Alloy ZK60.* Acta Materialia, 2001. **49**: p. 1199-1207.

62. Snir, Y., G. Ben-Hamu, D. Eliezer and E. Abramov, *Effect of compression deformation on the microstructure and corrosion behavior of magnesium alloys.* Journal of Alloys and Compounds, 2012. **528**: p. 84-90.

63. Ohtsuki, C. *How to prepare the simulated body fluid (SBF) and its related solutions, proposed by Kokubo and his colleagues*. 2012; Available from: http://mswebs.naist.jp/LABs/tanihara/ohtsuki/SBF/index.html.

64. *ASTM-G31-72: Standard Practice for Laboratory Immersion Corrosion Testing of Metals.*

65. Adams, B.L., et al., *Metallography and Microstructures*, in *ASM Handbook*, G.F.V. Voort, Editor 2004, ASM International: United States of America. p. 1184 pages, ISBN: 0-87170-706-3.

66. Wang, Y., M. Wei, J. Gao, J. Hu and Y. Zhang, *Corrosion process of pure magnesium in simulated body fluid.* Materials Letters, 2008. **62**(14): p. 2181-2184.

67. Baliga, c.B. and P. Tsakiropoulos, *Development of corrosion resistant magnesium alloys Part 2 Structure of corrosion products on rapidly solidified Mg-16AI alloys.* Materials Science and Technology, 1993. **9**: p. 513-519.

68. DAS, S.K. and L.A. DAVIS, *High Performance Aerospace Alloys via Rapid Solidification Processing.* Materials Science and Engineering, 1988. **98**: p. 1-12.

69. Zainal Abidin, N.I., A. D. Atrens, D. Martin and A. Atrens., *Corrosion of high purity Mg, Mg2Zn0.2Mn, ZE41 and AZ91 in Hank's solution at 37°C.* Corrosion Science, 2011. **53**(11): p. 3542-3556.

70. Ng, W.F., K.Y. Chiu, and F.T. Cheng, *Effect of pH on the in vitro corrosion rate of magnesium degradable implant material.* Materials Science and Engineering: C, 2010. **30**(6): p. 898-903.

71. Hanzi, A.C., I. Gerber, M. Schinhammer, J. F. Löffler and P. J. Uggowitzer, *On the in vitro and in vivo degradation performance and biological response of new biodegradable Mg-Y-Zn alloys.* Acta Biomater, 2010. **6**(5): p. 1824-33.

72. Xin, Y. and P.K. Chu, *Influence of Tris in simulated body fluid on degradation behavior of pure magnesium.* Materials Chemistry and Physics, 2010. **124**(1): p. 33-35.

73. Rettig, R. and S. Virtanen, *Composition of corrosion layers on a magnesium rare-earth alloy in simulated body fluids.* J Biomed Mater Res A, 2009. **88**(2): p. 359-69.

74. Waizy, H., A. Weizbauer, C. Modrejewski, F. Witte, H. Windhagen, A. Lucas, M. Kieke, B. Denkena, P. Behrens, A. Meyer-Lindenberg, F-W. Bach and F. Thorey, *In vitro corrosion of ZEK100 plates in Hank's Balanced Salt Solution.* Biomed Eng Online, 2012. **11**: p. 12.

75. Witte, F., *The history of biodegradable magnesium implants: a review.* Acta Biomater, 2010. **6**(5): p. 1680-92.

76. Mueller, W.D., M. Lucia Nascimento, and M.F. Lorenzo de Mele, *Critical discussion of the results from different corrosion studies of Mg and Mg alloys for biomaterial applications.* Acta Biomater, 2010. **6**(5): p. 1749-55.

77. Donald Garlotta, *A Literature Review of Poly(Lactic Acid).* Journal of Polymers and the Environment, 2001. **9**(2):p. 63-84.